THE UNIVERSITY OF WISCONSIN–MILWAUKEE

COLLEGE OF ENGINEERING AND APPLIED SCIENCE

DISCLAIMER

INTERFACIAL AREA AND INTERFACIAL TRANSFER IN TWO-PHASE FLOW SYSTEMS

Volume I. Chapters 1 – 5

T. Guo, J. Park and G. Kojasoy

Department of Mechanical Engineering
University of Wisconsin-Milwaukee, Milwaukee
Milwaukee, Wisconsin 53201

March 2003

Prepared for
U.S. DEPARTMENT OF ENERGY
Under Contract No. DE-FG02-87ER13764

DOE Patent Clearance Granted
Jay Ahn for Mark Peterson
14 May 2003

TABLE OF CONTENTS

VOLUME II

VOLUME III

VOLUME IV

EXECUTIVE SUMMARY

Advances in the study of two-phase flow increasingly require detailed internal flow structure information upon which theoretical models can be formulated. The void fraction and interfacial area are two fundamental parameters characterizing the internal flow structure of two-phase flows. However, little information was available on these parameters, and it is mostly limited to vertical flow configuration. Particularly, there was virtually no database for the local interfacial area concentration in spite of its necessity in multidimensional two-fluid model analysis.

In view of the above, a research program, which has been sponsored by the DOE/BES, has been underway at the University of Wisconsin-Milwaukee. The overall objectives of the research program were to develop instrumentation methods, an extensive database and analysis leading to predictive models for describing the internal flow structure and behaviors of two-phase flow in horizontal configurations.

Experimental efforts were directed at developing instrumentation technique for measurements of the local interfacial area concentration and void fraction in the bubbly flow, plug/slug flow, stratified smooth and stratified wavy and annular flow patterns encountered for two-phase flows in horizontal configurations. Chapters 5 through 12 describe several conductivity probe techniques that have been developed under this research program. More specifically:

- Chapters 5 and 6 present the development and utility of the two-sensor conductivity probe for a bubbly flow,
- Chapter 7 describes the utility of hot-film anemometry method for a bubbly flow whereas Chapters 9 and 10 documents the development of hot-film probe method for a plug/slug flow,
- Chapter 8 describes the four-sensor conductivity probe design for measuring the large bubble interfacial area concentration in a plug/slug flow-pattern,
- Chapter 11 summarizes the development and utility of a two-sensor parallel-wire conductivity probe for the stratified, i.e., stratified-smooth,

stratified-wavy and stratified-atomizing, flow patterns encountered in horizontal two-phase flows, finally,

- Chapter 12 involves with the development of eight-sensor parallel-wire probe method designed for a horizontal annular flow-pattern.

Analytical efforts were focused on deriving predictive mechanistic models describing the interfacial structure in various adiabatic two-phase flow patterns as well as predicting fluid particle behavior in boiling channels. Chapters 13 through 18 summarize these efforts. More specifically, they are summarized as follows:

- Chapter 3 deals with the derivation of the interfacial area transport equation and discusses the basic mechanisms affecting the source and sink terms appearing in the interfacial transport equation.
- Chapter 13 is devoted to studies of interfacial instabilities of horizontal stratified flows,
- Chapter 14 describes mechanistic scaling methodologies and derivation of similarity requirements for two-phase flow-regime transitions,
- Chapter 15 presents an analysis of the spherically symmetric phased change (moving boundary) problem to describe the bubble growth and/or collapse in boiling channels,
- Chapter 16 describes several droplet disintegration mechanisms and offers droplet size and size distributions model for an annular flow-pattern, whereas Chapter 17 is devoted to bubble break-up processes and describes a detailed mechanistic model describing the averaged bubble size and size distributions in bubbly flow, finally,
- Chapter 18 deals with modeling of void fraction and interfacial area concentration and concludes that the core break-up is a dominant break-up mechanism, which determines the interfacial area concentration in the core whereas the Taylor break-up mechanism becomes dominant around the pipe perimeter.

LIST OF FIGURES

VOLUME I

VOLUME II

VOLUME III

VOLUME IV

LIST OF TABLES

VOLUME I

VOLUME III

VOLUME IV

1. INTERNAL FLOW STRUCTURE AND INTERFACIAL AREA IN TWO-PHASE FLOW SYSTEMS

1.1 Introduction

The simultaneous flow of two phases or of several components occurs in a large number of engineering systems as well as in many natural phenomena. At first glance it might appear that various multiphase systems and components and phenomena have very little in common. Actually, the contrary is true. If we recall that the singular characteristic of two-phase or of two immiscible mixtures is the presence of one or several interfaces, between the phases or components, it can be noticed that many of the two-phase systems have a common structure, i.e., a common topography of the interface. Furthermore, whereas single-phase flows can be classified according to the geometry of the flow in laminar, transitional and turbulent flow, the flow of two-phases or of a mixture of immiscible liquids can be classified according to the geometry of the interface into three main classes, i.e., in separated flows, transitional or mixed flows and dispersed flows.

In view of this topographical and structural classification into separated, mixed and dispersed flows, it could be expected that many of the two-phase systems of importance should exhibit a large number of steady state and dynamic similarities. This indeed is the case. For example, it was shown in Refs. [1-3] that the theory of kinematic waves, which was developed by Lighthill and Whitman [4] to analyze the flow of cars on roads, can be extended to analyze and predict transient response of two-phase systems with applications to fluidized beds, boiling water nuclear reactors, and cryogenic heat exchanger.

It is evident that if a firm understanding of the thermo-fluid dynamic characteristics of two-phase flow is attained, then these results could be applied to predict the operational performance of systems and components in a variety of technologies. Indeed, such a generalized method of analysis has been attained and used in the field of single-phase flows. There, studies of the thermo-fluid dynamic characteristics of laminar and of turbulent flows have been first carried out, and then the results have been applied to various technologies. However, in the field of two-phase flow, the opposite approach has been followed most often. There, the tendency has been to analyze the thermal and/or

fluid dynamic problems of a particular system, component or process, say of a nuclear reactor, refrigerator, pollutant separator, liquid propellant rocket or open channel sediment transport.

Consequently, a broad understanding of the thermo-fluid dynamic behavior of two-phase systems has not been attained yet, nor is a generalized method available at the present time to analyze and predict the performance of the systems. The design of engineering systems and the ability to predict their performance depend on the availability of experimental data and of conceptual models, which can be used to describe a physical process with a required degree of accuracy. From a scientific, as well as from a practical point of view, it is essential that the various characteristics and properties of such conceptual models and processes should be formulated clearly, on a rational basis, and supported by experimental data. For this purpose specially designed experiments are required which must be conducted in conjunction with and in support of analytical investigations.

It is well established in continuum mechanics that the conceptual model for single-phase flow of a gas or of a liquid, is formulated in terms of field equations which describe the conservation laws of mass, momentum, energy, charge, etc. These field equations are then complemented by appropriate constitutive equations such as the constitutive equations of state, stress, chemical reactions, etc., which specify the thermodynamic, transport and chemical properties of a given constituent material, i.e., of a specified solid, liquid or gas. It is to be expected, therefore, that the conceptual models, which describe the steady state and dynamic characteristics of structured multi-phase or multi-component media, should also be formulated in terms of the appropriate field and closure relations. However, the derivation of such equations for the flow of structured media is considerably more complicated [5] than for continuous media, i.e., for single-phase flow.

In multi-phase or multi-component flows the presence of interfaces introduces great difficulties in the mathematical and physical formulation of the problem. From the point of view of physics, the difficulties which are encountered in deriving the field and closure equations appropriate to multiphase flow systems stem from the presence of the interface and the fact that both the steady and dynamic characteristics of multi-phase

flows depend upon the structure of the flow. For example, the steady state and the dynamic characteristics of dispersed two-phase flow systems depend on the collective dynamics of solid particles, bubbles or droplets interacting with each other and with the surrounding continuous phase; whereas, in the case of separated flows these characteristics depend upon the structure and dynamics of the interface. In order to determine the collective interaction of particles and the dynamics of the interface, it is necessary to describe first the local properties of the flow and then to obtain a macroscopic description by means of appropriate averaging procedures, [5]. For dispersed flows, for example, it is necessary to determine the rates of nucleation, evaporation or condensation, motion and disintegration of single droplets (bubbles) as well as the collisions and coalescence processes of several droplets (or bubbles).

For separated flows, the structure and the dynamics of the interface greatly influence the rates of mass, heat and momentum transfer as well as the stability of the system. For example, the performance and flow stability of a condenser for space application depend on the dynamics of the interface. Similarly, the rate of droplet entrainment from a liquid film, and therefore, the effectiveness of film cooling, depend on the stability of the vapor-liquid interface.

It can be concluded from this discussion that in order to derive the field and closure relations appropriate to structured, multi-phase media it is necessary to describe the local characteristics of the flow from which the macroscopic properties should be obtained by means of an appropriate averaging procedure. It is evident also that the design, performance and very often the safe operation of a great number of important technological systems depend on the availability of realistic and accurate field and closure equations. In particular, the interfacial transfer terms in a two-phase flow formulation play the essential roll by describing the interfacial transport of mass, momentum and energy. However, it can be said that these interfacial transfer terms are the weakest link in a two-phase flow formulation, because of considerable difficulties in terms of experimentation as well as modeling, [5]. The interfacial area concentration and flow-pattern transition criteria are the most important basis for driving reliable closure relations for two-phase flow.

1.2 Two-Phase Flow Field Formulations and Importance of Interfacial Area Measurements

Two-Phase flow is characterized by the existence of the interfaces between phases and discontinuities of properties associated with them. The internal structures of two-phase flow are classified by two-phase flow patterns. Various transfer mechanisms between the mixture and wall as well as between phases strongly depend on these two-phase patterns. This leads to the use of flow-pattern dependent correlations and closure equations together with appropriate flow-pattern transition criteria. On the other hand the basic structure of flow can be characterized by two fundamental geometrical parameters. These are the void fraction and interfacial area concentration. The void fraction expresses the phase distribution whereas the interfacial area describes available area for the interfacial transfer of mass, momentum and energy. Therefore, an accurate knowledge of these parameters is necessary for any two-phase flow analysis. This fact can be further substantiated with respect to two-phase flow formulation.

The rational approach to develop a macroscopic two-phase flow formulation is to use proper averaging of the local instant formulation, which is based on the single-phase flow balance equations and interfacial jump conditions at the interfaces. The averaging procedure is basically a filtering process, which eliminates or smooth out some unwanted high frequency random signals from local instant fluctuations of variables. However, various statistical properties of these fluctuations and collective contribution from the interfacial transfer are taken into account through the closure relations for the bulk fluids and interface. Many of the difficulties in developing the two-fluid model formulation are associated with this interfacial transfer modeling.

Various averaging procedures which can be used for two-phase flow analysis are reviewed in detail [5J. There are three main groups based on the physical concepts used to formulate dynamical problems, namely, Eulerian, Lagrangian and Boltzman statistical averages. Among them, the Eulerian averaging is particularly important in most practical engineering problems.

Besides these different averaging methods for developing a model, there are two fundamentally different formulations of the macroscopic balance equations for two-phase flow systems. These are the mixture models and two-fluid model. The mixture model

informulated by considering the motion of a two-phase mixture as a whole in terms of the mixture momentum equation. The relative motion between phases is taken into account by a closure equation for the relative velocity. The most important assumption associated with the mixture model is that a strong coupling exists between the motions of two phases. This implies that the mixture model is an accurate approximation to the two-fluid model whenever there is a sufficient interaction time or length for two phases. Certain two-phase flow problems involving a sudden acceleration of one phase, with respect to the other on a flow in a very short tube or vessel, may not be appropriately described by this model. In these cases inertia terms of each phase should be considered separately by use of a two-fluid model.

Depending on the form of the closure equation for the relative velocity and on the treatment of the thermal non-equilibrium between phases, a number of different mixture models have been proposed, i.e., the homogeneous flow, slip flow, and drift-flux models. When the effect of gravity is important as in the flooding, flow reversal, and counter-current flow, only the drift-flux model, [6 -9] is satisfactory. The use of the slip flow model based on a slip ratio correlation or void-quality correlation is limited to a high-speed unidirectional flow. The effect of thermal non-equilibrium can be taken into account by a phenomenological model in which the vapor generation rate is specified, or by the mechanistic model in which energy equation for each phase is used and the energy transfers to the interfaces are specified by closure relations.

The two-fluid model is formulated by considering each phase separately in terms of two sets of conservation equations which govern the balance of mass, momentum, and energy of each phase. These balance equations represent the macroscopic fields of each phase and are obtained from proper averaging methods. Since the macroscopic fields of each phase are not independent of the other phase, the interfacial interaction terms, which couple the transport of mass, momentum and energy of each phase appear in the field equations. It is expected that the two- fluid model can predict mechanical and thermal non-equilibrium between phases accurately. However, it is noted that the interfacial transfer terms should be modeled accurately for the two- fluid model to be useful. In the present state of the arts, the closure relations for these interfacial terms are the weakest link in the two-fluid model. The difficulties arise due to the complicated transfer

mechanisms at the interfaces coupled with the motion and geometry of the interface. Furthermore, the closure relations should be modeled by measurable macroscopic variables based on proper averaging.

A three-dimensional two-fluid model has been obtained by using temporal or statistical averaging [5]. For most engineering applications, the model developed by Ishii can be simplified to the following forms [6,7]:

Continuity Equation

$$\frac{\partial}{\partial t}\alpha_k \rho_k + \nabla \cdot \alpha_k \rho_k u_k = \Gamma_k \tag{1}$$

Momentum Equation.

$$\frac{\partial}{\partial_t}(\alpha_k \rho_k u_k) + \nabla \cdot (\alpha_k \rho_k u_k u_k) = -\alpha_k \nabla \rho_k + \nabla \cdot \alpha_k (\bar{\bar{\tau}}_k + \tau_k^t) + \alpha_k \rho_k g + u_{ki}\Gamma_k + M_{ki} - \nabla \alpha_k \cdot \tau_i \tag{2}$$

Enthalpy Energy Equation

$$\frac{\partial}{\partial_t}(\alpha_k \rho_k H_k) + \nabla \cdot (\alpha_k \rho_k H_k u_k) = -\nabla \cdot \alpha_k (\bar{\bar{q}}_k + q_k^t) + \alpha_k \frac{D_k}{D_t}\rho_k + H_{ki}\Gamma_k + q''_{ki} a_i + \Phi_k \tag{3}$$

Here Γ_k, M_{ik}, τ_i, q''_{ki} and Φ_k are the mass generation, due to phase change, generalized interfacial drag, interfacial shear stress, interfacial heat flux, and dissipation, respectively. The subscript k denotes the k-th phase and i stand for the values at the interface. a_i which is defined as the interfacial area concentration denotes the interfacial area per unit mixture volume.

The above field equations indicate that several interfacial transfer terms appear on the right- hand sides of the equations. Since these interfacial terms also should obey the balance laws at the interface, interfacial transfer conditions could be obtained from an average of the local interfacial conditions, [7]. They are given by:

$$\sum \Gamma_k = 0 \tag{4a}$$

$$\sum M_{ik} = 0 \tag{4b}$$

$$\sum H_{ki}\Gamma_k + q''_{ki} a_i = 0 \tag{4c}$$

In the above set of time-averaged balance equations, the dependent variables are listed in Table 1. Since the number of variables is larger than the number of equations,

constitutive equations need to be added to close the formulation. Extensive discussions of the requirements for the closure laws were given by Ishii [5] and Boure [8]. In view of the above formulation, it is evident that, closure relations for the interfacial area concentration (a_i), the interfacial transfer terms ($\Gamma_k, M_{ik}, and\ q''_{ki}a_i$) and the Reynolds stress in two-phase flow (τ'_k) are necessary for the interfacial transfer terms. The enthalpy interfacial transfer condition indicates that specifying the heat flow at the interface for both phases is equivalent to the closure relation for Γ_k if the mechanical energy transfer terms can be neglected. This aspect greatly simplifies the development of the closure relations for the interfacial transfer terms.

By introducing the mass flux, $\dot{m}''_k$ defined by

$$\Gamma_k \equiv a_i \dot{m}''_k \tag{5}$$

the interfacial energy transfer term appearing in Eqs. (1.3) and (1.4c) can be written as

$$\Gamma_k H_{ki} + a_i q''_{ki} = a_i (\dot{m}''_k H_{ki} + \dot{q}''_{ki}) \tag{6}$$

The heat flux at the interface should be modeled using the driving force or the potential for an energy transfer. Thus,

$$q''_{ki} = h_{ki}(T_i - T_k) \tag{7}$$

where T_i is the temperature at the interface and T_k is the k'th phase bulk mean temperature based on the average enthalpy, H_k, and h_{ki} is the interfacial heat transfer coefficient. A similar treatment of the interfacial momentum transfer term is also possible [9].

Table 1 Balance Equations and Associated Variables

Conservation Equations	Department Variables	Interfacial Transfer Terms
Mass	ρ_k, a_k, u_k	Γ_k
Momentum	$\rho_k, a_k, u_k, p, \bar{\bar{\tau}}_k, \tau'_k$	u_i, M_{ik}, τ_i
Energy	$\rho_k, a_k, u_k, H_k, p, \bar{\bar{q}}_k, q'_k, \Phi_k$	$H_{ki}\Gamma_k, q''_{ki}a_i$

In view of the above, the importance of the interfacial area concentration is developing closure relations for the interfacial transfer is evident. Thus, in general, the interfacial transfer terms can be written as a product of the interfacial area concentration, a_i, *and* the mean driving force:

$$\text{(Interfacial Transfer Term)} = a_i \times \text{(Driving Force)} \qquad (8)$$

As demonstrated by Ishii [5], and further detailed by Ishii and Kocamustafaogullari [10] and Ishii et al. [11], interfacial area concentration defined as the available interfacial area per unit volume of the two-phase mixture, characterizes the first order geometrical effects; therefore, it must relate to the interfacial structure of the two-phase flow field. On the other hand, the driving forces for the interfacial transport characterize the local transport mechanisms such as the local turbulence and molecular transport properties and must be related to the respective potentials. It is essential to make a conceptual distinction between the effects of these two parameters; thus, closure relations should be developed separately for each of these effects.

As the above formulation indicates, closure relations for the local interfacial are concentration and the driving forces are essential for a detailed analysis and prediction of the behavior of a two-phase flow system. In this study, efforts will be focused on the closure relations of the interfacial area concentration, the momentum driving force (momentum flux) and the Reynolds stress in two-phase flow, from both the theoretical and experimental point of views. Any attempt to formulate a two-phase flow system in terms of the two-fluid model would not be complete unless accurate models for these terms are also included. The general, interfacial area concentration relation can be used in the models of the interfacial mass and energy transfer as well. In order to highlight the research needs on the interfacial area concentration as well as the momentum flux and two-phase flow turbulence, the current state and problems in the modeling practice relevant to these closure relations are summarized below.

1.3 Interfacial Area Concentration

Most of the current two-phase flow formulations use the traditional flow-regime maps and flow-regime transition criteria and the flow-regime dependent interfacial area correlations in terms of basic flow parameters. As a result, the closure relations for the

interfacial area concentration are different from one regime to another with obvious discontinuities between them. Although this approach results in simple algebraic relations for the interfacial area concentration, it has the following shortcomings:

(1) The flow regime transition criteria are algebraic relations obtained for steady-state, fully developed flows conditions. They do not fully reflect the true dynamic nature of changes in the interfacial structure. Hence, the effects of the entrance or boundary and developing flow cannot be taken into account correctly, nor the gradual transition between regimes.

(2) The method based on the flow regime transition criteria is a two-step method that requires the flow regime dependent closure relations for the interfacial area in a form of bubble size or droplet size correlations. Therefore, the compound errors from this approach can be significant.

(3) The existing flow regime dependent correlations and criteria are valid in limited parameter ranges for certain specific operational conditions. Most of them are obtained from simple air- water flow experiments and phenomenological models. Often the scale effects of geometry and fluid properties are not taken into account correctly. When applied to high pressure, steam-water transients, these models may cause significant discrepancies, artificial discontinuities and numerical instability.

In reality, flow regime transition in two-phase flow is a gradual evolutional process, rather than sudden switching of flow characteristics, except for certain transitions such as CHF. For instance, as studied and observed by Radovicich and Moissis [12] and Griffith and Snyder [13], the transition from bubbly flow to slug flow occurs mainly due to agglomeration and coalescence of smaller bubbles into cap bubbles. Once a cap bubble is formed, further coalescence follows in the wake region of a cap bubble. These observations indicate that for good mechanistic modeling, it is necessary to study bubble coalescence and breakup criteria. The latter will give information on the maximum bubble size and bubble size distribution. These are important in the formation of a link between the flow-regime transition and the characteristics of the interfacial

structure, such as interfacial area concentration and void fraction distributions. In terms of heat transfer, the nucleation phenomena would be important.

Since the flow-regime dependent models have the inherent shortcomings, for complicated two-phase flow thermal hydraulics analysis, it is necessary to use an appropriate model, which can characterize changes in the interfacial structure. Based on the current development in multi- phase studies, most researchers agree [14-16] that interfacial area transport equation is a rational choice for such a purpose. This transport equation is in the form of a conservation equation of interfacial area concentration with the right-hand-side representing the source and sinks due to the physical process for the creation and destruction of interfacial area. In this way, the two- phase flow evolution across flow regime transition boundaries is closely modeled, and thus any artificial discontinuities can be prevented. The elimination of artificial bifurcation in a mathematical formulation of the two-phase flow field is highly desirable in terms of computational efficiency and numerical stability. It is expected that the interfacial area transport equation can expand the current capability of the two-fluid model from both scientific and practical point of view.

1.4 Objectives of the Research Program

The overall objectives of the research program sponsored by the DOE/BES at the University of Wisconsin-Milwaukee were to develop instrumentation methods, an extensive database and analysis leading to predictive models for describing the interfacial structure and behaviors of two-phase flow in horizontal configurations. In terms of the flow structure, development of the interfacial area transport equation, distributions of the local void fraction, interfacial area, fluid particle size and their axial development from the entrance to the exit were the primary focal point of the research program. For the purpose of understanding the dynamic behaviors of the interfacial velocity, interfacial wave characteristics and coalescence and disintegration of fluid particles were studied. The special emphasis were placed on developing instrumentation techniques for measurements of the interfacial area concentration in the stratified smooth and stratified wavy, plug/slug flow, bubbly flow and annular flow patterns encountered for two-phase flows in horizontal configurations.

1.5 Highlight of Accomplishments

One of the long term goals of the DOE/BES is to provide a technological base for the field related to energy engineering and science. The scope of the research program have addressed this goal in terms of the fundamental understanding of interfacial transfers in two-phase flow which is important to many energy systems.

Under the research program sponsored by the DOE/BES at the University of Wisconsin-Milwaukee (Principal Investigator Dr. Gunol Kojasoy), a number of important results have been obtained. They are briefly summarized in this report. The highlight of the major accomplishments in the instrumentation development, measurement and modeling is summarized below:

We have established the following:

1. The interfacial area transport equation can be derived from the statistical model of the fluid particle number transport equations.
2. The mathematical theory relating the interfacial area concentration to the interfacial velocity is correct and it can be implemented in the measurement method.
3. Measurement of the interfacial area concentration through the interfacial velocity can be applied to practical two-phase flow conditions by the use of multi-sensor resistivity probes.
4. For bubbly flow pattern, it is sufficient to use a double-sensor resistivity probe.
5. For large bubbles such as the plug/slug flow patterns, it is necessary to use a four-sensor resistivity probe.
6. For the horizontal annular two-phase flow pattern, the circumferential interfacial characteristic can be measured by the use of an eight-point electrical resistivity probe.
7. For the horizontal stratified/smooth and stratified/wavy flow pattern, the parallel-wire double-sensor resistivity probe can be used to measure the interfacial characteristics of the horizontal stratified-smooth and stratified-wavy flow pattern.

We have demonstrated the following:

1. For bubbly flow-pattern, the double-sensor probe method simultaneously give following parameters over a wide range of flow conditions:
   - Local void-fraction and void distribution,
   - Local interfacial area concentration and distribution,
   - Local Sauter-Mean Diameter of Bubbles,
   - Local Interfacial Velocity, i.e., bubble velocity,
   - Bubble passing frequency
   - Probability density function of bubble chord length.
2. The changes in the void-fraction and interfacial area concentration characterize and quantify the development of interfacial flow structure and two-phase flow regimes.
3. The four-sensor probes are very effective to characterize the detailed flow structure in bubbly and slug flows. For example, the contributions of large bubbles and small bubbles to void fraction and interfacial area concentration can be measured separately at once.
4. The integration of these local measurements over the cross section gives excellent agreements with the well-established global measurements such as quick closing valves and flow meters.
5. For bubbly and slug flow, the hot-film anemometry method can be used to
   - Identify liquid and gas phases, i.e., phase identification,
   - Measure the local time-averaged void fraction,
   - Construct the local time-averaged liquid velocity distribution,
   - Measure the local liquid-phase turbulent velocity fluctuations and turbulent intensity.
6. For slug flow, the hot-film anemometry method can differentiate the small spherical/distorted bubble and large slug bubble void fractions which is essential for the development of the two-group drag coefficient and turbulence models.

7. A simultaneous application of two hot-film probes can be used to investigate the intermittent and transient characteristics of the slug flow pattern. This method is very effective to investigate the local variations in the three distinctive regions of a horizontal slug flow:
   - Liquid ahead of large gas bubble nose,
   - Liquid in the wake region of large gas bubbles,
   - Liquid layer below the large bubbles, i.e., near the nose and wake.
8. Combination of the hot-film anemometry and multi-sensor resistivity probe methods yields information on the local gas and liquid velocities and, hence, the local relative velocity in the horizontal bubbly and slug flow patterns.
9. Double-sensor parallel wire resistivity probe technique can be used to measure
   - Average liquid height,
   - Average wave height,
   - Wave velocity,
   - Wave frequency and wave length, and
   - The cross-correlation technique for analyzing wave velocity and Fourier transform method for analyzing wave frequency spectrum and eventually determining the most dominant wave frequency.
10. For horizontal annular flow pattern, eight-point electrical resistivity probe can be used to measure the interfacial wave structure and its variation through the circumferential position.

This is the first time that such detailed local instrumentation methods for the measurement of local interfacial structure have been developed and their accuracy and reliability over wide ranges of parameters have been demonstrated.

As indicated in the preceding section, the traditional approach to describe the interfacial structure in terms of flow regimes and flow regime transition criteria has a number of shortcomings for complicated transient thermal-hydraulic analysis. In view of this a new approach was initiated to develop an interfacial area transport equation for the

first order characterization of interfacial structures. The highlight of the major accomplishments in modeling the interfacial area transport equation and the fluid particle (bubbles and droplets) break-up and size distributions can be summarized as follows:

1. The interfacial transport equation is developed from the statistical model of fluid particle number transport equation which includes the source and sink terms due to the particle interactions and interfacial phase change.
2. The consistency of this approach is demonstrated in terms of the macroscopic continuity equation of a bubbly flow field.
3. The general framework to develop the closure relations for the fluid particle interactions and phase change terms is presented.
4. Based on bubble break-up mechanism, maximum and mean bubble size and interfacial area concentration are mechanistically modeled:
   - The mean bubble size in the case of horizontal flow is mainly controlled by the action of stresses from surface forces and liquid turbulent velocity fluctuations acting across a bubble diameter,
   - However, in the vicinity of the pipe wall, the Taylor break-up mechanism becomes dominant factor in determining maximum bubble size and its distribution.
   - Verification of the model is established by experimental data.
5. Two Weber number criteria, one based on the classical Kolmogorov theory and other on Levich's theory, are studied for describing droplet disintegration mechanism in annular flow:
   - When $\rho_d < \rho_c$, the entrainment of fluid particles by turbulence may be complete, and that the Weber number criterion based on Kolmogorov's theory mechanistically describes the fragmentation of drops and bubbles in a turbulent liquid flow,
   - When $\rho_d < \rho_c$, the entrainment of droplets by turbulent eddies cannot be complete, and interfacial effects play a major role instead of turbulent eddies in the mechanism of droplet disintegration.

- A theoretical model developed to describe the break-up mechanism of entrained droplets in the gas core of an annular flow.

6. A simple mechanistic model is developed on the combination of Kelvin-Helmholtz and Raleigh-Taylor instability theories to describe the break-up of drops and bubbles rising or falling freely in a stagnant media.

7. A hydrodynamic model is developed to describe local variations in the liquid film thickness and local film velocity profiles with respect to radial and circumferential position within a horizontal annular flow:
   - Wave induced turbulence is dominant for $Re_g < 115{,}000$
   - Wave induced turbulence and shear pumping are equally dominant for $115 \leq Re_g \leq 205{,}000$ and
   - Shear pumping is dominant for $Re_g > 205{,}000$.

8. A long-wave stability analysis is performed to investigate the significance of
   - Viscosity Ratio
   - Density Ratio
   - Fluid Depth Ratio

   on interfacial stability of stratified flow.

1.6 Publications Generated From the Research Program

R. K. Schwartzbeck and G. Kocamustafaogullari, "Similarity Requirements for Two-Phase Flow-Pattern Transitions", J. Nucl. Engr. and Design, vol. 116, pp. 135-147 (1989)

J. Kitscha and G. Kocamustafaogullari, "Breakup criteria for Fluid Particles", Int. J. Multiphase Flow, Vol. 15, pp. 573-588 (1989).

J. Kitscha, C.T. Chang and G. Kocamustafaogullari, "Characteristics of Horizontal Annular Two-Phase Flow Determined by Experimental Techniques", Proc. 9th Int. Heat Transfer Conf. Vol. 6, pp. 15-23, Jerusalem, Israel, August 19-24, 1990

Z. Wang and G. Kocamustafaogullari, "Interfacial Characteristic Measurements in a Horizontal Two-Phase Flow", Proc. ANS Nuclear Thermal Hydraulics, Vol. 6, pp. 342-351 (1990). THIS PAPER RECEIVED THE BEST PAPER AWARD.

G. Kocamustafaogullari and Z. Wang, "An Experimental Study on Local Interfacial Parameters in a Horizontal Air-Wager Bubbly Two-Phase Flow", Int. J. Multiphase Flow, Vol. 17, pp. 553-572 (1991).

W.D. Huang, Z. Wang and G. Kocamustafaogullari, "Internal Flow Structure Development of Bubbly Two-Phase Flow in a Horizontal Pipe", Proc. Int. Conf. On Multiphase Flow, Vol. 1, pp. 479-484, Tsukuba, Japan.

G. Kocamustafaogullari, W.D. Huang and T. He, "Measurement and Modeling of Interfacial Area Concentration", Proc. ANS Nuclear Thermal Hydraulics, Vol. 7, pp. 53-62 (1992).

G. Kocamustafaogullari, W.D. Huang and J. Razi, "Measurement and Modeling of Average Void Fraction, Bubble Size and Interfacial Area", J. Nucl. Engr. and Design, Vol. 148, pp. 437-453 (1994).

D.L. Jackman and G. Kocamustafaogullari, "A Model for Predicting Liquid Film Thickness and Local Velocity Profiles in Horizontal Annular Two-Phase Flow", Phase Change Heat Transfer, ASME HTD, Vol. 262, pp. 75-84 (1993).

J. Shi and G. Kocamustafaogullari, "Interfacial Characteristic Measurements in Horizontal Stratified Flow", Proc. Sixth Int. Topical Meeting on Nucl. Thermal Hydraulics, NURETH6, Vol. 1. pp. 26-35, Grenoble, France, October 5-8, 1993.

S.R. Smits, J. Razi, W.D. Huang and G. Kocamustafaogullari, "Droplet Size Modeling in Annular Flow", Proc. Sixth Int. Topical Meeting on Nucl. Thermal Hydraulics, NURETH6, Vol. 2, pp. 1021-1030, Grenoble, France, October 5-8, 1993.

G. Wang, W.D. Huang and G. Kocamustafaogullari, "Experimental Description of Spatial Gas Distribution in Developing Bubbly Two-Phase Flow in Horizontal Channels", Proc. ANS Nucl. Thermal Hydraulics, Vol. 7, pp. 22-31, Atlanta, Georgia, August 8-11, 1993.

J. Shi and G. Kocamustafaogullari, "Interfacial Measurements in Horizontal Stratified Flow Patterns", J. Nucl. Engr. and Design, Vol. 149, pp. 81-96 (1994).

S.R. Smits, J. Razi and G. Kocamustafaogullari, "Maximum and Mean Droplet Sizes in Annular Two-Phase Flows", Int. J. Heat and Mass Transfer, Vol. 37, pp. 955-966 (1994).

G. Kocamustafaogullari and W.D. Huang, "Internal Structure and Interfacial Velocity Development for Bubbly Two-Phase Flow, "J. Nucl. Engr. and Design, Vol. 151, pp. 79-101 (1994).

G. Kocamustafaogullari and M. Ishii, "Foundation of Interfacial Area Transport Equation and Its Closure Relations", Int. J. Heat and Mass Transfer, Vol. 38, pp. 481-493 (1995).

N. Zuber, J. Riznic and G. Kojasoy, "Dynamics of Liquid-Vapor Phase Change as Applied to Bubbles and Droplets", ANS Nuclear Thermal Hydraulics, Vol. 8, pp. 11-12, Portland Oregon (1995).

S. Lewis, V. Davenport and G. Kojasoy, "Use of Hot-Film Anemometry in Horizontal Gas-Liquid Slug Flow" Proc. ANS Nuclear Thermal Hydraulics, Vol. 9, pp. 326-335, Houston, Texas (1996).

M.Rajkovic, J. Riznic and G. Kojasoy, "Dynamic Characteristics of Flow-Patterns Transitions in Horizontal Two-Phase Flow", Proc. 2nd European thermal-Sciences and 14th UIT Natl. Heat Transfer Confr., Rome, Italy, 1996 Edizioni ETS, pp. 1403-1408 (1996).

J. Riznic, S. Lewis and G. Kojasoy, "Experimental Studies of Interfacial Area in Horizontal Slug Flow", Proc. ASME-THD 334, pp. 27-7, Nov. 16-22, Atlanta, Georgia (1996)

S.Sharma, S. Lewis and G. Kojasoy, "Local Studies in Horizontal Gas-Liquid Slug Flow", OECDE/CSMI Specialist Meeting an Advanced Instrumentation and Measurement Techniques, March 17-20, 1997, Santa Barbara, California.

J. Riznic and G. Kojasoy, "An Experimental Study on Local Interfacial Parameters in Horizontal Slug Flow", Proc. ANS Nuclear Thermal Hydraulics HTC-10, pp. 100-109, Baltimore, Maryland (1997).

J. Riznic, J. Meinacke and G. Kojasoy, "Interfacial Area Velocity and Void Fraction in Two-Phase Slug Flow", Proc. 3rd Int. Conf. on Multiphase Flow, ICMF '98, Lyon, France, June 8-12, 1998.

S. Sharma, S, Lewis and G. Kojasoy, "Liquid Velocity Field Measurements in Horizontal Slug Flow," Proc. 3rd. Int. Conf. on Multiphase Flow. ICMF '98, Lyon, France, June 8-12, 1998.

S. Sharma, S. Lewis and G. Kojasoy, "Local Studies in Horizontal Gas-Liquid Slug Flow", J. Nucl. Engr. and Design, Vol. 184, pp. 305-318 (1998).

N. Zuber, J. Riznic and G. Kojasoy, "On the Spherically Symmetric Phase Change Problem", Int. J. Fluid Mechanics Research, Vol. 26, No. 2, pp. 136-171 (1999).

A. Iskandrani and G. Kojasoy, "utility of Hot-Film Anemometry Technique in Horizontal Bubbly Two-Phase Flow", Proc. 33rd Natl. Heat Transfer Conf., Albuquerque, New Mexico, August 15-17, 1999. THIS PAPER RECEIVED THE BEST PAPER AWARD.

A. Iskandrani and G. Kojasoy, "Local Void Fraction and Velocity Field Description in Horizontal Bubbly Flow", Proc. 9th Int. Topical Meeting on Nuclear thermal Hydraulics, NURETH-9, San Francisco, California, October 3-8, 1999.

W.L. Fu, J.H. Park, T.W. Guo and G. Kojasoy, "Scaling Effects on Interfacial Area Transition", Proc. 5th Int. Symposium on Heat Transfer, Vol. 1, pp. 795-803, Beijing, China, August 12-16, 2000.

A. Iskandrani and G. Kojasoy, "Local Void Fraction and Velocity Description in Horizontal Bubbly Flow", J. Nucl. Engr and Design, Vol. 204, pp, 117-128 (2001).

G. Kojasoy, T. Guo and J. Riznic, "Internal Flow Structure Measurements in Horizontal Slug Flow", Proc. 6th Biennial Conf. on Engr. System Design and Analysis, pp. 1-11, Istanbul, Turkey, July 8-11, 2002.

S. Lewis, W.L. Fu and G. Kojasoy, "Internal Flow Structure Description of Slug Flow-Pattern in a Horizontal Pipe", Int. J. Heat and Mass Transfer, Vol. 45, pp. 3897-3910 (2002)

Nomenclature

a_i	Interfacial Area Concentration
H	Specific Enthalpy
h	Convective Heat Transfer Coefficient
g	Gravitational Acceleration
L_s	Length Scale at the Interface
$\dot{M}_{ki}$	Interfacial Momentum Flux for k'th Phase
$\dot{m}_{ki}$	Interfacial Mass Flux for the k'$_{th}$ Phase
P	Pressure
$\dot{q}''_i$	Interfacial Heat Flux
$\dot{q}''^{t}$	Turbulent Heat Flux
T	Temperature
T	Time
$\vec{v}$	Velocity Vector

Greek Letters

α	Void Fraction
Γ	Mass Generation per Unit Volume of the Mixture
ρ	Density
$\overset{=}{\tau}$	Viscous Shear Stress
$\overset{=t}{\tau}$	Turbulent Shear Stress
Φ	Dissipation Rate

Subscripts

f	Liquid Phase
g	Gaseous Phase
I	Value at the Interface
k	k'th Phase (gas or liquid)

References

1. N. Zuber and F.W. Staub,"The Propagation and the Wave form of the Volumetric Concentration in Boiling Water Forced Convection Systems under oscillatory Condition." Intl. J. Heat & Mass Transfer, Vol. 9, pp. 87-95 (1966)
2. M. Ishii and N. Zuber, "Thermally Induced Flow Instabilities in Two-Phase Mixtures", Proc. 4th Intl. Heat Transfer Conf., Paris 1970, Elsevier Pub. Co., Amsterdam (1970)
3. M. Ishii,"Study of Flow Instabilities in Two-Phase Mixtures", Argenne Natl. Lab. Report, ANL-76-23 (1976)
4. M. H. Lighthill and G. B. Whitham, "On the Kinematic Waves: Theory of Tranffic Flow on Long Crowded Road", Proc. Royal. Soc., Vol. 229, 99. 317 (1955)
5. M. Ishii, Thermo-Fluid Dynamic Theory of Two-Phase Flow, Collection de la Direction des Etudes et Reserches d'Electricite de France, Eyrolles, Paris (1975).

6. M. Ishii and G. Kocamustafaogullari, "Two-phase flow models and their limitations," NATO Advanced Research Workshop on Advances in Two-Phase Flow and Heat Transfer, Spitzingsee, BRD, August 31-September 3 (1982).
7. M. Ishii and K. Mishima, "Two-fluid model and hydrodynamic constitutive relations," Nuclear Engineering and Design, Vol. 82, p107-126 (1984).
8. J. A. Boure, "Mathematical modeling of two-phase flows," Proc. of CSNI Specialist Meeting, S. Banerjee and K.R. Weaver, Eds. A.E.C.L., Vol. 1, 85, Aug. 3-4, Toronto (1978).
9. M. Ishii and K. Mishima, "Study of two-fluid model and interfacial area," Argonne National Laboratory Report, ANL-80-111 (1980).
10. M. Ishii and G. Kocamustafaogullari, "Two-phase flow models and their limitations, "NATO Advanced Research Workshop on Advances in Two-Phase Flow and Heat Transfer, Spitzingsee, BRD, August 31, September 3 (1982).
11. M. Ishii, K. Mishima, I. Kataoka and G. Kocamustafaogullari, "Two-fluid model and importance of the interfacial area in two-phase flow analysis," Proc. 9th U.S. National Congress of Applied Mechanics, p. 73-80, Ithaca, New York, June 21-25 (1982).
12. N.A. Radovicich and R. Moissis, "The transition from two-phase bubble flow to slug flow," MIT Report No. 7-7633-22 (1962).
13. P. Griffith and G. A. Snyder, "The bubbly-slug flow transition in a high velocity two-phase flow," MIT Report No. 5003-29 (1964).
14. D. Grand, " Closure relation needs for two-fluid model formulation," DECD/CSNI Workshop on Advanced Instrumentation and Measurement Techniques, Santa Barbara, California, March 17-20, 1997.
15. S. Banerjee, "Perspectives on muiltifeild models," OECD/CSNI Workshop on Transient Thermal Hydraulics, Annapolis, Maryland, Nov. 5-8, 1996.
16. M. Ishii, "Views on future of Thermal Hydraulics Modelings", OECD/CSNI Workshop on Thermal Hydraulics, Annapolis, Maryland, Nov. 5-8, 1996.

2. INTERFACIAL AREA MEASUREMENT METHODS

Several methods are available at present to measure interfacial area concentrations in gas-liquid and liquid-liquid two-phase flows. These are photography, light attenuation, ultrasonic, probing and chemical methods. Detailed reviews of all these methods have been given by Veteau and Morel [1], Veteau and Charlot [2,3], Veteau [4] and Ishii and Mishima [5]. In what follows, we shall briefly describe the principles of the measurement methods and discuss the advantages and limitations of each method.

2.1 Chemical Method

In this technique, integral values of interfacial areas are obtained by absorption experiments. This requires knowledge of gas solubility, dispersion characteristics of both phases, and either mass transfer coefficient in the case of physical absorption or diffusivity and reaction rate constants in the case of chemical absorption. Many chemical systems have been proposed for determination of interfacial areas by the chemical method, including non-aqueous systems. A suitable reaction has to be chosen carefully, as the result may be specific to the system used, the properties of which can hardly be varied. The value of the interfacial area concentration obtained thus is usually referred to as "effective interfacial area" indicating that it may deviate from the geometrical interfacial area and depends strongly on the particular conditions employed.

Several factors have to be considered when choosing a chemical reaction for measuring interfacial areas if the results are to be free of excessive error. The systems useful for such measurements have been reviewed by Sharma and Danckwerts [6]. The topic has been dealt with in the literature [6-33] and will be discussed here only to the extent directly relevant to the measurement principles.

For an irreversible reaction of a gas phase component A with a liquid phase reactant B,

$$\nu_A\, A + B \rightarrow \text{Products} \qquad (1)$$

which is of order m, n in A and B, respectively. An approximate expression for the enhancement factor is given by Danckwerts [6] as

$$E = \frac{\sqrt{M}[(E_i - E)/(E_i - 1)]^{n/2}}{\tanh\{\sqrt{M}[(E_i - E)/(E_i - 1)]^{n/2}\}} \qquad (2)$$

where

$$E \equiv \frac{R_A}{a_i k_{LA} C_A^*} \tag{3}$$

$$E_i \equiv 1 + \frac{\nu_A C_B D_B}{C_A^* D_A} \tag{4}$$

and

$$M \equiv \frac{1}{k_{LA}^2}[(\frac{2}{m+1})k_{mn} D_A (C_A^*)^{m-1} C_B^n] \tag{5}$$

In these equations, ν_A is the stoichiometric factor, R_A is the rate of absorption of gas A per unit volume of the gas-liquid two-phase mixture, k_{LA} is the mass transfer coefficient of A in the liquid phase, k_{mn} is the reaction rate constant, and D_A and D_B are the diffusion coefficients of A and B, respectively. C_B is the concentration of the component B in the bulk of the liquid phase, whereas C^*_A is the concentration of A at the gas-liquid interface which is assumed to be equal to the equilibrium concentration of A in the bulk liquid phase. A pseudo-m'th, n'th order reaction is approximated when $\sqrt{M} << E_i$. In this case, Eq. (2) can be approximated by

$$E = \sqrt{(1+M)} \tag{6}$$

For purposes of measuring interfacial areas, only fast reactions, which are characterized by

$$1 << \sqrt{M} << E_i \tag{7}$$

are relevant. In such cases, Eq. (6) can, in turn, be approximated by

$$E = \sqrt{M} \tag{8}$$

Substituting E and M from Eqs. (3) and (5), respectively, the following equation is obtained for the rate of absorption of A in an irreversible, fast m'th, n'th, order reaction:

$$R_A \equiv a_i[(\frac{2}{m+1})k_{mn} D_A (C_A^*)^{m+1} C_B^n]^{1/2} \tag{9}$$

Equation (9) states that the absorption rate is independent of k_{LA} that is of the hydrodynamic conditions. Instead, it is governed by the physiochemical parameters, reactant concentration and the area of contact surface. For the type of reaction so far

discussed, the means to influence the values of M and E_i, in order to justify the inequality expressed by Eq.(7) to be valid, are rather limited.

In principle, selecting a suitable chemical reaction confirming Eq. (7) and measuring the absorption rate, R_A, the local interfacial area concentration, a_i, can be evaluated directly from Eq. (9) provided that the physiochemical parameters appearing in the right-hand side bracket are known. Thus, knowledge of reaction kinetics, solubility of gas-phase component A, the diffusion coefficient of A in the liquid-phase B, and, finally, the experimental capability of measuring the local rate of absorption are required for determining a. from Eq. (9). While *the* chemical systems confirming Eq. (7) for such measurements have been reviewed by Sharma and Danckwerts [7], in principal it is extremely difficult, if not impossible, to measure the local rate of absorption. Therefore, instead of the local interfacial area measurements, in practice an averaged interfacial area concentration is obtained in terms of measurable quantities by incorporating Eq. (9) into a molar balance on the liquid phase over the total volume of the test section used in the experiment. Since the average of a product differs from the product of the averages, the interfacial area concentration obtained from the integral of Eq. (9) would be considered as an "effective interfacial area concentration" instead of the actual volume-averaged interfacial area concentration. If the fast reaction condition expressed by Eq. (7) is not fulfilled and the absorption takes place at the transition from slow to fast reaction regime, absorption measurements at different reaction rates must be carried out. In this case, the interfacial area concentration is obtained from the so-called Danckwerts plot [7].

Based on the above principle, many chemical systems have been proposed for determination of effective interfacial areas by using the chemical method [6-33]. The relevant literature has been recently reviewed by DeJesus and Kawaji [34]. It has been observed by Schumpe and Deckwer [20,21] that in the pseudo-homogeneous flow regimes, the values of the interfacial area determined by the photographic method were greater than those obtained by the chemical method by about 35%. However, in the heterogeneous flow regime the values obtained by the photographic method were twice as high as those obtained by the chemical method. They have also observed that two different chemical methods yielded largely different values, even under similar conditions. This may be due to the fact that the effective area is evaluated on the basis of

simplified reactor models, which do not account for the mixing phenomena of the gas phase. Bubble shrinkage due to absorption is also neglected. They have, however, also shown that this discrepancy can be reduced greatly by accounting for bubble shrinkage and hydrostatic head. Deviation between the effective interfacial area determined by chemical methods and the geometrical interfacial area is largely dependent on the properties of the reaction system such as rate constant, diffusivity and solubility, the operating conditions, bubble size, and bubble size distribution.

It can be seen that even though the chemical method is a common technique for determination of interfacial area, systematic investigation of the effects of the liquid phase properties on the interfacial area is extremely difficult. It is also difficult to measure the local rates of absorption. The method seems to be highly dependent on the reaction chosen and also the geometry of the reactor. Depending on the application, a suitable reaction has to be chosen with great care, and the experiments can be time consuming. The results are not suitable for obtaining information of a more general nature, as the results are specific to the property of the system. It seems, however, to be the only method, which does not require verification by any other kind of measurement, and yields an overall value of the interfacial area from a single measurement.

2.2 Photographic Method

The photographic method has been used innovatively in the two-phase flow measurements of various parameters. This method involves, first, the determination of the mean particle diameter of the dispersion, which could be either a droplet or a bubble. The specific interfacial area is then calculated from the relation:

$$a_i = \frac{6\alpha}{D_{sm}} \tag{10}$$

there D_{sm} is the Sauter mean diameter.

The above relation gives good results for the case of spherical bubbles. However, for non-spherical bubbles, the projected area and the perimeter for each bubble under consideration is to be obtained. Hence, in this case two Sauter mean diameters are obtained, one based on the projected area and the other based on the perimeter. The shape factor is then calculated based on the ratio of the perimeter of the projected non-spherical

bubble to that of the spherical bubble having the same projected area. With this information the interfacial area in the case of non-spherical bubbles can be obtained.

The photographic method seems to be a very expensive method. Rapid advances have been made in terms of the availability of equipment including sophistication combined with ease of use. These advances include the high-speed movie camera and the high-speed video camera. High-speed movie cameras offer the advantage of a better resolution at a considerably lower cost than a video camera. But it has a disadvantage in that it needs an additional digitizer or a projector for analysis. Instant analysis is also not possible due to the time involved in film processing. Speeds up to 60,000 frames per second are available in these types of cameras. The video cameras have an advantage in that there is no processing time and, hence, the results can be analyzed almost instantaneously. But the tremendous cost involved, which can be almost four times that of a movie camera, offsets this advantage on most occasions. The resolution also leaves much to be desired.

It is, however, to be borne in mind that it becomes absolutely necessary to conduct experiments in transparent sections in order to enable us to use the photographic method. Photographs taken through a transparent wall are representative of the conditions at the focal point and may not be representative of those over the entire cross section. This section of the experimental setup must be carefully chosen to minimize the effects of refraction and reflection, as they could have disastrous effects on the end results. It also appears that selection of the lighting equipment is something of a trial and error process before yielding photographs of the right quality. Analysis of photographs can be very tedious, time consuming, and at times even subjective. It also seems unlikely that a large body of data can be generated by this method.

Studies on the determination of the interfacial area by the photographic method have been conducted by various investigators [3,11,20,35-42]. Burgess and Calderbank [38] have shown that the photographic method yields interfacial areas which are more than twice those obtained by other methods. Kawecki et al. [39], applied the photographic technique so that a continuous stream of the liquid and dispersed gas was withdrawn from the apparatus into a translucent rectangular chamber, and photographs were taken through the chamber wall. As pointed out by Reith [40], however, the procedure cannot be used

with higher gas void fractions because of coalescence of bubbles during transfer from the apparatus into the chamber. Instead of photographing through the wall, a special probe can be placed inside the vessel as suggested by Weiss and Ziegel [41]. Only small volumes can be sampled by such a device and, also, especially at higher gas void fractions, the alteration of the flow conditions by the probe can lead to non-representative results. Landau et al. [11] used diffused side lighting for the photographs. Information regarding bubble size and shape was obtained from photographs with the aid of a digitizer. Bubble contours were traced with a stylus on an enlarged print placed on the digitizer. They obtained two Sauter mean diameters, one based on the perimeter and the other based on the projected area. In addition, Landau et al. [11] have shown that the photographic technique, when applicable, can be used in combination with a suitable means for photographic analysis to provide additional information on the dispersion, such as mean bubble diameter, bubble size distribution and shape factor.

Gunn and Doori [42] have compared the photographic method and the electrical probe method to study bubbles in a fluidized bed. A 16 mm cine-camera was used at a film speed of 24 frames per second. A digitizer was used by them, as by most other investigators, for analysis. They have studied the volumetric bubble flow rate, the mean equivalent diameter, the bubble velocity and the effects bubble orientation near a probe. They, in fact, compared the bubble measurements by the optical and electrical methods with very good results.

2.3 Light Attenuation Method

The method of light attenuation to measure the interfacial area was first used by Vermeulen et al. [43] and later by Calderbank [44]. The theory for the attenuation of a light beam passing through dispersion is well established [3,44-49].

In this method, a narrow beam of light travels through the fluid containing bubbles or drops and the intensity, I, of the beam leaving the fluid is measured with a photoelectric detector such as a photodiode or photomultiplier. The access to the detector is carefully collimated to be in line with the original beam. When the beam passes through a droplet or bubble, it is scattered, and this leads to a reduction in the intensity

received, as compared to the intensity I_0 received in the absence of the bubbles or drops. I is related to I_0 through the classical photo-extinction law by

$$\frac{I}{I_0} = \exp(-\beta l) \tag{18}$$

where l is the distance the light beam travels through the fluid, and β is the attenuation coefficient.

There are three basic assumptions in evaluating the attenuation coefficient β. They are as follows:

1. There is no interaction between the scattering of bubbles or droplets. This condition can be met for dispersed two-phase flow of volumetric concentration less than ten percent composed of small fluid particles randomly spaced and separated by several fluid particle diameters.
2. The dispersed phase should be limited to spherical fluid particles. There are great differences in the scattering behavior of spherical and non-spherical fluid particles. Thus, the solution for scattering cross sections presently available for spherical fluid particles is a rather poor approximation of the total scattering cross section for large diameter non-spherical fluid particles.
3. Finally, it is assumed that there are no effects of forward scattering.

In view of the above assumptions, the attenuation coefficient is expressed as

$$\beta = \frac{\pi n}{8}\int_0^\infty D^2 f(D) S_{app}(2\pi D/\lambda) dD \tag{12}$$

where n is the fluid particle number density, D is the fluid particle diameter, $f(D)$ is the particle size distribution, λ is the wave length, and S_{app} is the apparent scattering coefficient.

Noting that the interfacial area concentration can be expressed by

$$a_i = \frac{\pi n}{2}\int_0^\infty D^2 f(D) dD \tag{13}$$

from Eqs. (12) and (13), n can be eliminated to obtain a relation between β *and* a_i. *Thus,*

$$\frac{\beta}{a_i} = (\frac{1}{4}) \frac{\int_0^\infty D^2 f(D) S_{app}(2\pi d/\lambda) dD}{\int_0^\infty D^2 f(D) dD} \quad (14)$$

In general, the apparent scattering coefficient depends on the real scattering coefficient, $S_n(2\pi D/\lambda)$, and the geometry of the actual experimental apparatus. To determine the scattering coefficient, the normalized extinction cross section which consists of scattering and absorption cross-sections are used. Neglecting the absorption cross section with respect to the scattering cross-section, Stravs and von Stockar [50] showed that

$$S_{app}(2\pi D/\lambda) \cong S_n(2\pi D/\lambda) \quad (15)$$

The theoretical expression of S_n for an air bubble in water was derived by Marston et al. [51]. Stravs and von Stockar [50] showed that for a sufficiently large spherical gas bubble, the scattering coefficient rapidly approaches its final value of 2 with increasing values of $(2\pi D/\lambda)$. This means the bubble removes an amount of energy from the incident light beam as if it were a completely absorbing disc of twice its projection area. In reality, one-half of this energy is reflected backwards, whereas the other half is diffracted forward around the bubble. Furthermore, as shown by Stravs and von Stockar [50] with light, where $(2\pi D/\lambda) > 700$, the diffracted energy is confined in such a narrow angle that under normal measuring conditions, it will be measured together with non-disturbed parallel light. This reduces the, apparent scattering coefficient S_{app} to 1. Thus,

$$S_{app} \approx S_n \approx 1.0 \quad (16)$$

With Eq. (16), Eq. (14) reduces to

$$\beta = a_i/4 \quad (17)$$

indicating that the attenuation coefficient β is equal to one-fourth of the interfacial area concentrations, which is four times larger than the projection area of the bubble size distribution. Furthermore, combining Eq. (17) with the photo-extinction law expressed by Eq. (11) leads to the following equation [44-46]:

$$I = I_0 \exp(-a_i l/4) \quad (18)$$

In principle, measuring I, I_0 and l, Eq. (18) allows the line-averaged interfacial area concentration, a_i. However, it is important to note here that in arriving at Eq. (18) a

series of assumptions have been made regarding the interaction between scattering of fluid particles, the particle shape, the effects of forward scattering, and the particle size D in relation to the wavelength λ. These assumptions limit the applicability of the light attenuation technique to optically dilute, transparent, dispersed two-phase flow with a volumetric concentration of less than a few percent. The method becomes inaccurate as the bubble or droplet concentration increases.

In fact, Eq. (18) has been extensively tested [52] and found to hold only up to

$$\ln(\frac{I_0}{I}) = \frac{a_i l}{4} < 5 \tag{19}$$

Above this value multiple scattering becomes important. This severe limitation of the light attenuation technique has evidently prevented its widespread use in dispersed two-phase flow. For example, Ohba and Itoh [48] showed a thousand fold attenuation in intensity for bubbly two-phase flow at a void fraction of about 30%. This implies a considerable number of inaccuracies in the measurements of the interfacial area concentrations at a void fraction of this magnitude and higher, although the method can be effectively used at lower void fractions of less than 10%. Evidently, the method cannot be applicable for horizontal, bubbly, two-phase flow, where the local void fraction toward the top of the pipe may reach as high as 60 - 65% corresponding to the maximum packing condition.

2.4 Ultrasonic Attenuation Method

For bubbly flows, the ultrasonic attenuation method as described by Stravs and von Stockar [50], Jones et al. [53], Oelhaye [54] and Bensler et al. [55] looks promising because of its simplicity and versatility. It compares fairly well with the photographic method and the light attenuation method at relatively low void fractions.

The interfacial area measurement by this method is based on the principle of energy attenuation as described in the preceding section. For the ultrasonic attenuation method measurements, a plane wave of ultrasound pulse is used instead of the visible light beam. As shown by Stravs and von Stockar[50], Eqs. (11) through (15) are valid in this technique, too. However, in the case of ultrasonic pulse attenuations, S varies with the bubble size, and the theoretical expression of S_n for an air bubble in water has been

given by Nishi [56]. With a known value of S_n as a function of the dimensionless size parameter $2\pi D/\lambda$, the interfacial area concentration can be calculated from Eqs. (14) and (15) as follows:

$$a_i = 4\beta \frac{\int_0^\infty D^2 f(D) dD}{\int_0^\infty D^2 f(D) S_n(2\pi d/\lambda) dD} \tag{20}$$

It is evident from Eq. (20) that one must know the bubble size distribution $f(D)$ in order to calculate a_i from the measured value of β from Eq. (11). However, the bubble size distributions are generally difficult to obtain, whereas the Sauter mean diameter D_{sm} may be found by a simultaneous measurement of the void fraction a and the interfacial area concentration a. through Eq. (10). Thus,

$$D_{sm} \equiv \frac{6\alpha}{a_i} \tag{21}$$

Stravs and von Stockar [50] used simulated size distribution f(D) over a frequency range from 1 to 5 MHz to show that the attenuation coefficient β calculated from Eq. (12) was in the worst case only 3% greater than a β value based on D_{sm}:

$$\beta^* = (\frac{\pi n}{8}) S_n(2\pi D_{sm}/\lambda) \int_0^\infty D^2 f(D) dD = (\frac{a_i}{4}) S_n(2\pi D_{sm}/\lambda) \tag{21}$$

β is approximated by β^*, Thus,

$$\beta \cong (\frac{a_i}{4}) S_n(2\pi D_{sm}/\lambda) \tag{23}$$

which can be rearranged to solve for a_i as

$$a_i = \frac{4\beta}{S_n(2\pi D_{sm}/\lambda)} = \frac{4\beta}{S_n(12\pi\alpha/a_i\lambda)} \tag{24}$$

From Eqs. (24) and (21), it follows that by knowing the local Sauter mean diameter, D_{sm} , *or* the local void fraction, α, one may determine the interfacial area concentration, a_i., from the measured attenuation coefficient, β, from Eq. (11).

Stravs and von Stockar [50] reported experimental results showing that for gas-liquid dispersions the interfacial area concentrations determined with the ultrasonic pulse attenuation method differed from those determined with the light attenuation method by

approximately 5%. Bensler et al. [55] indicated that the ultrasonic pulse attenuation method compared fairly well with the photographic technique in the determination of specific interfacial I areas in bubbly two-phase flows with a low void fraction.

As in the case of the light attenuation method, the ultrasonic pulse attenuation method has a limited success at relatively low void fractions. At high void fractions, the scattering and refraction at multiple interfaces becomes a very serious problem. Since the measurements of interfacial areas by the ultrasonic attenuation method can be made for non-transparent fluids in an opaque flow channel where measurements by the light transmissions method I fails, this method appears to be a powerful new technique over the light attenuation technique for measuring the interfacial area in bubbly two-phase flow.

2.5 Summary and Conclusion

The chemical absorption method is the most widely used technique and is applicable to all two-phase flow patterns. The value of the interfacial area is obtained by sampling and chemical analysis of concentrations. It is a global measurement over a certain length of a flow channel. Therefore, it does not give detailed local information on the interfacial area concentration. It is limited to steady-state flow without phase change. The experimental setup is cumbersome and time consuming. Furthermore, the errors associated with this method may be large depending on the experimental conditions.

The photographic method is applicable to relatively low concentration, dispersed two-phase flow. It involves the actual measurement of the fluid particle size from pictures of the flow. The combination of the fluid particle size and information on the void fraction yields the interfacial area. The method can be used for the case where the phase change occurs. However, it requires a transparent test section. Analysis of photographs may be very time consuming and highly expensive and even subjective in nature. The method seems to be useful when used in conjunction with other methods to provide additional information on the dispersion.

As in the case of the photographic method, the light attenuation method requires a flow channel with transparent walls. Basically, the attenuation of a visible light beam crossing a two-phase mixture is measured; and, relating the attenuation to the

concentration of fluid particles, the interfacial area is calculated. In this method the fluid particle size should be larger than the incident wavelength, and multiple reflections reaching the detector should be negligible. These assumptions limit the light attenuation method to an optically dilute, transparent, dispersed, two-phase flow with a volumetric concentration of less than a few percent. The method becomes inaccurate as the bubble or droplet concentration increases.

For bubbly flows the ultrasonic attenuation method is a relatively new technique for interfacial area measurements. It involves the measurement of pulse amplitude attenuation of an ultrasonic beam coupled with a sound scattering theory for calculating the interfacial area concentration. Although the photographic and the light attenuation methods cannot be used with opaque channel walls and are limited to transparent fluids, the ultrasonic technique is not restricted to such conditions. However, presently it can be used only for relatively low void fractions.

In conclusion, the presently available methods summarized above for measuring the interfacial area concentration are effective for certain idealized cases. Only an average interfacial area can be measured by the chemical absorption method. The photographic and light attenuation methods cannot be used with opaque walls and are limited to transparent bubbly flows. The ultrasonic method is not restricted to such conditions, and thus expands the measurement of the interfacial area concentration beyond the presently available range of fluids and non-opaque systems. However, the ultrasonic attenuation method is limited to low void fraction bubbly systems. In view of the intention of the present investigation to measure local interfacial variables in a horizontal bubbly two-phase flow with local void fractions possibly ranging from zero to 60 ~65%, it is inevitable that a probe method must be used. An evaluation of potential probe methods resulted in the selection of the electrical resistivity probe because of the relatively simple instrumentation and the positive results for conducting liquids reported in the literature.

Nomenclature

A	Area
a_i	Interfacial Area Concentration
B_o	Factor Defined in Eq. (36)
C	Concentration in Liquid Phase
C_A^*	Concentration of Component A at gas-liquid Interface
D_A	Diffusion Coefficient of A in Liquid Phase
D_B	Diffusion Coefficient of B in Liquid Phase
d	Fluid Particle Diameter
d_{SM}	Sauter Mean Diameter
E	Enhancement Factor
f(D)	Fluid Particle Size Distribution
g	Gravitational Acceleration
h	Specific Enthalpy
I	Intensity of a Light Beam
j	Superficial Volumetric Flux for Two-Phase Mixture
j_f	Superficial Volumetric Flux for Gaseous Phase
j_g	Superficial Volumetric Flux for Liquid Phase
k_{LA}	Mass Transfer Coefficient in Liquid Phase
k_{mn}	Reaction Rate Constant
l	Distance a Light Beam Travels Through Fluid
p	Pressure
$\dot{Q}_g$	Volumetric Flow Rate of Gas
$\dot{q}''$	Mean Conductive Heat Flux
$\dot{q}''_t$	Turbulent Heat Flux
$\dot{q}''_i$	Interfacial Heat Flux
R_A	Rate of Absorption of Gas A per unit Volume of Mixture
r	Radial Position
S	Root Mean Square of Fluctuating Component of Sensor Passing Velocity

S_{app}	Apparent Scattering Coefficient
S_n	Scattering Coefficient
V	Voltage Drop Across a Sensor
V_T	Threshold Voltage
T	Sampling Time
t	Time
$\vec{v}_i$	Interfacial Velocity Vector
α	Void Fraction
α_k	Volumetric Fraction of k'th Phase
β	Attenuation Coefficient
Δt_m	Most Probable Time Delay determined by cross correlation method
Δt_{max}	Time Limit Corresponding to Minimum Bubble Velocity
Δt_{min}	Time Limit Corresponding to Maximum Bubble Velocity
δ	Delta Function
λ	Wave Length
ν_A	Stoichiometric Factor
ρ	Mass Density

Subscripts

f	Liquid Phase, and also identifies front sensor
g	Gaseous Phase
i	Value at Interface
r	Identifies Rear Sensor

References

1. Veteau, J. M. and Morel, Y., "Techniques de measure des sires interfacials dans les ecoulements a bulles--II la methode chimique," CEA Report CEA -R-5092, France (1980).
2. Veteau, J. M. and Charlot, R., "Techniques de measure des sires interfacials dans les ecoulements a bulles--I Comparison de la methode d'attenuation d'un faisceau lumineux et de la methode photographiques," CEA Report CEA-R-5075, France (1980).

3. Veteau, J. M. and Charlot, R., "Techniques de measure des sires interfacials dans les ecoulements a bulles--III Comparison de la methode d'attenuation d'un faisceau lumineux et d'une methode locale," CEA Report CEA-R-5122, France (1981).
4. Veteau, J. M., "Contribution a 1'etude des techniques de measure de faire interfacial dans les ecoulements a bulles," These de docteaur es sciences, Universitye Scientifique et Medicale et Institute National Polytechnique de Grenoble (1981).
5. Ishii, M. and Mishima, K., "Study of Two-Fluid Model and Interfacial Area." Argonne National Laboratory Report, ANL-80-111 (1981).
6. Danckwerts, P. V., Gas-Liquid Reactions, McGraw-Hill, New York, 1970.
7. Sharma, M. M. and Danckwerts, P. V., "Chemical Methods of Measuring Interfacial Area and Mass Transfer Coefficients in Two-Fluid Systems," British Chem. Eng., Vol. 15, pp. 522-528 (1970).
8. Kasturi, G. and Stepanek, J. B., "Two-Phase Flow--III. Interfacial Area in Concurrent Gas-Liquid Flow," Chem. Eng. Sci., Vol. 29, pp. 713-719 (1974).
9. Robinson, C. W. and Wilke, C. R., "Simultaneous Measurement of Interfacial Area and Mass Transfer Coefficients for a Well-Mixed Gas Dispersion in Aqueous Electrolyte Solutions," AIChE J., Vol. 20, pp. 285-294 (1974).
10. Sridharan, K. and Sharma, M. M., "New Systems and Methods for the Measurement of Effective Interfacial Area and Mass Transfer Coefficients in Gas-Liquid Contactors," Chem. Eng. Sci., Vol. 31, pp. 767-774 (1976).
11. Landau, J., Boyle, J. Gomaa, H. G., and A1 Tawell, A. M., "Comparison of Methods for Measuring Interfacial Areas in Gas-Liquid Dispersions," Canadian J. of Chem. Eng., Vol. 55, pp. 13-18 (1977).
12. Shilimkan, R. V. and Stepanek, J. B., "Interfacial Area in Cocurrent Gas-Liquid Upward Flow in Tubes of Various Size," Chem. Eng. Sci., Vol. 32, pp. 149-154 (1977).
13. Shilimkan, R. V. and Stepanek, J. B., "Mass Transfer in Cocurrent Gas-Liquid Flow: Gas Side Mass Transfer Coefficients in Upflow, Interfacial Areas and Mass

Transfer Coefficient in Gas and Liquid in Downflow," Chem. Eng. Sci., Vol. 33, pp. 1675-1680 (1978).

14. Sridhar, T. and Potter, 0. E., "Interfacial Area Measurements in Gas-Liquid Agitated Vessels, Comparison of Techniques," Chem Eng. Sci., Vol. 33, pp. 1347-1353 (1978).
15. Watson, A. P., Cormack, 0. E., and Charles, M. E., "A Preliminary Study of Interfacial Areas in Vertical Cocurrent Two-Phase Upflow," Canadian J. of Chem. Eng., Vol. 57, pp. 16-23 (1979).
16. Dhanuka, V. R. and Stepanek, J. B., "Simultaneous Measurement of Interfacial Area and Mass Transfer Coefficient in Three-Phase Fluidized Beds," AIChe J., Vol. 26, pp. 1029-1038 (1980).
17. Farritor, R. E. and Hughmark, G. A., "Interfacial Area and Mass Transfer with Gas-Liquid Systems in Turbine-Agitated Vessels," Chem. Eng. Com., Vol. 4, pp. 143-147 (1980).
18. Hassan, I. T. M. and Robinson, C. W., "Mass-Transfer-Effective Bubble Coalescence Frequency and Specific Interfacial Area in a Mechanically Agitated Gas-Liquid Contractor," Chem. Eng. Sci., Vol. 35, pp. 1277-1289 (1980).
19. Vavruska, J. S. and Perona, J. J., "Measurements of Interfacial Areas in Cocurrent Gas-Liquid Downward Flow," Canadian J. of Chem. Eng., Vol. 58, pp. 141-144 (1980).
20. Schumpe, A. and Deckwer, W.-D., "Comparison of the Photographic and the Sulfite Oxidation Method for Interfacial Area Determination in Bubble Columns," Chem. Eng. Com., pp. 313-324 (1982).
21. Schumpe, A. and Deckwer, W. D., "Analysis of Chemical Methods for Determination of Interfacial Areas in Gas-in-Liquid Dispersions with Non-Uniform Bubble Sizes," Chem. Eng. Sci., Vol. 35, pp. 2221-2233 (1980).
22. Kulkarmi, A., Shah, Y., and Schumpe, A., "Hydrodynamics and Mass Transfer in Downflow Bubble Column," Chem. Eng. Com., Vol. 24, pp. 307-337 (1983).
23. Capuder, E. and Koloini, T., "Gas Hold-up and Interfacial Area in Aerated Suspensions of Small Particles," Chem. Eng. Res. & Design, Vol. 62, pp. 255-260 (1984).

24. Nagy, E., Borlai, 0., Laurent, E., and Charpentier, J.-C., "Determination of the Gas-Liquid Interfacial Area of a Perforated Plate Operating with Cross Flow," Intl. Chem. Eng., Vol. 26, pp. 637-646 (1986).
25. Schumpe, A. and Deckwer, W.-D., "Analysis of Chemical Methods for Determination of Interfacial Areas in Gas-in-Liquid Dispersions with Non-uniform Bubble Sizes," Chem. Eng. Sci., Vol. 35, pp. 2221-2233 (1980).
26. Shilimkan, R. V., "Mass Transfer in Co-Current Gas-Liquid Vertical Flows," Ph.D. Thesis, University of Salford (1975).
27. Tomida, T. Yuse, F., and Okezaki, "Effective Interfacial Area and Liquid-Side Mass Transfer Coefficient in the Upward Two-Phase Flow of Gas-Liquid Mixture," Chem. Eng. J., Vol. 16, pp. 81-88 (1978).
28. Benerjee, S., Scott, D. S., and Rhodes, E., "Studies on Cocurrent Gas-Liquid Flow in Helically Coiled Tubes," Can. J. Chem. Eng., Vol. 48, pp. 542-551 (1970).
29. Wales, C. E., "Physical and Chemical Absorption in Two-Phase Annular and Dispersed Horizontal Flow," AIChE J., Vol. 12, pp. 1166-1171 (1966).
30. Shah, A. K. and Sharma, M. M., "Mass Transfer in Gas Liquid Pipeline Contractors," Can. J. Chem. Eng., Vol. 53, pp. 572-574 (1975).
31. Gregory, G. A. and Scott, D. S., "Physical and Chemical Mass Transfer in Horizontal Cocurrent Gas-Liquid Slug Flow," Int. Symp. on Research in Gas-Liquid Flow, Waterloo, Canada, Sept. 19, 2, F3.1-F3.44 (1968).
32. Kulic, E. and Rhodes, E., "Chemical Mass Transfer in Co-Current Gas-Liquid Slug Flow in Helical Coils," Can. J. Chem. Eng., Vol. 52, pp. 114-116 (1974).
33. Radhkerishen, V. R. and Mitra, A. K., "Pressure Drop, Holdup and Interfacial Area in Vertical Two-Phase Flow of Multi-Jet Ejector Induced Dispersions," Can J. Chem. Eng., Vol. 62, pp. 170-178 (1984).
34. DeJesus, J. M. and Kawaji, M., "Measurement of Interfacial Area and Void Fraction in Upward, Cocurrent Gas-Liquid Flow," pp.137-145 (1989).
35. Akita, K. and Yoshida, F., "Bubble Size, Interfacial Area, and Liquid-Phase Mass Transfer Coefficient in Bubble Columns," Ind and Eng. Chem. Process Design and Development, Vol. 13, pp. 84-91 (1974).

36. Jeng, J. J. Jer, R. M., and Yang, Y. M., "Surface Effects and Mass Transfer in Bubble Column," Ind. and Eng. Chem., Process Design and Development, Vol. 25, pp. 974-978 (1986).
37. Yang, N. S., Shen, Z.-Q., Chem, B. H., and McMillian, A. F., "Pressure Drop, Gas Holdup, and Interfacial Area for Gas-Liquid Contact in Karr Columns," Ind. and Eng. Chem., Process Design and Development, Vol. 25, pp. 660-664 (1986).
38. Burgess, J. M. and Calderbank, P. H., "The Measurement of Bubble Parameters in Two-Phase Dispersions, I--The Development of an Improved Probe Technique," Chem. Eng. Sci., Vol. 30, pp. 743-750 (1975).
39. Kawecki, W., Reith, T., Van Heuven, J. W., and Beck, W., "Bubble Size Distribution in the Impeller of a Stirred Vessel," Chem. Eng. Sci., Vol. 22, pp. 1519-1523 (1967).
40. Reith, T. and Beck, W. J., Proc. 4th European Symp. Chem. Rect. Engng., pp. 191-197, Brussels, Belgium (1968).
41. Weiss, S. and Ziegel, G., Chem. Technik, Vol. 24, pp. 15-26 (1972).
42. Gunn, D. J. and Al-Doori, H. H., "The Measurement of Bubble Flows in Fluidized Beds by Electrical Probe," Int. J. Multiphase Flow, Vol. 11, pp. 535-551 (1985).
43. Vermeulen, T., Williams, G. M., and Langlois, G. E., "Interfacial Area in Liquid-Liquid and Gas-Liquid Contractors," AIChE J., Vol., pp. (1955).
44. Calderbank, P. H., "Physical Rate Processes in Industrial Fermentation, Part I: The Interfacial Area in Gas-Liquid Contacting with Mechanical Agitation," Trans. of the Inst. of Chem. Engineers, Vol. 36, pp. 443-463 Its-(1958).
45. McLaughlin, C. M. and Rushton, J. H., "Interfacial Areas of Liquid-Liquid Dispersions from Light Transmission Measurements," AIChE J., Vol. 19, pp. 813-822 (1973).
46. Curl, R. L., "Note on Light Transmission Through a Polydisperse Dispersion," AIChE J., Vol. 20, pp. 184-190 (1974).
47. Ohba, K. and Itoh, T., "Light Attenuation Technique for Void Fraction Measurement in Two-Phase Bubbly Flow, Part I. Theory," Technology Reports 4h$ of the Osaka University, Vol. 28, 1448, pp. 487-494 (1978).

48. Ohba, K. and Itoh, T., "Light Attenuation Technique for Void Fraction Measurement in Two-Phase Bubbly Flow, Part II. Experimental," Technology Reports of the Osaka University, Vol. 28, 1449, pp. 495-506 (1978).
49. Ohba, K., Itoh, T., and Yuhera, T., "Light Attenuation Technique for Void Fraction Measurement in Two-Phase Bubbly Flow, Part III. Effect of Some Parameters on Accuracy of Measurement," Technology Reports of the Osaka University, Vol. 28, 1450, pp. 507-516 (1978).
50. Stravs, A. A. and von Stockar, U., "Measurement of Interfacial Areas in Gas-Liquid Dispersions by Ultrasonic Pulse Transmission," Chem. Eng. Sci., Vol. 40, pp. 1169-1175 (1985).
51. Marston, P. L., Langley, 0. S., and Kingsbury, D. L., "Light Scattering by Bubbles in Liquids: Mie Theory, Physical-Optics Approximation, and Experiments," appl. Sci. Res. Vol. 38, pp. 373-383 (1982).
52. McLaughlin, C. M. and Rushton, J. H., "Interfacial Areas of Liquid-Liquid Dispersions from Light Transmission Measurements," AIChE J., Vol. 19, pp. 813-822 (1973).
53. Jones, S. W., Ambland, A., and Favreau, C., "Interaction of an Ultrasonic Wave with a Bubbly Mixture," Experiments in Fluids, Vol. 4, pp. 341-349 (1986).
54. Delhaye, J. M., "Recent Advances in Two-Phase Flow Instrumentation," in Heat Transfer, Tien, C. L., Canly, V. P., and Ferrel, J. K., Eds., Vol. 1, pp. 215-226, Hemisphere Publ. Corp. (1986).
55. Bensler, H. P. Delhaye, J. M., and Farreau, C., "Measurement of Interfacial Area in Bubbly Flows by Means of an Ultrasonic Technique," Proc. ANS, 1987 National Heat Transfer Conference, pp. 240-246.
56. Nishi, R., "The Scattering and Absorption of Sound Waves by a Gas Bubble in a Viscous Liquid," Acustica, Vol. 33, pp. 65-74 (1975).
57. Neal, L. G., and Bankoff, S. G., "A High Resolution Resistivity Probe for Determination of Local Void Properties in Gas-Liquid Flow," AIChE J., Vol. 9, pp. 490-494 (1963).

58. Park, W. H., Kang, W. K., Capes, C. E., and Osberg, G. L., "The Properties of Bubbles in Fluidized Beds of Conducting Particles as Measured by an Electroresistivity Probe," Chem. Eng. Sci., Vol. 24, pp. 851-865 (1969).
59. Rigby, G. R., van Blockland, G. P., Park, W. H., and Capes, C. E., "Properties of Bubbles in Three Phase Fluidized Beds as Measured by an Electroresistivity Probe," Chem. Eng. Sci., Vol. 25, pp. 1729-1741 (1970).
60. Hoffer, M. S., and Resnick, W., "A Modified Eiectroresistivity Probe Technique for Steady-and Unsteady-State Measurements in Fine Dispersions-I., Hardware and Practical Operating Aspects," Chem. Eng. Sci., Vol. 30, pp. 473-480 (1975).
61. Serizawa, A., Kataoka, I., and Michiyoshi, I., "Turbulence Structure of Air-Water Bubbly Flow-I. Measuring Techniques," Int. J. of Multiphase Flow, Vol. 2, pp. 221-233 (1975).
62. Herringe, R. A., and Davis, M. R., "Structural Development of Gas-Liquid Mixture Flows," J. of Fluid Mechanics, Vol. 73, pp. 97-123 (1976).
63. Kataoka, I., Ishii, M., and Serizawa, A., "Interfacial Area in Two-Phase Flow; Formulation and Measurement," Proc. 23rd Natl. Heat Trans. Conf. ASME, Denver (1985).
64. Hilgert, W. and Hofmann, H., "Characterization of Gas Phase Flow in Bubble Columns at Low Superficial Gas Velocities with the Aid of Ultrasonic Doppler Techniques," Ger. Chem. Eng. Vol. 9, pp. 180-190 (1986).
65. Wang, S. K., "Three-Dimensional Turbulence Structure Measurements in Air/Water Two-Phase Flow," Ph.D. Thesis, Rensselaer Polytechnic Institute, Troy, New York (1985).
66. Liu, T., Tay-Jian, "Experimental Investigation of Turbulence Structure inTwo-Phase Bubbly Flow," Ph.D. Thesis, Northwestern University, Evanston, Illinois (1989).

3. UNDERLYING THEORETICAL APPROACH FOR INTERFACIAL AREA TRANSPORT AND CLOSURE RELATIONS

3.1 Introduction

The interfacial transfer terms are strongly related to the interfacial area and to the local mechanisms, such as the degree of turbulence near the interfaces. Basically, the interfacial transport of mass, momentum and energy is proportional to the interfacial area concentration and to a driving force. This area concentration, defined as the interfacial area unit volume of the mixture, characterizes the kinematic effects; therefore, it must be related to the structure of the two-phase flow field. On the other hand, the driving forces for the inter-phase transport characterize the local transport mechanism, and they must be modeled separately.

Basic macroscopic parameters related to the internal structure of two-phase flows, particularly of a dispersed (bubbly or droplet) flow, are the void fraction, particle number density, interfacial area concentration and the particle shape factor. From geometric considerations, it is demonstrated by the principal investigators [1,2] that the particle number density is a key parameter in determining the interfacial area concentration, but it has not been sufficiently investigated in the literature.

Realizing the significance of the fluid particle number density as an important parameter for predicting the interfacial area concentration in a forced convective two-phase flow channel, the following are the objectives of this report:

1) To formulate the fluid particle number density transport in terms of the differential balance equation which takes into account various parameters such as the fluid particle generation and disintegration rates through the source and/or sink terms,
2) To develop the fluid particle interfacial area concentration transport equation,
3) To discuss the physical significance and possible mechanisms for particle interaction terms that give rise to the rate of change of number density due to sources and sinks,
4) To summarize preliminary modeling efforts for the interfacial source and sink terms,

5) To indicated a possible method to relate these source and sink terms to experimentally measured interfacial parameters, such that experiments can be used to establish a model for these terms.

3.2 Fluid Particle Transport Equations

3.2.1 Fluid Particle Number Density Transport Equation

The fluid particle interfacial transport equations for the interfacial area concentration and void fraction can be developed from a fluid particle number density transport equation analogous to Boltzman's transport equation. This approach recently was proposed by Reyes [3] to develop a set of fluid particle conservation equations for a distribution of chemically non-reacting, spherical fluid particles dispersed in a continuous medium. Here we shall follow a similar approach and extend the model for a general two-phase flow.

A simple procedure accounting for the fluid particle entering and leaving a control volume through different mechanisms yields the fluid particle number density transport equation of particles having volume ϑ:

$$\frac{\partial f}{\partial t} + \nabla \cdot (f \vec{v}_p) = \sum_j S_j + S_{ph} \qquad (1)$$

In this equation, $f(\vec{x}, \vartheta, t)$ is the particle density distribution function, which is assumed to be continuous and specifies the probable number density of fluid particles at a given time t, in the spatial range $d\vec{x}$ about a position $\vec{x}$, with particle volumes between ϑ and ϑ+dϑ. $\vec{v}_p(\vec{x}, \vartheta, t)$ is the particle velocity of volumes between ϑ and ϑ+dϑ at time t. S_{ph} is the fluid particle sink or source rate due to the phase change. For example, for one component bubbly flow S_{ph} represents the bulk liquid bubble nucleation rate due to the homogeneous and heterogeneous nucleation, and the collapse rate due to condensation for the subcooled boiling flow. The significance and methods evaluating S_{ph} are discussed in great detail by Kocamustafaogullari and Ishii [2]. The wall nucleation rate, which is not included in Sph, must be specified as a boundary condition.

The interaction term, $\sum_j S_j$, represents the net rate of change in the number density distribution function, f, due to the particle break-up and coalescence processes.

In essence, it serves as source and/or sink terms for fluid particles for two-component dispersed two-phase flow. Therefore, this term may be written as a sum of four components as follows:

$$\sum_{j=1}^{4} S_j = S_1 + S_2 + S_3 + S_4 \tag{2}$$

The following describes each term appearing in the above equation:

S1: represents the formation rate of particles of volume ϑ per unit volume of mixture due to break-up

S2: represents the loss rate of particles of volume ϑ per unit volume of mixture due to break-up

S3: represents the formation rate of particles of volume ϑ per unit volume of mixture due to coalescence,

S4: represents the loss rate of particles of volume ϑ per unit volume of mixture due to coalescence.

S1 can be formulated in terms of the break-up frequency, the distribution density of daughter particles by break-up and the number of daughter particles produced from a parent particle. Designating $g(\vartheta')$ as the break-up frequency of a particle having a volume of ϑ', $\beta(\vartheta',\vartheta)$ as the distribution of daughter particles produced upon break-up of a parent particle having volume ϑ', and $n(\vartheta')$ as the number of daughter particles produced by break-up of a parent particle of volume ϑ', the formation rate of particles of volume ϑ and be expressed by

$$S_1(\vec{x},\vartheta,t) = \int_{\vartheta}^{\vartheta_{max}} \beta(\vartheta',\vartheta) n(\vartheta') g(\vartheta') f(\vec{x},\vartheta',t) d\vartheta' \tag{3}$$

where ϑ_{max} is the maximum attainable particle volume.

S2, the loss rate of particles of volume ϑ per unit volume of the mixture due to break-up, can be readily evaluated in terms of $g(\vartheta)$ and the bubble number density distribution. Thus

$$S_2(\vec{x},\vartheta,t) = -g(\vartheta) f(\vec{x},\vartheta,t) \tag{4}$$

The formation due to a binary coalescence occurring at $(\vec{x},t)$ between two particles of volumes ϑ' and $(\vartheta-\vartheta')$ can be expressed in terms of collision frequency, $h(\vartheta,\vartheta')$, between particles of volumes ϑ and ϑ'. The collision frequency multiplied by the product of the number density of the respective particles $f(\vec{x},\vartheta,t)$ and $f(\vec{x},\vartheta-\vartheta',t)$ yields the collision rate density. Since every collision may not lead to coalescence, the total formation rate of particles of volume ϑ by coalescence can be given by multiplying the collision rate density by the coalescence efficiency $\lambda(\vartheta-\vartheta',\vartheta')$ and integrating over all possible volumes as follows:

$$S_3(\vec{x},\vartheta,t) = \int_{\vartheta_{min}}^{\vartheta/2} \lambda(\vartheta-\vartheta',\vartheta')h(\vartheta-\vartheta',\vartheta')f(\vec{x},\vartheta-\vartheta',t)f(\vec{x},\vartheta',t)d\vartheta' \qquad (5)$$

This equation describes how the coalescence between the two particles results in a new particle characterized by volume ϑ. A factor of (1/2) at the upper limit is included to prevent double counting of collision between particles of ϑ' and $\vartheta-\vartheta'$ for a given particle of ϑ'.

S4, loss rate of particles of volumes ϑ per unit volume of mixture due to coalescence, can be evaluated by

$$S_4(\vec{x},\vartheta,t) = \int_{\vartheta_{min}}^{\vartheta_{max}+\vartheta} \lambda(\vartheta,\vartheta')h(\vartheta,\vartheta')f(\vec{x},\vartheta',t)f(\vec{x},\vartheta',t)d\vartheta' \qquad (6)$$

where ϑ_{min} is the minimum particle volume.

The fluid particle number density transport equation of particles having volume of ϑ described by Eq. (1) is much too detailed for most flow studies where the primary focus is on the average fluid particle behavior. Therefore, it would be advantageous to develop a particle number density transport equation that has been averaged over all particle sizes it can be achieved by integration of Eq. (1) from the minimum particle volume to the maximum possible particle volume. Thus,

$$\int_{\vartheta_{min}}^{\vartheta_{max}} \frac{\partial f}{\partial t}d\vartheta + \int_{\vartheta_{min}}^{\vartheta_{max}} \nabla\cdot f\vec{v}_p d\vartheta = \sum_{j=1}^{4} \int_{\vartheta_{min}}^{\vartheta_{max}} S_j d\vartheta + \int_{\vartheta_{min}}^{\vartheta_{max}} S_{ph} d\vartheta \qquad (7)$$

Applying the Leibnitz rule for integration and noting that

$$\int_{\vartheta_{min}}^{\vartheta_{max}} f(\vec{x},\vartheta,t)d\vartheta = N(\vec{x},t) \tag{8}$$

the number density transport equation can be expressed at follows:

$$\frac{\partial N}{\partial t} + \nabla \cdot N\vec{v}_{pm} = \sum_{j=1}^{4} \int_{\vartheta_{min}}^{\vartheta_{max}} S_j d\vartheta + \int_{\vartheta_{min}}^{\vartheta_{max}} S_{ph} d\vartheta \tag{9}$$

where $N(\vec{x},t)$ is the total number of particles of all sizes per unit volume of mixture, and $\vec{v}_{pm}(\vec{x},t)$ is the average local particle velocity weighted by the particle number. It is defined by

$$\vec{v}_{pm}(\vec{x},t) \equiv \frac{\int_{\vartheta_{min}}^{\vartheta_{max}} f(\vec{x},\vartheta,t)\vec{\vartheta}_p(\vec{x},\vartheta,t)d\vartheta}{\int_{\vartheta_{min}}^{\vartheta_{max}} f(\vec{x},\vartheta,t)d\vartheta} \tag{10}$$

Equation (1) will serve as the basis for the development of the interfacial area concentration and void fraction transport equation.

3.2.2 Fluid Particle Interfacial Area Concentration Transport Equation

The interfacial are concentration transport equation of particles of volume ϑ can be obtained by multiplying the particle number density transport equation of particles having volume ϑ by the average interfacial area, $A_i(\vartheta)$, of particles of volume ϑ, which is independent of the spatial coordinate system. This yields the following equation:

$$\frac{\partial f A_i(\vartheta)}{\partial t} + \nabla \cdot (f A_i(\vartheta)\vec{v}_p) = \sum_{j=1}^{4} A_i(\vartheta) S_j + A_i(\vartheta) S_{ph} \tag{11}$$

As in the case of the fluid particle number density equation, the fluid particle interfacial area concentration transport equation of volume ϑ given by Eq. (11) is much too detailed for practical purposes. It would be much more useful to develop an interfacial area transport equation averaged over all particle sizes. This can easily be done by integrating Eq. (11) from ϑ_{min} to ϑ_{max}. Thus,

$$\int_{\vartheta_{min}}^{\vartheta_{max}} \frac{\partial f A_i(\vartheta)}{\partial t} d\vartheta + \int_{\vartheta_{min}}^{\vartheta_{max}} \nabla \cdot (f A_i(\vartheta)\vec{v}_p d\vartheta = \sum_{j=1}^{4} \int_{\vartheta_{min}}^{\vartheta_{max}} A_i(\vartheta) S_j d\vartheta + \int_{\vartheta_{min}}^{\vartheta_{max}} A_i(\vartheta) S_{ph} d\vartheta \tag{12}$$

Again applying the Leibnitz rule, the average interfacial area concentration transport equation can be expressed in a condensed form as follows:

$$\frac{\partial a_i}{\partial t} + \nabla \cdot a_i \vec{v}_i = \sum_{j=1}^{4} \Phi_j + \Phi_{ph} \tag{13}$$

where $a_i(\vec{x},t)$ is the average interfacial area concentration of all fluid particles of volumes between ϑ_{min} and ϑ_{max}, and $\vec{v}_i(\vec{x},t)$ is the interfacial velocity. These variables are defined as:

$$a_i(\vec{x},t) \equiv \int_{\vartheta_{min}}^{\vartheta_{max}} f(\vec{x},\vartheta,t) A_i(\vartheta) d\vartheta \tag{14}$$

and

$$\vec{v}_i(\vec{x},t) \equiv \frac{\int_{\vartheta_{min}}^{\vartheta_{max}} f(\vec{x},\vartheta,t) A_i(\vartheta) \vec{v}_p(\vec{x},\vartheta,t) d\vartheta}{\int_{\vartheta_{min}}^{\vartheta_{max}} f(\vec{x},\vartheta,t) A_i(\vartheta) d\vartheta} \tag{15}$$

Φ_j's, which are defined by

$$\Phi_j = \int_{\vartheta_{min}}^{\vartheta_{max}} A_i(\vartheta) S_j(\vec{x},\vartheta,t) d\vartheta ; \qquad j = 1,2,3,4 \tag{16}$$

represent the rate of change in the interfacial area concentration due to the particle break-up and coalescence processes. In line with definitions S1, S2, S3 and S4 expressed, respectively, by Eqs (3)-(6), the following describes each Φ_j:

$$\Phi_1 = \int_{\vartheta_{min}}^{\vartheta_{max}} A_i(\vartheta) \int_{\vartheta}^{\vartheta_{max}} \beta(\vartheta',\vartheta) n(\vartheta') g(\vartheta') f(\vec{x},\vartheta',t) d\vartheta' d\vartheta \tag{17}$$

$$\Phi_2 = -\int_{\vartheta_{min}}^{\vartheta_{max}} A_i(\vartheta) g(\vartheta) f(\vec{x},\vartheta,t) d\vartheta \tag{18}$$

$$\Phi_3 = \int_{\vartheta_{min}}^{\vartheta_{max}} A_i(\vartheta) \int_{\vartheta_{min}}^{\vartheta/2} \lambda(\vartheta-\vartheta',\vartheta') h(\vartheta-\vartheta',\vartheta') f(\vec{x},\vartheta-\vartheta',t) f(\vec{x},\vartheta',t) d\vartheta' d\vartheta \tag{19}$$

$$\Phi_4 = -\int_{\vartheta_{min}}^{\vartheta_{max}} A_i(\vartheta) \int_{\vartheta_{min}}^{\vartheta_{max}} \lambda(\vartheta,\vartheta') h(\vartheta,\vartheta') f(\vec{x},\vartheta',t) f(\vec{x},\vartheta',t) d\vartheta' d\vartheta \tag{20}$$

From the above equations, it is evident that $\Phi_1 and\ \Phi_2$, respectively, represent the rate of increase and decrease in the interfacial area concentration due to the fluid particle break-up process, whereas Φ_3 and Φ_4 describe the rate of increase and decrease due to the coalescence process.

Similarly, Φ_{ph}, which is defined by

$$\Phi_{ph} = \int_{\vartheta_{min}}^{\vartheta_{max}} A_i(\vartheta) S_{ph} d\vartheta \tag{21}$$

represents the rate of change in interfacial area concentration due to evaporation of condensation.

3.2.3 Fluid Particle Volume Fraction (Void Fraction) Transport Equation

The void fraction transport equation of particles having volume ϑ can be obtained by multiplying the particle number density transport equation of particles having volume ϑ by the average volume of particles. This yields the following equation:

$$\frac{\partial f\vartheta}{\partial t} + \nabla \cdot (f\vartheta \vec{v}_p) = \sum_{i=1}^{4} \vartheta S_j + \vartheta S_{ph} \tag{22}$$

As in the case of obtaining the interfacial area concentration transport equation, Eq. (22) can be integrated to obtain the void fraction transport equation as follows:

$$\int_{\vartheta_{min}}^{\vartheta_{max}} \frac{\partial f\vartheta}{\partial t} d\vartheta + \int_{\vartheta_{min}}^{\vartheta_{max}} \nabla \cdot (f\vartheta \vec{v}_p) d\vartheta = \sum_{j=1}^{4} \int_{\vartheta_{min}}^{\vartheta_{max}} \vartheta S_j d\vartheta + \int_{\vartheta_{min}}^{\vartheta_{max}} \vartheta S_{ph} d\vartheta \tag{23}$$

Noting that

$$\alpha(\vec{x},t) \equiv \int_{\vartheta_{min}}^{\vartheta_{max}} f(\vec{x},\vartheta,t) \cdot \vartheta d\vartheta \tag{24}$$

and using Eq. (8), it can be shown that

$$\frac{\partial \alpha}{\partial t} + \nabla \cdot \alpha \vec{v} = \int_{\vartheta_{min}}^{\vartheta_{max}} \left[\sum_{j=1}^{4} \vartheta S_j + S_{ph} \vartheta \right] d\vartheta \tag{25}$$

where $\vec{v}(\vec{x},t)$ is the average velocity of the center of volume of the dispersed phase. It is defined by

$$\vec{v}(\vec{x},t) \equiv \frac{\int_{\vartheta_{min}}^{\vartheta_{max}} f(\vec{x},\vartheta,t)\vartheta\vec{v}_p(\vec{x},\vartheta,t)d\vartheta}{\int_{\vartheta_{min}}^{\vartheta_{max}} f(\vec{x},\vartheta,t)\vartheta d\vartheta} \tag{26}$$

Equation (25) is the fluid particle volume fraction transport equation, which represents the volume balance for particles of constant density. Both the interfacial area concentration and void fraction transport equations are the moments of the number density transport equation. Since the weighting functions on these equations are the interfacial are and volume, respectively, the resulting equations yield macroscopic transport of the respective quantities.

The consistency of the above derivations can be justified by considering the gaseous phase continuity equation, which is given by

$$\frac{\partial \alpha\rho_g}{\partial t} + \nabla \cdot \alpha\rho_g \vec{v}_g = \Gamma_g \tag{27}$$

Where Γ_g is the amount of phase change pre unit volume of the mixture, and $\vec{v}_g(\vec{x},t)$ is the velocity of center of mass of gas phase.

For an incompressible flow with no phase change, Eq. (27) reduces to

$$\frac{\partial \alpha}{\partial t} + \nabla \cdot \alpha\vec{v}_g = 0 \tag{28}$$

In this case, the velocity of center of mass, $\vec{v}_g$ reduces to the velocity of center of volume $\vec{v}$ as follows:

$$\vec{v}_g(\vec{x},t) \equiv \frac{\int_{\vartheta_{min}}^{\vartheta_{max}} f\vartheta\vec{v}_p\rho_g d\vartheta}{\int_{\vartheta_{min}}^{\vartheta_{max}} f\vartheta\rho_g d\vartheta} = \vec{v}(\vec{x},t) \tag{29}$$

Finally, comparing Eq. (28) with Eq. (25), it can be noted that

$$\int_{\vartheta_{min}}^{\vartheta_{max}} \sum_{j=1}^{4} S_j \vartheta d\vartheta = 0 \tag{30}$$

Which indicates that the net volume change due to coalescence and break-up would be zero. This identify can be used for the purpose of measuring S_j's for a two-phase flow.

3.3 Closure Relation Requirements

The parameters involved in the break-up components of the S_j's and ϕ_j's terms are the maximum fluid particle volume, the average daughter particle distribution function, the average number of daughter particles produced by break-up of a parent fluid particle, and the average break-up frequency. On the other hand, the parameters involved in the coalescence component are the minimum fluid particle volume, the average collision frequency, and the average coalescence efficiency. These parameters which are needed to evaluate the fluid particle number density and the interfacial area concentration distributions are summarized as follows:

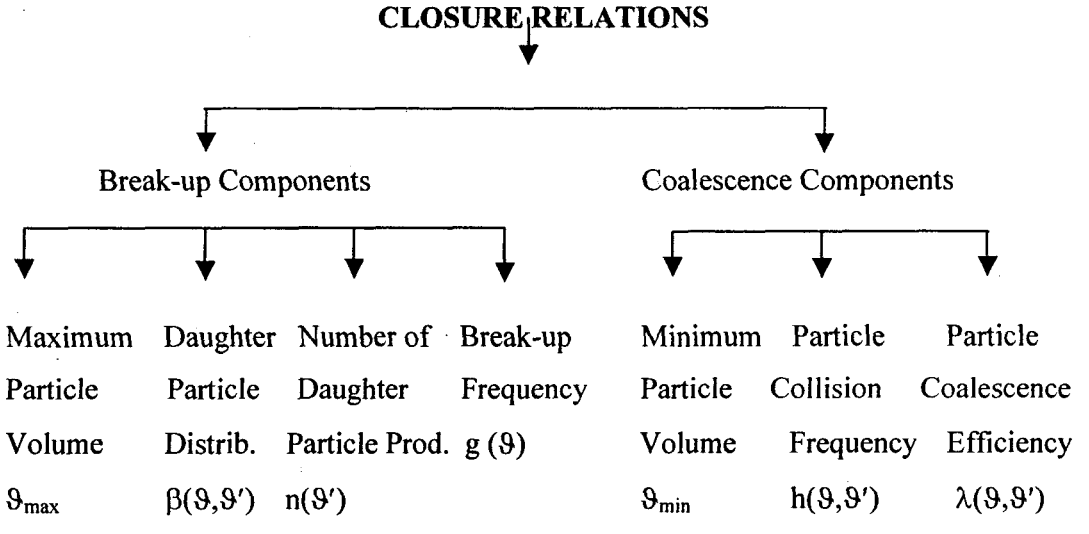

In order to evaluate these terms which serve as source and sink terms in Eqs. (9) and (13), accurate interaction rate models for fluid particle break-up and coalescence must be incorporated. These models are typically functions of the physical and operating conditions of the system. The overall behavior of the particle number density and interfacial area concentration in a region of space can then be predicted by solving the proper transport equation which has the form of an integro-differential equation.

3.4 Break-up and Coalescence Processes

In any two-phase flow field, the initial bubble or drop size is determined in terms of the mechanism of fluid particle generation such as formation of bubbles at an orifice or bubble entrainment mechanisms and generation of droplets by shearing off of

roll waves in separated two-phase flow patterns such as annular and stratified-wavy flows. However, in forced convective pipe flow or mechanically agitated systems, the initial fluid particle size may be too large or too small to be stable. In these cases the fluid particle size is further determined by a break-up and/or coalescence mechanism. In boiling systems, in addition to the break-up and coalescence mechanisms, the growth rate should also be considered.

When a fluid particle exceeds a critical value, the particle interface becomes unstable and break-up is likely to occur. Similarly, when fluid particles are smaller than some critical dimension, then the coalescence is likely to occur on a series of collision events. Therefore, the particle break-up can be related to the maximum attainable size of the particle; whereas particle coalescence can be related to the minimum size. The literature contains several models for determining the maximum and minimum sizes of fluid particles. These models have been developed from the first principle and have been used to develop break-up and coalescence criteria. These criteria, however, do not treat a distribution of fluid particles. Rather, they describe the particle size limits of break-up and coalescence.

In what follows, we shall briefly describe the basic mechanisms that have been used to obtain the closure relations listed in Section 3.3.

3.5 Break-up Parameters

3.5.1 Maximum Fluid Particle Size: d_{max} or ϑ_{max}. The fluid particle break-up controls the maximum bubble or droplet size and can be greatly influenced by the continuous phase hydrodynamics and interfacial interactions. Therefore, a generalized break-up mechanism can be expressed as a balance between external stresses, τ, that attempt to disrupt the bubble and the surface stress, σ/d, that resists the particle deformation. These stresses influence both the size of fluid particles, which are torn away from their point of formation, and also the maximum particle size, which is stable in the flow field. At the point of break-up, these forces must balance. Thus,

$$\tau \propto \frac{\sigma}{d/2} \tag{31}$$

This balance leads to the prediction of a critical Weber number, above which the fluid particle is no longer stable. It is defined by:

$$We_{cr} \equiv \tau d_{max} / 2\sigma \geq 1.0 \qquad (32)$$

where d_{max} is the maximum stable fluid particle, and τ reflects the hydrodynamic conditions responsible for particle deformation and eventual break-up. The mechanism of particle break-up can thus be related to the external conditions as illustrated below:

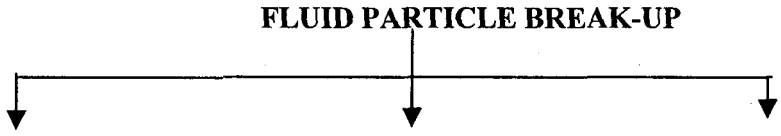

Turbulent Flow (Local Turbulence)	Laminar Flow (Viscous Shear)	Interfacial Instability (Rayleigh-Taylor & Kelvin-Helmholtz Instabilities)

In the case of turbulent flow, particle break-up is caused by fluctuating eddies resulting in the pressure variation along the particle surface. In laminar flow, viscous shear in the continuous phase will elongate the particle and cause break-up. However, even in the absence of net flow of continuous phase such as rising bubbles in a liquid and rising and falling drops in a continuous gas or immiscible liquid, the fluid particle break-up is caused by interfacial instabilities due to the Raleigh-Taylor and Kelvin-Helmholtz instabilities.

Aside from the break-up mechanism caused by interfacial instabilities, basically there are two external forces that are involved in the breaking up of fluid particles, namely viscous and turbulence induced inertial forces. In most applications, the Reynolds numbers that are characteristic of the flow field are so large that viscous effects are negligible. In other cases, however, inertial effects play a minor role and may be neglected. Existing experimental and theoretical information can, therefore, be classified into two categories, namely, in which surface tension and viscous forces interact, and another in which surface forces and turbulence induced dynamic pressure forces are dominant.

The first fundamental experiments on the break-up of drops and bubbles under the action of external viscous stresses and surface stress were made by Taylor [4]. Taylor made numerous observations, many of which were subsequently explained by

Tomotika [5]. The break-up criteria is expressed in terms of external viscous stress in Eq. (32). It is given by

$$We_{cr} \equiv \mu_c (\partial v / \partial r)_{\max} d_{\max} / 2\sigma \tag{33}$$

where μ_c, is the absolute viscosity of the continuous phase, and $(\partial v/\partial r)_{max}$ is the maximum velocity gradient in the external flow field. Equation (33) leads to capillary number criteria for break-up.

The Taylor mechanism of bubble and drop deformation applies if both the undeformed and the elongated particles are small compared with the local regions of viscous flow. Several predictive equations for the maximum particle size were derived from Eq. (33) for agitated vessels [6,7].

The fluid particle fragmentation phenomenon in a highly turbulent flow is related to the fact that the velocity in a turbulent stream varies from one point to another. The velocity of the fluid particle at the surface of the particle varies from point to point. The velocity of the continuous phase at the surface of the particle also varies from point to point. Therefore, different dynamic pressures will be exerted at different points on the surface of the fluid particle. Under certain conditions, this will inevitably lead to deformation and break-up of the fluid particle.

The force due to dynamic pressure may develop either through the local relative velocity around the particle, which appears because of inertial effects, or through the changes in eddy velocities over the length of the droplet. For both cases, however, the external stress appearing in Eq. (32) can be expressed in terms of the kinetic energy differences around the droplet. From Eq. (32), the former yields

$$We_{cr)1} \equiv \rho_c v_r^2)_{\max} d_{\max} / 2\sigma \geq 1.0 \tag{34}$$

where the latter gives

$$We_{cr)2} \equiv \rho_c \overline{v_c'^2} d_{\max} / 2\sigma \geq 1.0 \tag{35}$$

The mean-square spatial fluctuating velocity term, $\overline{v_c'^2}$ describes the turbulent pressure forces of eddies of size d_{max} and is defined as the average of the square of the differences in velocity over a distance equal to the fluid particle diameter. $v_{r)max}$ is that limiting local relative velocity at which a fluid will flow around a particle suspended in it. The subscript c identifies the continuous phase.

Considering the simplest case of turbulence, namely, an isotropic homogeneous turbulence, the main contribution to the kinetic energy, $\overline{v_c'^2}$, is made by the fluctuations in the region of wavelengths where the Kolmogoroff energy distribution is valid. In this region, the local turbulence pattern is solely determined by the energy dissipation per unit mass, ε. The mean square velocity difference between two points of length d_{max} is given by Batchelor [8] as follows:

$$\overline{v_c'^2} \sim (\varepsilon d_{max})^{2/3} \tag{36}$$

Where $v_{r)max}$ is given by Levich [9] as

$$v_{r)max} \sim [\varepsilon d_{max}(\rho_d / \rho_c)]^{2/3}(|\Delta\rho|/\rho_d)^{1/2} \tag{37}$$

where the subscript d identifies the dispersed phase.

When Eqs. (36) and (37) are inserted into their respective places in Eqs. (34) and (35), and the resulting equations are solved for d_{max}, the following equations can be obtained for the maximum particle size:

$$d_{max} = (\sigma We_{cr)2} / k_2 \rho_c)^{3/5} \varepsilon^{-2/5} \tag{38}$$

and

$$d_{max} = (\sigma We_{cr)1} / k_1 \rho_c)^{3/5} \varepsilon^{-2/5} (\rho_c / \rho_d)^{2/5} (\Delta\rho / \rho_d)^{-3/5} \tag{39}$$

where k_1 and k_2 are proportionality coefficients. These numerical coefficients probably have no great significance. They are set forth here only in order to stress the absence of large numerical coefficients in these formulas. Both k_1 and k_2 are the same order of magnitude of one.

Equations (38) and (39) have been used in literature to determine the maximum stable particle size in liquid-liquid, liquid-gas and gas-liquid dispersions irrespective of their differences in terms of fluid properties. The differences can be explained by comparing the expressions for fluid velocity relative to the particle, $v_{r)max}$, with the change in velocity of turbulence eddies over a distance equal to the dimension d_{max} of the particle $\overline{v_c'^2}$.

A comparison of Eqs. (36) and (37) shows, that with $\rho_c \geq \rho_d$, $v_{r)max} << \overline{v_c'^2}$. In these cases, large-scale eddies of continuous phase completely entrain the fluid particle together with portions of fluid adhering to it, and transfer both as a single unit. The

entrainment of particles by turbulence eddies is complete. Therefore, the second Weber number criterion, $We_{cr)2,}$ which is based on $\overline{v_c'^2}$, mechanistically describes the fragmentation of drops and bubbles in a turbulent liquid flow for $\rho_c \geq \rho_d$. However, the disintegration of a drop in a turbulent gas stream occurs in a somewhat different manner. In this case, the entrainment of particles by turbulence eddies cannot be complete. The smaller-scale fluid motions are unable to entrain the particle, and in relation to them, the particle acts as a motionless solid body. The fluid participating in these small-scale motions flows over the surface of the particle. In this case, inertial effects used in derivation of Eq. (37) play an important role in the mechanism of the drop's motion. In the case of $\rho_c >> \rho_{d,}$ from Eqs. (36) and (37), it is evident that

$$v_{r)\max} / \overline{v_c'^2} = (\rho_d / \rho_c)^{1/3} \tag{40}$$

which indicates that $v^2_{r)\max} >> \overline{v_c'^2}$. Therefore, the disruptive forces based on $v_{r)max.}$ become much larger than the disruptive forces generated by changes in eddies. In view of this brief discussion, the first critical Weber number criterion, $We_{cr)1}$, describes the disintegration of drops in a turbulent gas stream.

Several fluid particle break-up mechanisms have been discussed and applicability of each mechanism has been clarified. However, as it is evident from Eqs. (38) and (39), the key parameter in determining local $d_{max.}$ is the turbulent energy dissipation rate, ε. Local turbulence and dissipation models for two-phase flow have not been established. Therefore, it is a challenge to develop a model for local correlation. First a one-dimensional model will be developed, and it is expected that in the turbulent core region this model can be used as a local correlation, since the turbulent characteristics may be approximated as uniform. However, in the wall shear layer, both turbulence and viscous effects become important. In this region, shear induced turbulence should be investigated.

3.5.2 Break-up Frequency: g(ϑ'). Several phenomenological models have been developed to predict the break-up frequency in liquid-liquid dispersions [7,10-12]. These models are heavily influenced by flow conditions and can be classified according to the hydrodynamic flow regime as follows:

BREAK-UP FREQUENCY MODELS

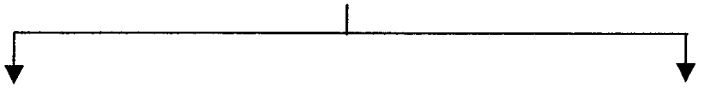

Turbulent Flow Models

Laminar Flow Model [7]

- Molecular Decomposition Analogy Model [7]
- Dispersion Hydrodynamics Break-up Models [10-12]
- Critical Velocity Break-up Frequency Model [7]
- Drop Oscillation Break-up Frequency Model [11]

As indicated above, models should be chosen with regard to the flow conditions. As an example, for dispersions in turbulent flow, the kinetic energy transferred by the eddies plays a dominant role in the break-up process. The imbalance between the kinetic energy and the surface energy is used to define the break-up frequency. In laminar flow or transition regimes, the imbalance would be between the shear forces and the surface forces on the particle, and many expressions for the break-up frequency in such environments can be found in the literature. The following model for break-up frequency in turbulent flow based on dispersion hydrodynamics is given here as an example. It is dependent on the physical properties, particle size, and energy dissipation rate per unit mass as shown below:

$$g(\vartheta') = c_1(\varepsilon/\vartheta'^2)^{1/3}\exp[-c_2\sigma/\rho_d(\varepsilon^{2/3}\vartheta'^{5/3})] \qquad (41)$$

where the constants c_1 and c_2 are adjustable to be determined from experiments according to the flow environment. It is to be noted that this expression is very similar to the one that can be derived using the molecular decomposition model except in the latter, the continuous phase density was used instead of the dispersed phase density.

In the above derivation, the break-up rate was taken to be a function of the dispersed phase density. However, in gas-liquid systems, break-up is primarily governed by the density of the continuous liquid phase. The lack of an independent measurement of the break-up rate, as well as the use of several adjustable constants appearing in Eq. (41), prevent a direct use of Eq. (41) in bubbly flow systems. For example, comparisons of experimental data, for bubble break-up frequency with Eq.

(41), which was originally derived for drop break-up frequency, resulted in poor agreement [14].

In the course of future research, an effort will be placed on identifying those liquid-liquid dispersion models, which have features that would also be applicable to gas-liquid dispersions, and those models which are best suited for use in bubbly two-phase flow systems. In this development, the bubble break-up frequency will be determined by examining the interaction rate of bubbles with turbulent eddies.

3.5.3 Number of Daughter Particle Production: n(ϑ'). This parameter determines the average number of daughter particles produced by break-up of a parent particle of volume ϑ'. Various experimental data indicate that 2 to 7 particles are produced in each break-up of liquid-liquid dispersions [l l].

In the area of bubble break-up process, the break-up process was considered to occur by break-up of a bubble into two daughter bubbles in random size. However, recently Prince et al. [15] and others have noted that bubble break-up is often accompanied by the production of two primary bubbles and a number of smaller fragments. Incorporation of this effect instead of binary break-up is expected to significantly alter the number of smaller bubbles and the interfacial area concentration predicted by the proposed transport equations.

3.5.4 Daughter Particle Distribution: $\beta(\vartheta, \vartheta')$. This parameter is introduced due to the possible random production of non-equal daughter particles upon break-up. The simplest representation of daughter droplets volume density is to assume that two equal volume daughter particles are produced upon break-up. In relativity, a large number of non-equal daughter particles are produced upon break-up in a random fashion. It is reasonable to assume that these particles are distributed normally [10] and therefore

$$\beta(\vartheta', \vartheta) = (1/\sqrt{2\pi}\delta)\exp[-(\vartheta - \bar{\vartheta})^2 / 2\delta^2] \qquad (42)$$

This relation is based on the variance δ^2 which is chosen in such a manner that 99.6 % of the particles density lies within the volume range 0 to ϑ'. ϑ' is the volume of the breaking parent drop and $\bar{\vartheta}$ is the mean volume of the daughter droplets.

The distribution given by Eq. (42) is only one example of several distribution functions that are available. It is important to note that $\beta(\vartheta',\vartheta)$ can be expressed in terms of any other suitable distribution function.

3.6 Coalescence Parameters

3.6.1 Description of Coalescence Processes. While the maximum particle size was used as a criterion for the break-up process (where the particle size is considered stable when its size is below the maximum value), the minimum particle size can be used as a criterion for the initiation of the coalescence process (which is enhanced by the presence of small particles). It is assumed that there is a minimum stable particle size below which a pair of particles will coalesce upon colliding, and the ultimate coalescence process can be described in three consecutive stages. First, particles collide, and upon the collision of two particles, the surfaces of the colliding particles flatten against each other; trapping a thin film between them under the action of the continuous phase. This film then drains over a period of time from an initial thickness of h to a critical thickness, h_c, under the action of the film hydrodynamics. The hydrodynamics of the film depend on whether the film surface is mobile or immobile, and the mobility, in turn, depends on whether the continuous phase is pure or a solution. Finally, once the film reaches its critical thickness, it ruptures due to film instability resulting in coalescence.

From the first step, it is seen that the coalescence rate is intimately connected to the particle collision frequency. In order to determine whether a given collision will result in coalescence, it is necessary to determine the collision efficiency. Two fluid particles will coalesce, provided they remain in contact for a period of time sufficient for the film between them to thin to the critical value necessary for rupture.

Considering a bubbly two-phase flow, collision may occur due to a variety of mechanisms summarized below:

COLLISION PROCESSES

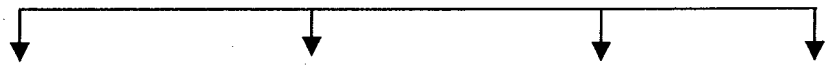

Turbulent Fluctuations	Size Dependent Rise Velocity Differences	Wake Entrainment	Shear Layer Induced Velocity Differences

From the above, it is clear that collisions may result from the random motion of bubbles due to turbulence. In addition, bubbles of different sizes will have different rise velocities relative to continuous liquid phase, which may lead to collision. Flow field generated at the wake of large Taylor bubbles entrains small bubbles into the Taylor bubble, resulting in a collision of small bubbles with a large bubble. Finally, bubbles located in a region of relatively high liquid velocity may collide with bubbles in a slower section of the velocity field. The first mechanism is a random process, which largely depends on the fluctuating bubble motion and the inter-bubble distance. However, the latter three mechanisms highly depend on the particle size distribution and internal flow structure.

The coalescence process described above indicates that a clear understanding of the coalescence process depends on accurate knowledge of the minimum particle size, collision frequency and coalescence efficiency. These parameters are briefly discussed below.

3.6.2 Minimum Fluid Particle Size. As described in Section 3.1, it is assumed that there is a minimum stable particle size below, which a pair of particles will coalesce upon colliding. The equation that describes the minimum diameter for the absence of coalescence (i.e., the diameter below which coalescence will occur) can be obtained in the same way as the break-up equation. The adhesion force acts to hold the colliding fluid particles together. The energy of adhesion of two particles of equal diameter is given by Shinnar and Church [16] and Shinnar [17] as:

$$AE = C_1 d \tag{43}$$

where C_1 is a parameter dependent upon the critical rupture thickness, h_c.

A coalescence criterion can be developed by determining the critical value of the kinetic energy, which is given by $C_2\rho_c(\varepsilon d)^{2/3}$, to the adhesion energy. That is,

$$\frac{KE}{AE} = C_2\rho_c(\varepsilon d_{\min})^{2/3}/C_1 d_{\min} = C_2\rho_c\varepsilon^{2/3}d_{\min}^{8/3}/C_1 = const. \tag{44}$$

or

$$d_{\min} = C_3/\rho_c^{3/8}\varepsilon^{1/4} \tag{45}$$

Thomas [18] developed a coalescence criterion by performing a force balance similar to that presented above. However, the adhesion force was replaced by the surface tension force acting at the time of rupture. Thomas predicted the coalescence to occur if the drop diameter is less than the minimum diameter defined by

$$d_{\min} \cong 2.4[\sigma^2 h_c^2 / \mu_c \rho_c \varepsilon]^{1/4} \tag{46}$$

Equations (45) and (46) have been employed extensively in correlations for the minimum and mean diameters of dispersed-phase drops in mechanically-agitated liquid-liquid systems [13,19-21]. The development of phenomenological models for minimum bubble size in gas-liquid dispersions, however, has received comparatively little attention, even though such dispersed systems are of significant interest to bubbly two-phase flow hydrodynamics and heat transfer. This problem will be addressed for bubbly two-phase flow in pipes.

3.6.3 Collision Frequency: h(ϑ,ϑ′). Based on the type of flow as described in the section of Coalescence Parameters, a variety of definitions for the collision frequency between two particles of diameters d and d′ in liquid-liquid dispersions were proposed [22]. The suggested expression for the velocity averaged collision frequency in a uniform shear flow can be expressed as:

$$h(d,d') = 1.366(d+d')^3(\partial v/\partial r) \tag{47}$$

where $(\partial v/\partial r)$ is the velocity gradient perpendicular to the direction of liquid particle motion.

For turbulent flow, the velocity gradient can be replaced by

$$\partial v/\partial r \cong (\varepsilon/\nu)^{1/2} \tag{48}$$

Therefore, the collision frequency becomes

$$h(d,d') = 1.366(d+d')^3(\varepsilon/\nu)^{1/2} \tag{49}$$

It should be noted that the drop size relative to the turbulent eddy size will affect the collision frequency. When the drops are small compared to the turbulent eddies, the drop velocity will be significantly affected by the eddies. When the drop density is equal to the density of the continuous phase, the drop velocity will be very close to the velocity of the continuous phase flow field. Under these conditions, the collision

frequency will be determined by local turbulent flow characteristics. In this case, the collision frequency is given by

$$h(d,d') = 0.618(d+d')^3(e/\nu)^{1/2} \tag{50}$$

The only difference between Eqs. (49) and (50) is the constant coefficient.

When the drops are large compared to the turbulent eddies, the drop will be exposed to the eddies' stresses from all directions. This results in a random drop motion. This randomness in drop motion led researchers to consider the analogy between the collision of drops and the collision of molecules, as in the kinetic theory of gases. Based on this analogy, Rietema [23] proposed the collision frequency in terms of the average turbulent velocity fluctuations.

In addition to the collision frequency's dependence on particle size, the density of both dispersed and continuous phases play an important role in shaping the collision frequency. When the drop density is significantly different than the density of the continuous phase, the drops move with different velocities based on their sizes. Therefore, the relative velocity between drops will be the primary cause of collision. This is known as the acceleration mechanism or size dependent rise velocity difference mechanism for collisions. This mechanism plays an important role whenever there is a significant difference in dispersed and continuous phase densities as in the case of bubbly flow.

Many correlations can be found in the literature for small and large sizes with equal or non-equal phase distributions. Recently, Prince and Blanch [14] in their predictive model for the coalescence rate in gas-liquid dispersions considered the cumulative contribution of three collision mechanisms due to turbulence, buoyancy and laminar shear.

In future research work, the major coalescence mechanisms will be examined. Contribution of each mechanism to the overall collision process will be evaluated to arrive at predicting the coalescence frequency.

3.6.4 Coalescence Efficiency: $\lambda(\vartheta,\vartheta')$. In order to determine what fraction of fluid particle collision leads to coalescence events, it is necessary to define a coalescence or collision efficiency. The coalescence efficiency $\lambda(\vartheta,\vartheta')$ may be defined as the fraction

of collisions between fluid particles of volumes ϑ and ϑ' that result in coalescence. This efficiency will be a function of the average contact time between bubbles and the average time required for particles to coalesce (the average coalescence time). The average coalescence time is the time required for the continuous fluid film trapped between the two colliding particles to thin to a critical value so that rupture, and consequently coalescence, can occur.

An expression for the efficiency is given by Coulaloglu and Tavlarrides [10]:

$$\lambda(d,d') = \exp(-t_{coa}(d,d')/t_{con}(d,d')) \tag{51}$$

where $t_{coa}(d, d')$ is the average coalescence time of particles of diameters d and d′, while $t_{con}(d, d')$ is the contact time for the particles.

Different models have been used to determine the coalescence efficiency in turbulent and laminar flow regimes for liquid-liquid dispersions. These models are based on the biomolecular gas reaction analogy, sufficiency of the time of contact, impact of colliding particles as well as combined approaches for collision efficiency [22]. An expression for the coalescence efficiency in gas-liquid dispersions was proposed by Prince and Blanch [14].

In future research, these models will be evaluated. A model that combines the deformable particle approach, which considers the existence of an attracting force between two particles, and the impact of the colliding particle approach will be developed for bubbly flow coalescence efficiency.

3.7 Summary of Modeling Efforts Related to Fluid Particle Interactions

A series of phenomenological analytical studies have been undertaken to mechanistically model:

1. The droplet break-up and its distribution in an annular flow core [24,25],
2. The bubble break-up in a high speed horizontal bubbly flow [26],
3. The fluid particle break-up in a stagnant fluid media, i.e., break-up of freely rising bubbles in a liquid and freely rising or falling droplets in a gas or liquid [27,28],
4. The non-linear wave growth leading to break-up of large bubbles [29].

In what follows, we shall briefly summarize significant achievements of each study.

3.7.1 Droplet Size Modeling in Annular Flow [25]

Two Weber number criteria, one based on the classical Kolmogorov theory and the other on the dynamics thrust, which appears because of inertial effects along a fluid particle, were discussed and compared to each other. It was concluded that when $\rho_d \leq \rho_c$, the entrainment of fluid particles by turbulence may be complete, and that Weber number criterion based on the Kolmogoroff's theory mechanistically describes the fragmentation of drops and bubbles in a turbulent liquid flow. However, in the case of droplets in a gas stream with $\rho_d >> \rho_c$, the entrainment of droplets by turbulent eddies cannot be complete, and inertial effects play a major role instead of eddies in the mechanism of disintegration.

Based on the competing stresses between stabilizing surface forces and disruptive dynamic thrust, a theoretical model was developed to describe the break-up of entrained droplets in the gas core of an annular flow. The experimental data of the maximum droplet size were correlated in terms of Re_g, Re_f, We_m, and the physical property groups of $(\rho_f/\rho_g), (\mu_f/\mu_g)$ and $N\mu$ as follows:

$$d^*_{max} = 2.61 C_w^{-4/15} We_m^{=3/5} (Re_g^4/Re_f)^{1/15} [(\rho_g/\rho_f)(\mu_g/\mu_f)]^{4/15} \equiv 2.61K \qquad (52)$$

The dimensionless groups appearing in the above equation are defined as follows:

- Dimensionless maximum drop size: $d^*_{max} \equiv d_{max}/d_h$
- Gas Reynolds number: $Re_g \equiv \rho_g < j_g > d_h/\mu_g$
- Liquid Reynolds number: $Re_f \equiv \rho_f < j_f > d_h/\mu_f$
- Modified Weber number: $We_m \equiv \rho_g d_h < j_g >^2 /\sigma$
- Viscosity number: $N\mu \equiv \mu_f /[\rho_f \sigma(\sigma/g\Delta\rho)^{1/2}]^{1/2}$

and

- $C_w = 1/35.34\, N\mu^{4/5}$ *for* $N\mu \leq 1/15$
- $C_w = 0.25$ *for* $N\mu > 1/15$

Effects of each group in determining the maximum stable droplet size were discussed in the context of available experimental data. It was concluded that the functional dependence of d_{max} on these groups could be experimentally verified. Figures 1 through 3 show comparisons between experimental and predicted maximum stable droplet size. A good agreement between experimental data and Eq. (52) reveals that the maximum stable droplet size in annular flow is controlled by the action .of forces resulting from pressure fluctuations of the turbulent flow of the gas around the droplet.

Having obtained a relation between d^*_{max} and We_m, Re_g, Re_f and fluid property groups (μ_f / μ_g) and (ρ_f / ρ_g) as shown in Eq. (52), it was evident that the droplet size distribution could be correlated in terms of the similar dimensionless groups. The upper limit log-normal distribution function was applied to the data as shown in Fig. 4. The distribution function for all data was found to be given by

$$\frac{d\vartheta_d}{d\xi} = \frac{\eta}{\sqrt{\pi}} \exp(-\eta^2 \xi^2) \tag{53}$$

where ϑ_d is the volume fraction of droplets having diameter less than the droplet diameter, d, η is the size distribution parameter, and ξ is the dimensionless function of d defined by

$$\xi \equiv \ell n(ad/(d_{max} - d)) \tag{54}$$

Available experimental data indicated that a = 193 and η=0.75. Based on these parameters, predictive equations were developed for the most representative mean droplet sizes, the volume median diameter and Sauter mean diameter. As illustrated in Figs. 5 and 6, the mean sizes were found to agree reasonably well with those measured mean sizes. This indicates that the principal mechanisms involved in the droplet break-up process in a turbulent gas stream were properly accounted for in the development of the theoretical model.

The mechanistic model summarized in this work was based on the break-up of droplets to determine the maximum particle size by turbulent fluctuations. However, in a very high speed gas flow it is possible that the entrained droplet is exposed to velocity gas core flow and goes through subsequent disintegration. In a fluid particulate flow, break-up and coalescence occur simultaneously. Therefore, it is necessary to have both

break-up and coalescence criteria for a meaningful size distribution. In this research program, these two criteria will be utilized for a complete size distribution.

3.7.2 Bubble Size and Interfacial Area Modeling in Horizontal Bubbly Flow [26]

A generalized break-up mechanism was expressed as a balance between external stresses caused by the shear in continuous liquid phase, the dynamic pressure forces and the turbulent fluctuations of the velocity and pressure and the stabilizing surface stresses by surface tension. It was concluded that the maximum stable size in a high-speed horizontal flow is mainly controlled by the action of stresses resulting from pressure fluctuations acting across a bubble diameter. A detailed model of the maximum bubble size and the Sauter mean diameter was developed based on the balance between the surface stresses and the dynamic pressure variations induced by the turbulent fluctuations in the liquid phase. The Sauter mean diameter of bubbles was found to be given by

$$< d_{sm} >= 1.06\left[\frac{\sigma}{\rho_f^{1/3}}\right]^{1/3} [\alpha(1-\alpha)d_h^2]^{2/9} /[< j > (-dp/dz)]^{2/9} \qquad (55)$$

where $<d_{sm}>$ is the area-averaged Sauter mean diameter, and (dP/dz) is the axial pressure gradient. $<d_{sm}>$ predictions from Eq. (55) are compared in Fig. 7 with the measured values of Sauter mean diameters. From these figures, a good agreement between the predicted and experimental values can be observed. Irrespective of good comparisons, however, limitations of the experimental work and theoretical modeling have to be taken into account when applying Eq. (55):

a) The pipe diameter dependence of the mean bubble size seems relatively large. Presently an investigation has been underway to carry out experimentation in a 25.4 mm ID pipe with the same bubble generation mechanism. Based on very few data, the bubble size is somewhat smaller in the present set-up. However, the number of data does not warrant a conclusion yet.

b) Only one bubble size generation mechanism was used during the course of experimentation. Therefore, effects of initial bubble size were not systematically investigated. However, fundamental studies regarding the initial bubble size effects were undertaken in horizontal bubbly two-phase flow configurations by Sevik and Park

[30] and Sleicher [31]. Both indicated that irrespective of initial bubble size the maximum fluid particle size was uniquely defined as long as the pipe was long enough. The residence time of a bubble was in all cases very much longer than the following characteristic times: natural period of bubble vibration, mean time of diffusion of bubble from core toward the top of tube wall and Lagrangian time scale. Then intuition based on the above reasoning suggested that a pipe length of 13 meters was sufficient for bubble interactions resulting in a relatively uniform bubble size distribution due to coalescence and break-up processes. Recently, a series of photographic studies was undertaken. It was observed that the majority of bubble break-up was complete in about 65 - 75 cm downstream of the bubble generation. The importance of the effects of initial bubble size on flow modeling has been emphasized by Zun [32], Serizawa and Kataoka [33], Lahey [34] and Liu [35]. However, all these investigations were concerned with vertical flow configurations, where the bubbly flow-pattern is limited to relatively much lower velocities than those experienced in horizontal flow situations.

c) The simplest case, namely, an isotropic homogenous turbulence was considered in developing the bubble break-up model. For this case, Kolmogoroff's Universal Equilibrium theory implies that energy transfer through the spectrum is independent of viscosity resulting in the mean fluctuating velocity as follows:

$$\overline{v_c'^2} = 2(\varepsilon d_{max})^{2/3} \tag{56}$$

This case can be justified if the Reynolds number of the flow is sufficiently high. However, derivation leading to bubble size cannot be applicable for highly viscous liquids. In this case, the break-up should be based on Taylor's break-up mechanism.

Assuming that the bubbles are spherical, the area-averaged void fraction and Sauter mean diameter have been used to calculate the interfacial area concentration as follows:

$$\langle a_i \rangle = 6 \langle \alpha \rangle / \langle d_{sm} \rangle \tag{57}$$

Equations (55) to (57) were used to calculate $\langle a_i \rangle$. Thus,

$$\langle a_i \rangle = \frac{6 < \alpha > [(< j_f > + < j_g >)(-dp/dz)]^{2/9}}{1.06(\sigma/\rho_f^{1/3})^{1/3}[< \alpha > (1 - < \alpha >) d_h^2]} \tag{58}$$

Predictions for the average interfacial area concentration are compared with the present experimental data in Fig. 8 for each value of the superficial liquid velocity.

From this figure it is evident that the newly developed interfacial area concentration expression predicts the experimentally measured values within a small mean deviation. Surprisingly, good estimates of bubble sizes based on competing surface forces and dynamic pressure fluctuations are a good indication of the mean bubble size and interfacial area occurring in practice.

A preliminary study has been initiated to mechanistically model the local interfacial area concentration. As it is indicated above, the model for the averaged interfacial area was based upon a balance between the dynamic stresses induced by turbulent fluctuations in the continuous phase and the surface stress. Furthermore, in this model, the dynamic stresses were evaluated through the turbulent energy dissipation, which, in turn, was approximately estimated from the two-phase flow kinetic energy equation.

In order to use the same model for modeling the local interfacial area concentration, a_i, information on the local turbulence structure in the liquid phase is needed. Unfortunately, this information has not been readily available at this time. However, Eq. (58) has been used with locally measured void fraction, a, and superficial velocities, j_f and j_g, rather than average values as follows:

$$a_i = \frac{6\alpha[(j_f + j_g)(-dp/dz)]^{2/9}}{1.06(\sigma/\rho_f^{1/3})[\alpha(1-\alpha)d_h^2]^{2/9}} \tag{59}$$

Local interfacial area concentration as predicted by Eq. (59) is presented together with experimentally measured values in Fig. 9. It is evident from this comparison that the local interfacial area concentration follows very closely in the core of the pipe. However, discrepancies occur in the vicinity of the pipe wall. A uniform bubble size distribution that was observed in the core except near the wall, indicates that the bubble size is primarily determined by the local turbulence in the bulk fluid. However, in the vicinity of the pipe wall where a steep velocity gradient exits, it is expected that break-up must be governed by the Taylor break-up mechanism, which, as shown by Levich [9], usually yields smaller bubbles.

From the above description, it can be concluded that the core break-up which is a dominant break-up mechanism will determine the interfacial area concentration in the

core. However, Taylor break-up mechanism becomes dominant around the pipe perimeter.

A theoretical work along the above lines has been underway at the University of Wisconsin-Milwaukee. However, the theoretical work should be checked against the experimental local turbulent structure measurements, which have not been available. The present research program will enable us to measure local turbulent structure in the continuous phase. Hopefully, the experimentally measured local turbulence properties will lead to the local mechanistic modeling of bubble interactions and eventually to a better understanding of these phenomena and predictive methods.

3.7.3 Fluid Particle Break-up Modeling [27]

A simple mechanistic model was developed based on the combination of Kelvin-Helmholtz and Raleigh-Taylor instability theories to describe the break-up of drops and bubbles rising or falling freely in a stagnant media. Referring to a rising cap bubble illustrated in Fig. 10, the break-up was modeled to occur if the growth rate of interfacial waves on the leading front is faster than the rate at which waves propagate around the interface to the side of the particle. The generalized break-up criterion was expressed as

$$2.25\left[\frac{2\pi}{\theta_w}\right]^2\left[\frac{\rho^*}{1+\rho}\right]\sin^2\left[\frac{\theta_w}{2}\right]+\frac{1}{We}\left[\left[\frac{2\pi}{\theta_w}\right]c_e d_e^{*2}-\left[\frac{1}{c_e}\right]\left[\frac{2\pi}{\theta_w}\right]^3\right]$$
$$\geq 1.09\left[\frac{2+3\rho^*}{1+\rho^*}\right]^{2.27}\cdot(1+N\mu_c)^{0.36}\left\{\ell n\left[\frac{\left|\tan\left(\frac{\theta_w}{2}\right)\right|}{\tan\left(\frac{\theta_w}{2}\right)}\right]\right\}^{-2} \qquad (60)$$

Where d_e^*, We, ρ^* and $N\mu_c$, are the dimensionless particle equivalent diameter, Weber number, density ratio, and continuous phase viscosity number, respectively. They are defined as

$$d_e^* \equiv \left[\frac{g|\Delta\rho|d_e^2}{\sigma}\right]^{1/2} \quad ; \quad We=\frac{\rho_d d_e v_c^2}{\sigma}$$
$$\rho^* \equiv \frac{\rho_d \coth(k_{\min}h_d)}{\rho_c} \quad ; \quad N\mu_c \equiv \left[\frac{\mu_c^2}{\rho_c(\sigma^3/g\Delta\rho)^{1/2}}\right]^{1/2} \qquad (61)$$

where v_c is the relative velocity of the continuous phase with respect to the dispersed phase, and k_{min}, is the minimum unstable wave number.

Equation (60) was used to predict the maximum fluid particle diameter at break-up. The break-up diameter suggested by this equation is general in the sense that it is applicable for gas-liquid bubbly systems as well as liquid-liquid and liquid-gas droplet systems for low viscosity fluids. The results were extended to predict the maximum droplet size in a high-velocity gas field.

Predicted values of the maximum particle size were compared with experimental data in Fig. 11. An average deviation of ± 13.94 % between predicted and experimental values can be observed from the figure. Considering the various simplifications and idealizations made in the analysis leading to Eq. (60), the agreement is favorably good, and much better than that obtained from the Rayleigh-Taylor instability analysis.

From practical applications, the general break-up criterion was simplified for four separate cases as follows:

- freely falling drops in a gas,
- droplets in a high-velocity gas stream,
- freely rising bubbles,
- freely falling or rising drops in liquids.

Simple correlations were developed for each case. With the proper form of the terminal velocity it was demonstrated that the dimensionless break-up diameter could be expressed in terms of ρ^*, $N\mu_c$, and (μ_d / μ_c)

The theoretical model developed in this study was approximate in nature, including such simplifications as the treatment of growth of three-dimensional disturbances on curved interfaces by means of two-dimensional, small-amplitude waves on a flat interface. Despite these approximations, the agreement with experimental results indicate that the principal physical mechanisms involved were properly accounted for by the model.

3.7.4 Nonlinear Wave Growth and Break-up Process of Large Cap Bubbles [29]

The major objective of this study is to develop a better understanding of the interfacial wave phenomenon and how it contributes to particle break-up. Both the wave growth and the wave propagation were studied in detail for air bubbles rising in an extended, stagnant liquid column. The detailed observation on the break-up process (Fig. 12) and the wave growth of breaking waves (Fig. 13) were measured. All air bubbles analyzed exceeded the critical Weber number for bubbles in water, and most exceeded the maximum bubble diameter measured in previous studies. In addition, other characteristic effects resulting from the wave behavior were investigated.

Examination of the interfacial wave height growth for all bubbles analyzed resulted in a relatively constant initial exponential growth rate of

$$kc_i = 25.5/\sec \tag{62}$$

The good exponential fit to the data indicates that the initial stage of growth is dominated by the Kelvin-Helmholtz instability model. This result is comparable to that previously measured by Henriksen and Ostergaard (1974).

A very well defined exponential growth rate of 13.7/sec. for the larger wave heights ($\eta > \lambda_T/2$) was determined. From this result, the linear theory describes the growth rate well beyond the range of heights allowed for linear theory. It can be presumed that the nonlinearities in wave growth do not significantly alter the growth rate dependence for air-water systems.

As it is seen in Fig. 13, a transitional wave height measured to be 9.12 mm, or 0.53 λ_T, was encountered when a plot to measure the linear acceleration was produced.

$$for\ \eta > 9.12mm = 0.53\lambda_T,\quad \frac{\delta_\eta^2}{\delta t^2} = 2.51m/s^2 = 0.26g \tag{63}$$

The second state of growth had an acceleration of 0.26 g which agrees with the results obtained by Emmons et al. (1959) for the Rayleigh-Taylor instability. Additionally, after a wave height of 15 mm was reached, corresponding to half of the most dangerous wavelength, a spherical bulb of liquid is produced that matches that observed by Emmons, and strongly suggests that the second growth state is dominated by the Rayleigh-Taylor instability. The existence of the bulb was always linked to bubble splitting.

Calculations of the wavelength from a linearized perturbation of the potential flow theory equations produced wavelengths comparable to the Taylor wavelength, but smaller than those measured. Measured wavelengths matched the most dangerous wavelength, A, produced by maximizing the growth rate with respect to the wave number. The wavelength produced by two adjacent waves also agreed with this result. The relative velocities of the fluids were found to be minor contributors to the wavelength calculation, which does not justify the need to incorporate them as in the Kelvin-Helmholtz instability theory. The Rayleigh-Taylor theory is sufficient for the system analyzed to adequately predict the phenomenon.

Interfacial wave propagation followed potential flow theory very well. The growth rate agreed well with the direct calculation of the average rise velocity and the average radius of curvature.

$$\tan\frac{\theta}{2} = \tan\frac{\theta_0}{2} e^{(10.2/s)t} \tag{64}$$

An angular acceleration of 21.0 rad/s^2 was also correlated, but has no theoretical basis. The location of the initial disturbance, important in determining the propagation time for a wave, suggests that the bubble nose is an antinode for wave development.

$$\theta_0 = 8.7^\circ \cong \lambda_{cr} 2r \tag{65}$$

This contradicts the suggestion that the bubble nose is a node. The maximum initial location measured with wave propagation of 5.3 mm, 0.18 λ_{cr}, more closely follows this suggestion, but results in a propagation time 25 % larger than that calculated using the average initial wave location.

Other behavior observed during wave development is the existence of a spherical bulb of liquid at the base of the wave once the wave height reached 1/2 λ_{cr}, This bulb, observed in the Rayleigh-Taylor instability model, averaged 1.48 cm, equating well with the diameter determined by the critical Weber number criterion,

$$d_{bulb} = 1.48\,cm = d_{\max} We \tag{66}$$

and, more importantly, 1/2λ_{cr} to validate the notion that particles of diameter λ_{cr} will cause break-up of the larger particle.

Broadening of the bubble diameter during wave growth suggests that wave development for slug bubbles will be restricted due to the physical confines of the walls.

The most significant results from this analysis include the following:

- potential flow theory is valid for interfacial wave propagation,
- linear potential flow theory describes the initial wave height growth, but it is uncertain which instability mechanism is more adequate,
- later wave growth ($\eta > 1/2\lambda_T$) closely follows Rayleigh-Taylor instability theory despite being outside of the linear theory range,
- an initial wave height growth rate of 25.5/s was consistent for all bubble sizes,
- measured wavelengths agree well with the most dangerous wavelength, $1/2\ \lambda_{cr}$,
- the bubble nose should be considered an antinode for better accuracy,
- particles of minimum diameter $1/2\lambda_{cr}$, are sufficient to cause bubble splitting,
- initial wave heights were below 0.7 mm and could not be measured accurately.

3.8 Formulation of Interfacial Area Transport Equation

3.8.1 General Functional Dependence of Various Source and Sink Terms

As derived from the statistical distribution transport equation, the local interfacial area transport equation is given by Eq. (13). For the purpose of completeness, it is duplicated here as follows:

$$\frac{\partial a_i}{\partial t} + \nabla \cdot a_i \vec{v}_i = \sum_{j=1}^{4} \phi_j + \phi_{ph} \tag{13}$$

For simplicity, it is also possible to combine two terms related to the break-up process. Thus the break-up source term is defined as

$$\phi_{dis} \equiv \phi_1 + \phi_2 \geq 0 \tag{67}$$

whereas the coalescence sink term is defined by

$$\phi_{co} \equiv -(\phi_3 + \phi_4) \geq 0 \tag{68}$$

Hence, the interfacial area transport equation becomes

$$\frac{\partial a_i}{\partial t} + \nabla \cdot a_i \vec{v}_i = \phi_{dis} - \phi_{co} + \phi_{ph} \tag{69}$$

The various local mechanisms affecting the break-up and coalescence terms have been discussed in Section 3. Here we study the general functional dependence of these two terms. The fluid particle disintegration occurs mainly due to the turbulent fluctuation and interfacial stability. Therefore, locally it should depend on the particle size, r_d, turbulent intensity, $\overline{v_c'^2}$, and local relative velocity, v_r. Hence

$$\phi_{dis} = \phi_{dis}(\overline{v_c'^2}, r_d, We) \tag{70}$$

where the Weber number is given by

$$We \equiv \frac{2\rho_c r_d v_r^2}{\sigma} \tag{71}$$

which scales the interfacial instability.

The coalescence process depends on the random collisions and the systematic wake entrainment. The collision is a strong function of the inter-particle distance and the amplitude of the fluctuating particle velocity. The latter depends on the continuous phase turbulent fluctuations. The wake flow structure depends on the particle Reynolds number, Re_d, and the particle size. The coalescence probability after a collision depends on the particle sizes and fluctuating velocity components. Thus

$$\phi_{co} = \phi_{co}(\alpha_d, r_d \overline{v_c'^2}, \mathrm{Re}_d) \tag{72}$$

The turbulence intensity in dispersed flow may be related to the continuous phase Reynolds number, Re_c, and a distance from a wall.

3.8.2 One-Dimensional Formulation and Relation to Experimental Measurements

The simplest form of the interfacial area transport equation can be obtained by applying the cross-sectional area averaging and reducing it to a one-dimensional form. This form of the interfacial area transport equation may have the most useful and practical applications in the existing one-dimensional two-fluid model. It can replace the traditional flow regime maps and regime transition criteria. The changes in the two-phase flow structure are predicted mechanistically by introducing the interfacial area transport equation. The effects of the boundary conditions and flow development are efficiently modeled by this transport equation. Such a capability does not exist in the

state-of-the arts. Thus a successful development of the interfacial area transport equation can make a quantum improvement in the two-fluid model formulation.

By applying the cross-sectional area averaging, the one-dimensional area transport equation becomes

$$\frac{\partial < a_i >}{\partial t} + \frac{\partial}{\partial z} < a_i > \bar{v}_{iz} = < \phi_{dis} > + < \phi_{co} > + < \phi_{ph} > + < \phi_w > \tag{73}$$

where $<a_i>$ denotes the area averaged interfacial area concentration. The term $< \phi_w >$ stands for the wall nucleation source which can be important in boiling and condensation processes.

The constitutive relation for this wall source term is discussed in Section 5.3. The average interfacial velocity is defined by

$$\bar{v}_{iz} \equiv \frac{< a_i v_{iz} >}{< a_i >} \tag{74}$$

By using the local interfacial area measurement method developed under the program, the following parameters are measured simultaneously.

$$a_i = a_i (r,z) \tag{75}$$

$$v_{iz} = v_{iz}(r,z) \tag{76}$$

Under the adiabatic and steady conditions, there are no effects of phase changes, thus

$$\frac{d}{dz} < a_i v_{iz} > = < \phi_{dis} > - < \phi_{co} > \tag{77}$$

which shows the way to measure the right hand side source and sink terms. First, two limiting cases are studied to isolate the break-up source term and the coalescence sink term. It is considered that there is a critical Reynolds number, Re_c^*, for a break-up process. Below this value, the break-up of fluid particle becomes insignificant. Hence, for $Re_e << Re_c^*$

$$\frac{d}{dz} < a_i v_{iz} > \cong - < \phi_{co} > \tag{78}$$

Typically, this happens in low velocity bubbly flow. The gradual coalescence leads to the formation of Taylor cap bubbles. This is followed by the wake entrainment and development into slug flow. Hence, by measuring the left hand side terms at two different axial locations, one obtains

$$< \phi_{co} >= -\frac{1}{\Delta z}[< a_i \, v_{iz} >_2 - < a_i \, v_{iz} >_1] \tag{79}$$

This data represents the global changes in the interfacial area concentration.

For bubbly to slug flow transition, both the random coalescence and wake entrainment by Taylor bubbles can be significant. In order to measure the process of the wake entrainment, it is necessary to measure the characteristics of the large Taylor bubbles and small wake bubbles separately. The rate of coalescence due to the wake entrainment can be obtained from the separate measurements of interfacial velocities, interfacial area and void fractions of these two groups of bubbles using the five sensor probe method.

From a geometrical consideration, the interfacial area concentration of a slug or churn-turbulent flow [36] is given by

$$a_i = \frac{4.5}{D}\frac{< \alpha > -\alpha_{gs}}{1-\alpha_{gs}} + \frac{3\alpha_{gs}}{r_{sm}}\frac{1- < \alpha >}{1-\alpha_{gs}} \tag{80}$$

where $< \alpha >$, α_{gs}, D and r_{sm} are the average overall void fraction, average void fraction in the liquid slug section, hydraulic diameter and the Sauter mean radius of the small bubbles in the liquid slug section, respectively. The five sensor probe gives all the parameters in the above equation. The first and second terms on the right hand side give the separate contributions from the large Taylor bubbles and small bubbles in liquid slug. Thus, the total coalescence effect on the interfacial area can be measured. Furthermore, by measuring the velocity of Taylor bubbles, v_{lgs}, and that of small bubbles, v_{ib}, by the five sensor probe, the influx of the small bubbles into the large slug bubble can be directly measured. This will give the sink term due to the entrainment alone. Without the use of the five sensor probe, such a detailed measurement of various contributions is nearly impossible.

For a break-up dominated section at high Reynolds number, Re, > Re*, the coalescence process may be neglected when the particle sizes are relatively large. Then

$$\frac{d}{dz} < a_i \, v_{iz} > \cong < \phi_{is} > \tag{81}$$

or

$$< \phi_{dis} >= \frac{1}{\Delta z}[< a_i \, v_{iz} >_2 - < a_i \, v_{iz} >_1] \tag{82}$$

The boundary conditions for $<a_i>$ can be changed by using different bubble injectors. For this group of experiments, relatively large bubbles, which are unstable, are injected at the inlet.

One extreme limit of this type of experiment has been already performed [29]. The detailed observation on the break-up process such as the wave growth of breaking bubbles are measured, see Fig. 13.

When two-phase flow is fully established, the break-up process and coalescence process should reach an equilibrium, thus

$$< \phi_{dis} > - < \alpha_{co} >= 0 \tag{83}$$

which is a good check of the constitutive relations for break-up and coalescence processes.

The above three types of experimental data, namely

1) coalescence sink term data,

2) break-up source term data, and

3) fully developed equilibrium data

will be analyzed based on the general functional dependence of the constitutive relations for $< \phi_{dis} >$ and $< \phi_{co} >$. These phenomenological models should form the basis for the more mechanistic models discussed in Sections 2, 3 and 4.

3.8.3 Wall Nucleation Source Term $< \phi_w >$

For boiling flow, the wall nucleation source $<\phi_w>$ is the most important term. In view of this, an effort has been made to develop a reliable constitutive relation for $<\phi_w>$ [2,36]. It can be expressed by the following form

$$< \phi_w >= \frac{\xi_h}{A} N a f_d \pi D_d^2 \tag{84}$$

Here ξ_h, Na, f_d and D_d are the heated perimeter, flow area, nucleation site density, bubble departure frequency and bubble departure diameter, respectively. For boiling system, the nucleation site density [2] is given approximately by

$$Na = \frac{1}{D_d^2}\left\{\frac{2\sigma T_{sat}}{(T_w - T_{sat})\rho_g \Delta i_{fg}}\right\}^{-4.4} f(\rho^*) \tag{85}$$

where $f(\rho^*)$ is a known function of a density ratio. The bubble departure diameter is given by

$$D_d = 2.64\times10^{-5}\theta\left[\frac{\sigma}{\Delta\rho g}\right]^{0.5}\left[\frac{\Delta\rho}{\rho_g}\right]^{0.9} \tag{86}$$

Here, θ is the contact angle. The bubble departure frequency is expressed by

$$f_d = \frac{1.18}{D_d}\left[\frac{\sigma g\Delta\rho}{\rho_f^2}\right]^{0.25} \tag{87}$$

Combining the above expressions, the nucleation site density can be calculated.

3.9 Conclusions

The interfacial area transport equation has been derived from the statistical model of the fluid particle number transport equations. The basic mechanisms affecting the source and sink terms in the interfacial transport equation have been discussed in detail. The underlying physics and modeling approach to develop the closure relations for these terms are presented. The hydrodynamic effect can be divided into the break-up and coalescence of fluid particles. There are a number of different potential mechanisms which can lead to the break-up of fluid particles. For example, the local turbulence, high shear flow and interfacial instability can lead to substantial particle break-up. The coalescence process is caused by fluid particle collisions and subsequent break-up of the particle interface. The collision can be produced by turbulent fluctuations, size dependent rise velocity, wake entrainment and shear layer induced velocity difference. These phenomena affecting the break-up and coalescence of fluid particles are reviewed and preliminary modeling approach is indicated. Some of the important results obtained under the present programs are summarized.

The development of the one-dimensional interfacial area transport equation and the necessary experimental data to support the modeling effort are discussed. The use of the presently developed two, four and five sensor resistivity probes is essential to generating the experimental data required to develop the closure relations for the source and sink terms in the interfacial area transport equation. The changes in the flow regime can be predicted mechanistically by the introduction of the interfacial area transport equation. The effects of the initial and boundary conditions on the flow structure

development are effectively modeled by the present approach. Such capability does not exist in the present state-of-the-arts. Therefore, a successful development of this interfacial area transport equation can make a substantial improvement in the two-fluid model formulation.

Acknowledgement

This research is supported by the U.S. Department of Energy under the Office of the Basic Energy Sciences as a joint research program between Purdue University and the University of Wisconsin-Milwaukee. The authors would like to express their sincere appreciation to Dr. O. P. Manley of DOE/BES for his support of this program and encouragement.

Nomenclature

A_i	Interfacial Area
a_i	Interfacial Area Concentration
d	Diameter
d_{SM}	Sauter Mean Diameter
f	Particle Density Distribution Function
g	Breakup Frequency
h	Collision Frequency
i	Specific Enthalpy
j	Superficial Velocity
k	Wave Number
N	Total Number of Particles of All Sizes per Unit Volume of Mixture
n	Number of Daughter Particle Production
Re	Reynolds Number
S	Fluid Particle Number Density Rate due to Breakup and/or Coalescence
S_{ph}	Fluid Particle Sink or Source Rate due to Phase Change
T	Temperature
t	Time
$\vec{v}$	Velocity Vector

$\overrightarrow{v_p}$	Particle Velocity
$\overrightarrow{v_{pm}}$	Average Local Particle Velocity Weighted by Particle Number
$\vec{x}$	Position Vector
We	Weber Number

Greek Letters

α	Void Fraction
β	Distribution of Daughter Particles
ε	Energy Dissipation per Unit Volume
ν	Coalescence Efficiency
μ	Dynamic Viscosity
ϑ	Particle Volume
Φ	Rate of Change in Interfacial Area Concentration due to Particle Breakup and/or Coalescence Processes
Φ_{ph}	Rate of Change in Interfacial Area Concentration due to Evaporation and/or condensation
ρ	Density
σ	Surface Tension
τ	External Stress
θ	Contact Angle

Subscripts

c	Continuous Phase
c_o	Coalescence Process
cr	Critical Value
d	Dispersed Phase
f	Liquid Phase
i	Value at Interface
g	Gaseous Phase
max	Maximum

min	Minimum
p	Particle
ph	Phase Change
sat	Saturation

References

1. G. Kocamustafaogullari, M. Ishii and 1. Y. Chen, "Correlation for Nucleation Site Density and Its Effect on Interfacial Area," Argonne National Laboratory Report, ANL-82-32 (1982).
2. G. Kocamustafaogullari and M. Ishii, "Interfacial Area and Nucleation Site Density in Boiling Systems," Int. J. Heat and Mass Transfer, Vol. 26, p. 1377 (1983).
3. J. N. Reyes, "Statistically Derived Conservation Equations for Fluid Particle Flows," Proc. ANS-THD, Vol. 5, pp. 12-19, ANS Winter Annual Meeting, San Francisco (1989).
4. G. E. Taylor, "The Formation of Emulsion in Definable Field of Flow," Proc. Roy. Soc. (London) Series, Vol. A146, p. 501 (1934).
5. S. Tomotika, "Breaking Up of a Drop of Viscous Liquid Immersed in Another Viscous Fluid which is Extending at a Uniform Rate," Proc. Roy. Soc. (London) Series, Vol. A153, p. 302 (1936).
6. R. Kumar and N. R. Kulsor, "The Formation of Bubbles and Drops," Adv. in Chem. Eng., Vol. 8, p. 255 (1970).
7. L. L. Tavlarrides and M. Stamatoudis, "The Analysis of Interphase Reactions and Mass Transfer in Liquid-Liquid Dispersions," Adv. in Chem. Eng., Vol. 11, p. 199 (1981).
8. G. K. Batchelor, "Pressure Fluctuations in Isotropic Turbulence," Proc. Cambridge Phil. Soc., Vol. 47, p. 359 (1951).
9. V. G. Levich, "Physicochemical Hydrodynamics," Prentice Hall, Englewood Cliffs, New Jersey (1962).
10. C. A. Coulaloglu and L. L. Tavlarrides, "Description of Interaction Processes in Agitated Liquid-Liquid Dispersions," Chem. Eng. Sci., Vol. 32, p. 1289 (1977).

11. E. G. Chatzi and I. M. Lee, "Analysis of Interactions for Liquid-Liquid Dispersion in Agitated Vessels," Ind. Chem. Eng. Res., Vol. 26, No. 11, p. 2263 (1987).
12. E. G. Chatzi, A. D. Garrielides and C. Kiparissides, "General Model for Prediction of the Steady-State Drop Size Distribution in Batch Stirred Vessels," Ind. Eng. Chem. Res., Vol. 28, p. 1704 (1989).
13. S. G. Hatzikiriakos, R. P. Gaikwad, P. R. Nelson and J. M. Shaw, "Hydrodynamics of Gas-Agitated Liquid-Liquid Dispersions," AIChE J., Vol. 36, p. 677 (1990).
14. M. J. Prince and H. W. Blanch, "Bubble Coalescence and Break-up in Air-Sparged Bubble Column," AIChE J., Vol. 36, No. 10, p. 1485 (1990).
15. M. J. Prince, S. Walters and H. W. Blanch, "Bubble Break-up in Air-Sparged Biochemical Reactors," First Generation of Bioprocess Engineering, T. K. Ghose, ed., p. 160 (1989).
16. R. Shinnar, "On the Behavior of Liquid Dispersions in Mixing Vessels," J. Fluid Mech., Vol. 10, p. 259 (1961).
17. R. Shinnar and J. M. Church, "Predicting Particle Size in Agitated Dispersions," Ind. Eng. Chem., Vol. 52, p. 253 (1960).
18. R. M. Thomas, "Bubble Coalescence in Turbulent Flows," Ind. J. Multiphase Flow, Vol. 7, p. 709 (1981).
19. M. F. Nishikawa, F. Mori and S. Fujieda, "Average Drop Size in Liquid-Liquid Phase Mixing Vessel, J. Chem. Eng. Japan, Vol. 28, p. 12 (1987).
20. C. A. Coulaloglu and L. L. Tavlarrides, "Drop Size Distributions and Coalescence Frequencies of Liquid-Liquid Dispersion in Flow Vessels," AIChE J., Vol. 22, p. 289 (1976).
21. M. Stamatoudis and L. L. Tavlarrides, "Effect of Continuous Phase Viscosity on the Drop Sizes of Liquid-Liquid Dispersions in Agitated Vessels," Int. Eng. Chem. Process Des. Dev., Vol. 24, p. 1175 (1985).
22. L. L. Tavlarrides and M. Stamatoudis, "The Analysis of Interface Reactions and Mass Transfer in Liquid-Liquid Dispersions," Adv. in Chem. Eng., Vol. 11, p. 199 (1981).
23. K. Rietema, Adv. in Chem. Eng., Vol. 5, p. 237 (1964).

24. S. R. Smits, W. D. Huang, J. Razi and G. Kocamustafaogullari, "Droplet Size Modeling in Annular Flow," to be presented in NURETH 6, Grenoble, France, October 5-8 (1993).
25. G. Kocamustafaogullari;` S. R. Smits and J. Razi, "Maximum and Mean Droplet Sizes in Annular Two-Phase Flow," Int. J. Heat Mass Transfer, Vol. 37, pp. 955-965 (1994).
26. G. Kocamustafaogullari, W. D. Huang and J. Razi, "Measurement and Modeling of Average Void Fraction, Bubble Size and Interfacial Area," J. Nucl. Engr. and Des., in print (1993).
27. G. Kocamustafaogullari, M. Ishii and I. Y. Chen, "Unified Theory for Predicting Maximum Fluid Particle Size for Drops and Bubbles," Argonne National Laboratory Report, NUREG/CR-4028 (1984).
28. J. Kitscha and G. Kocamustafaogullari, "Break-up Criteria for Fluid Particles," Int. J. Multiphase Flow, Vol. 15, p. 573 (1989).
29. J. W. Miller, "An Experimental Analysis of Large Spherical Cap Bubbles Rising in an Extended Liquid," M.S. Thesis, School of Nuclear Engineering, Purdue University (1993).
30. M. Sevik and S. H. Park, "The Splitting of Drops and Bubbles by Turbulent Fluid Flow," *J. Fluids Eng., Vol.* 95, p. 53 (1973).
31. A. Sleicher, "Maximum Drop Size in Turbulent Flow," *AIChE J., Vol.* 8, p. 471 (1962).
32. A. Serizawa and I. Kataoka, "Phase Distribution in Two-Phase Flow," Transient Phenomena in Multiphase Flow," ICHMT Int. Seminar, Dubrovnik, p. 179 (1988).
33. R. T. Lahey, Jr., "The Analysis of Phase Separation and Phase Distribution Phenomena Using Two-Fluid Models," Nucl. *Eng. and Des., Vol.* 122, p. 17 (1989).
34. T. J. Liu, "The Effect of Bubble Size on Void Fraction Distribution in a Vertical Channel," Proc. *Int. Conf. on Multiphase Flow,* Tsukuba, Japan, Vol. 1, p. 453 (1991).
35. M. Ishii and K. Mishima, "Two-Fluid Model and Hydrodynamic Constitutive Relations, " *Nucl. Eng. and Des., Vol.* 82, p. 107 (1984).

36. J. Riznic and M. Ishii, "Bubble Number Density and Vapor Generation in Flashing Flow, " *Int. J. Heat and Mass Transfer, Vol.* 32, p. 182 (1989).

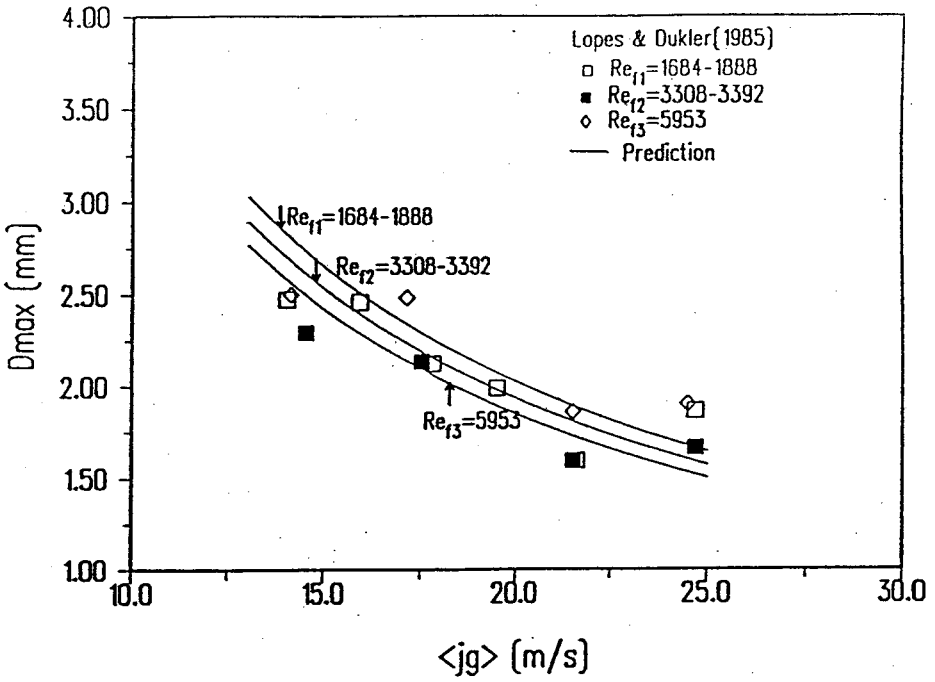

Figure 1 Theoretical and Experimental Values of the Maximum Stable Drop Diameter, Lopes and Dukler (1985)

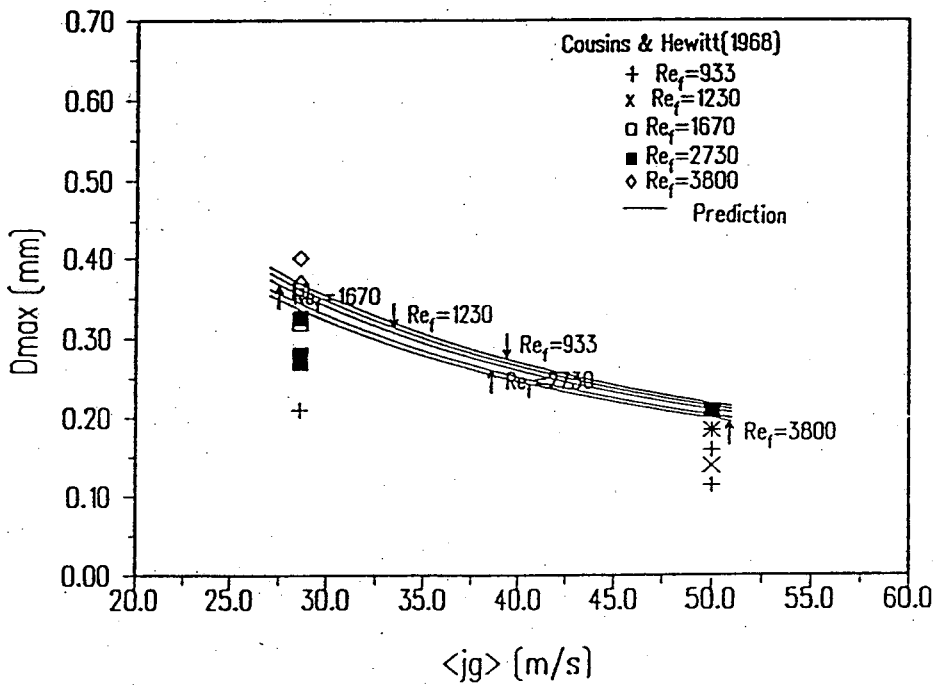

Figure 2 Theoretical and Experimental Values of the Maximum Stable Drop Diameter, Cousins and Hewitt (1968)

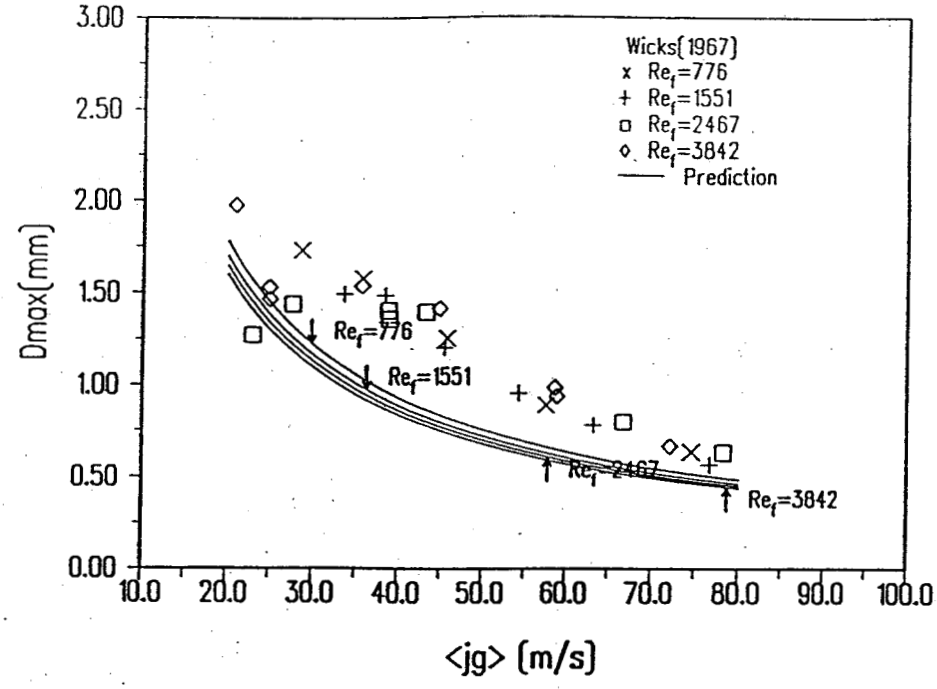

Figure 3 Theoretical and Experimental Values of the Maximum Stable Drop Diameter, Vicks (1967)

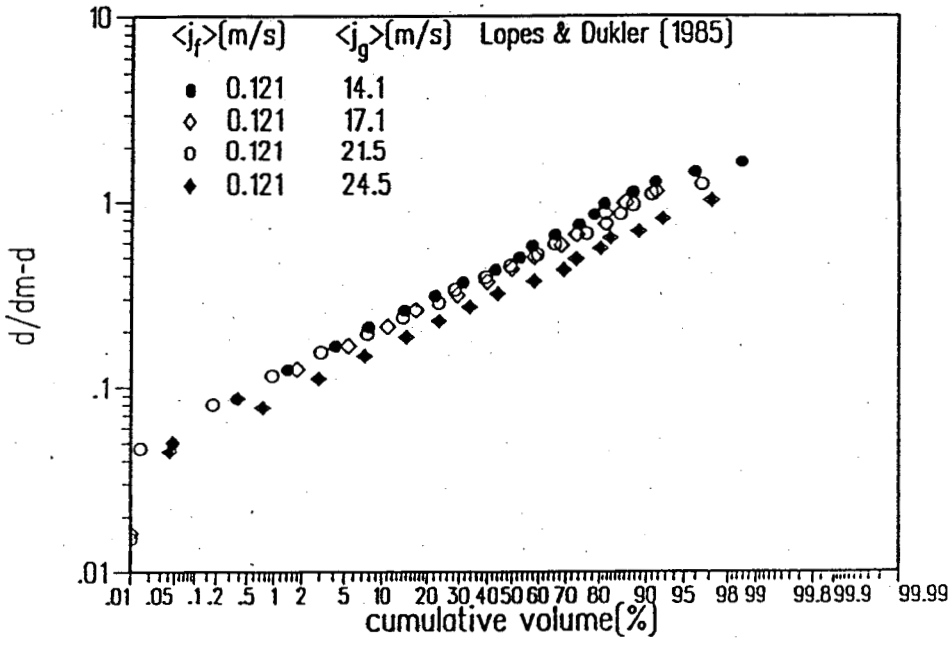

Figure 4 Example of Upper Limit, Log-Normal Distribution, Lopes and Dukler (1985)

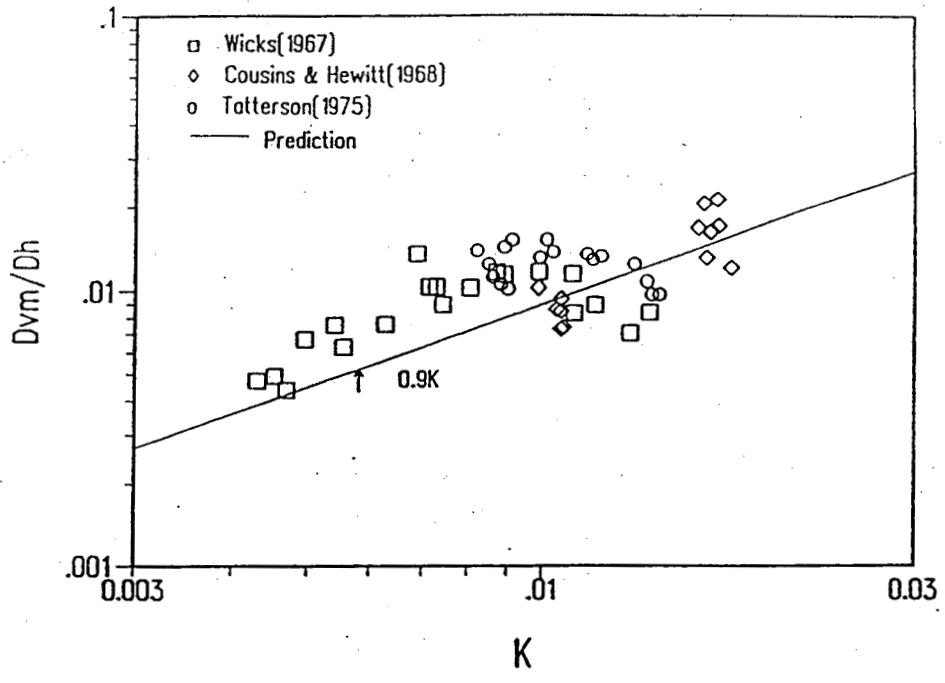

Figure 5 Theoretical and Experimental Values of Volume Median Diameter

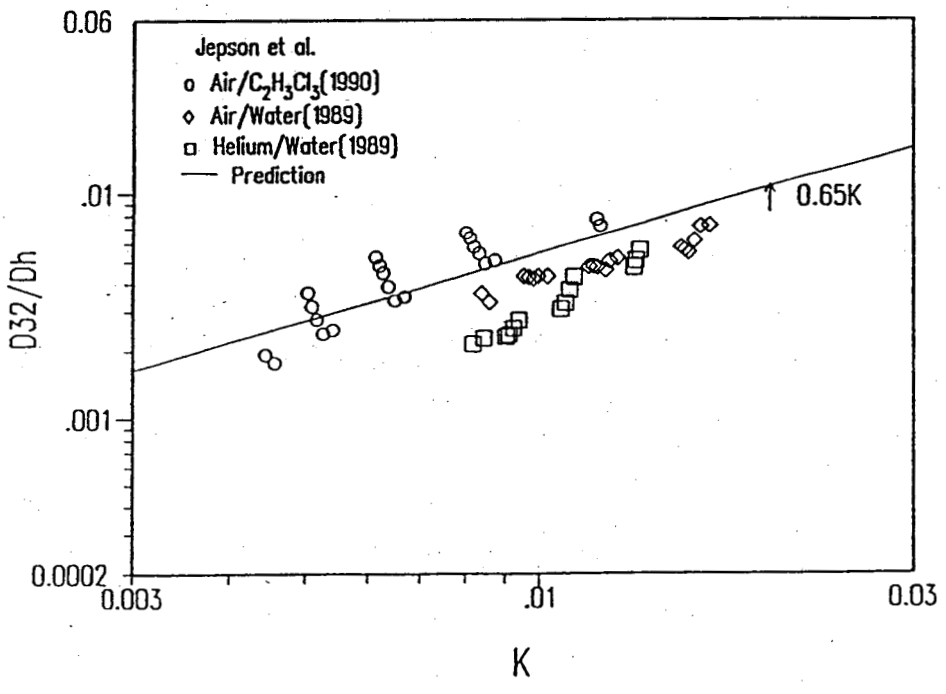

Figure 6 Theoretical and Experimental Values of Sauter Mean Diameter

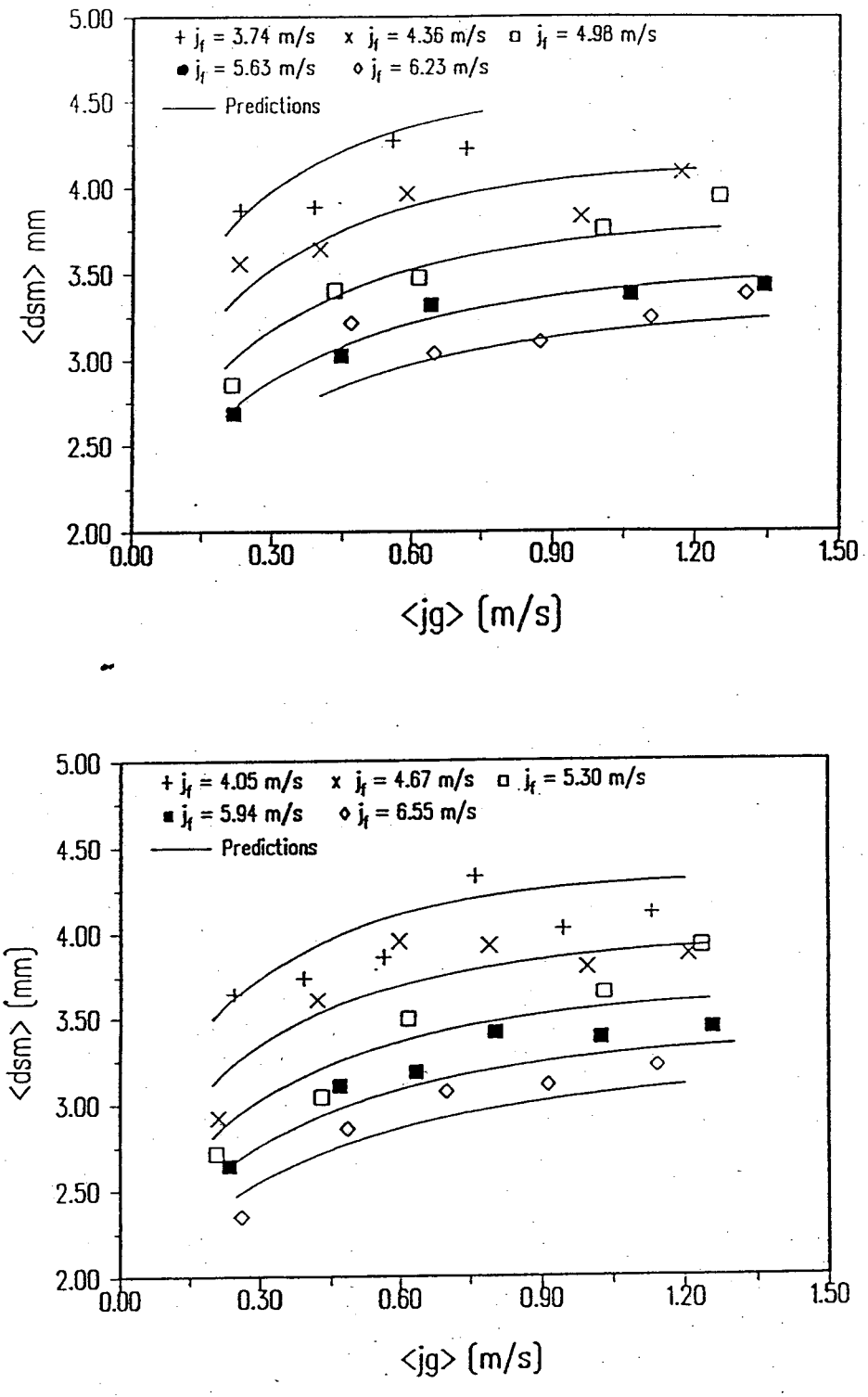

Figure 7 Variation of Average Sauter Mean Diameter of Bubbles with Superficial Gas Velocity

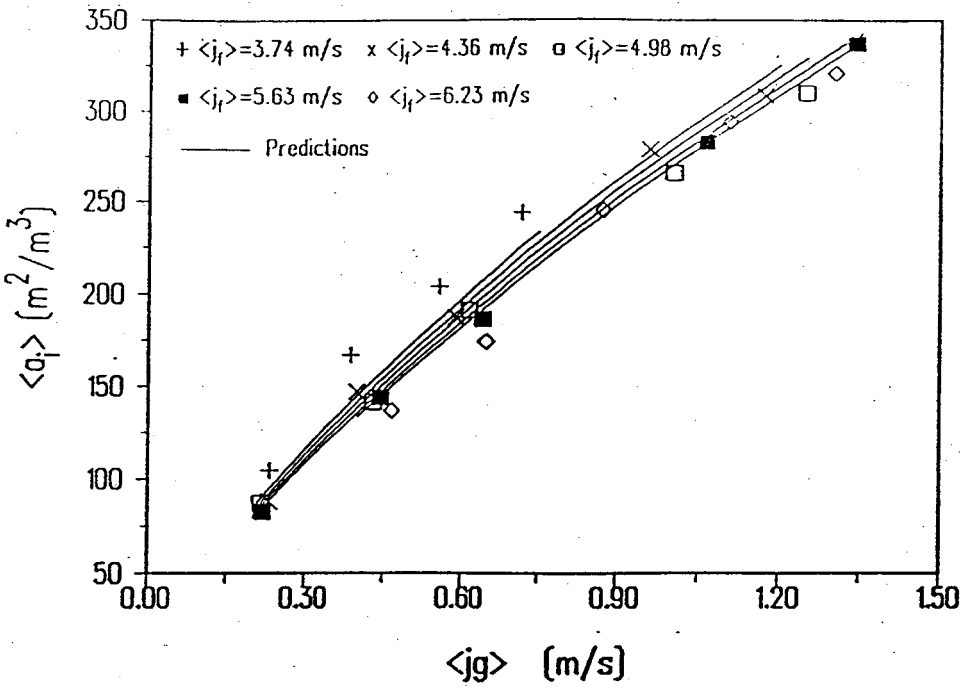

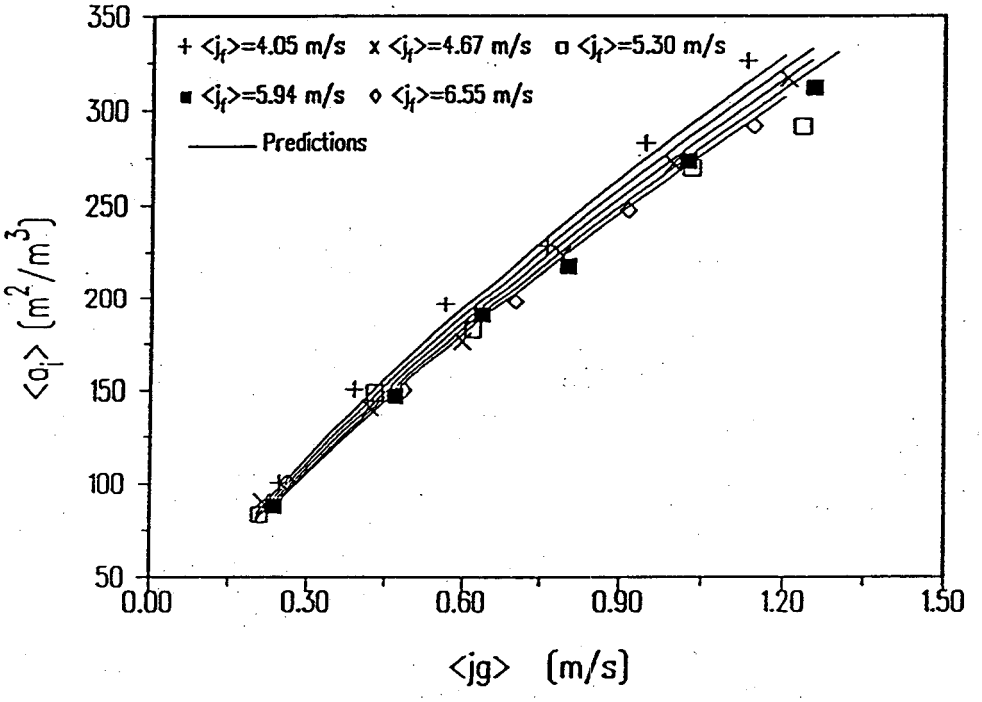

Figure 8 Variation of Average Interfacial Area Concentration with Superficial Gas Velocity

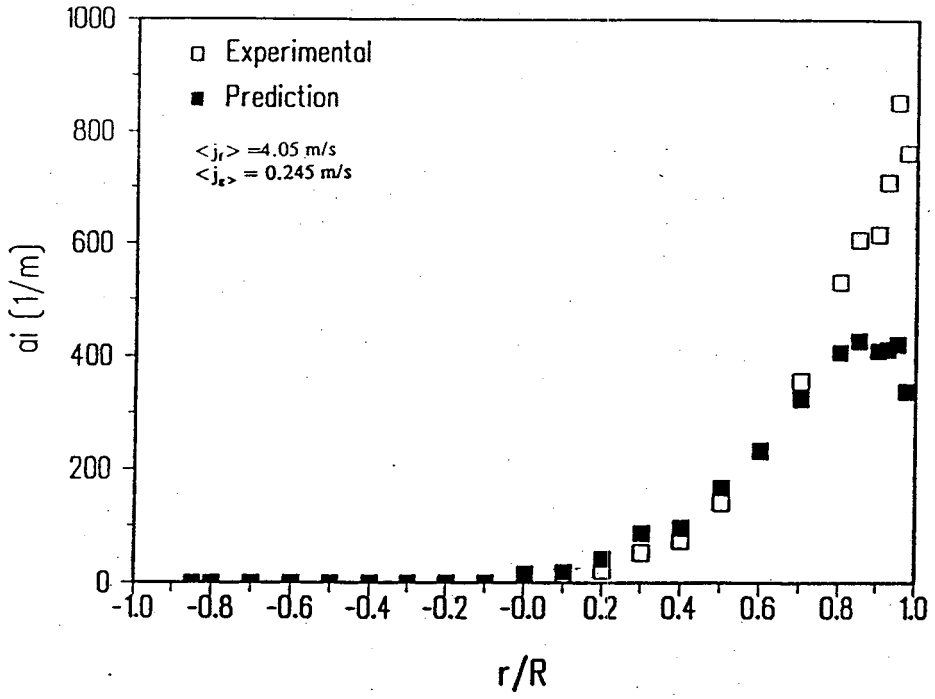

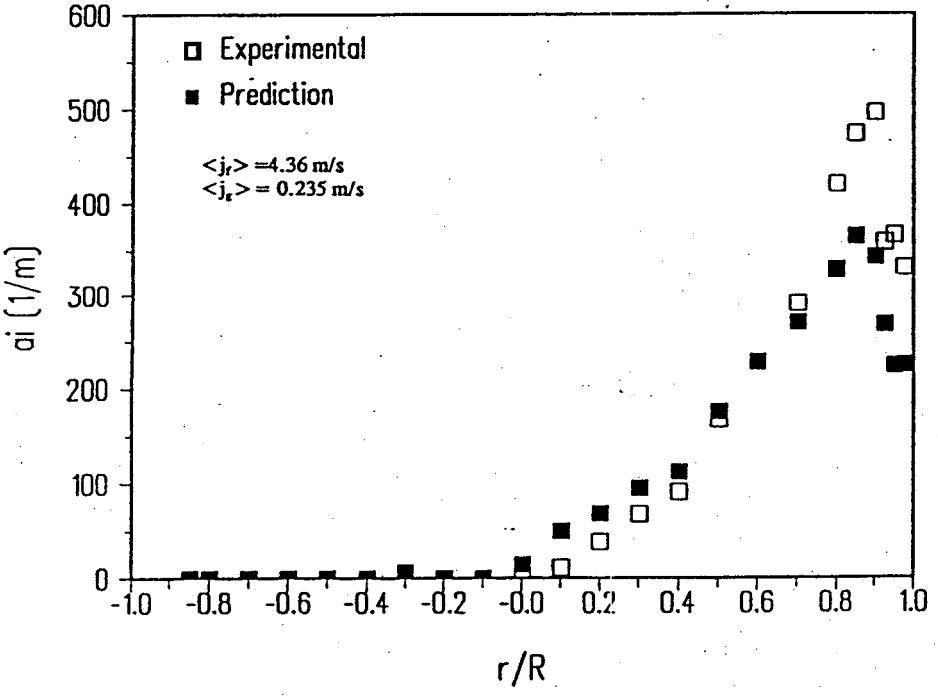

Figure 9 Comparison of Local Interfacial Area Concentration Predictions with Experimental Data for Two Flow Conditions

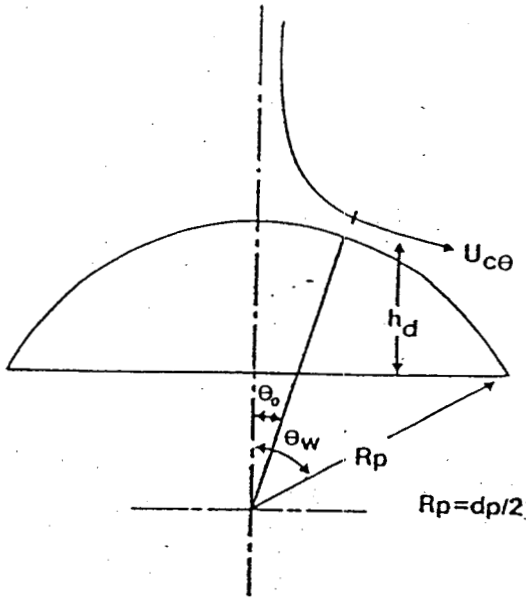

Figure 10 Schematic Illustration of Flow Around a Rising Cap Bubble

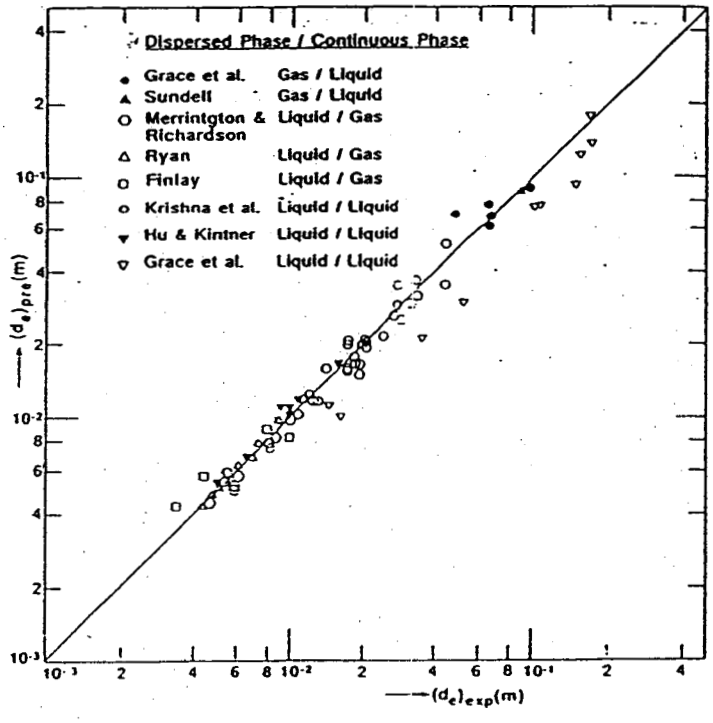

Figure 11 Comparison of Predicted Break-up Diameters with Experimental Data

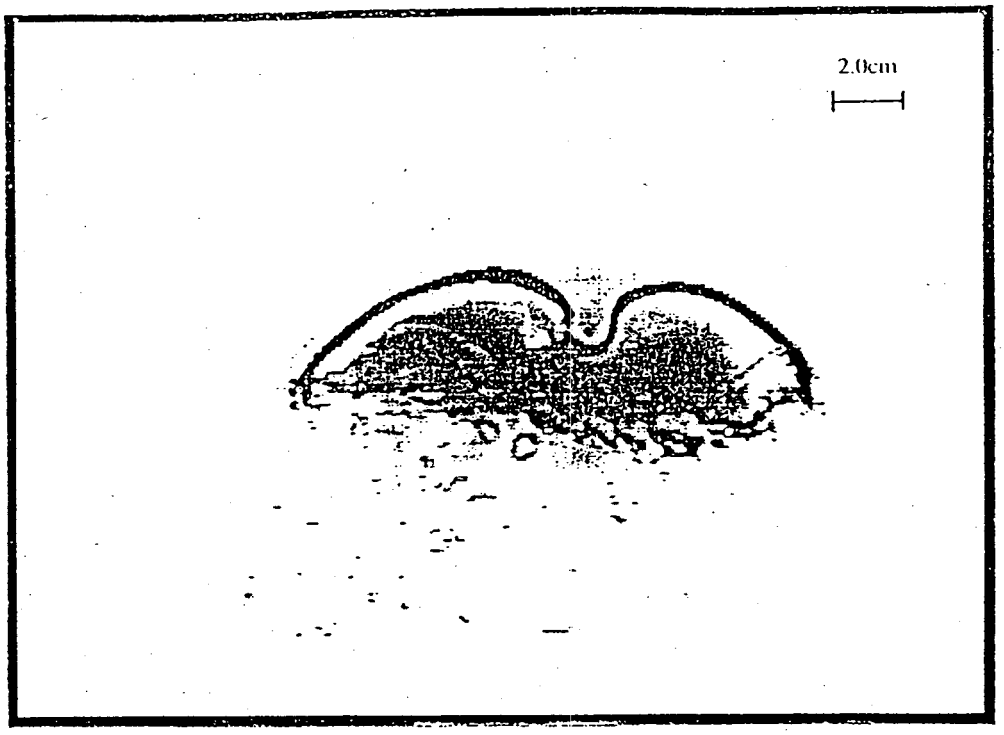

Figure 12 Image of a Small Bubble with Liquid Bulb
(P_o = 114 kPa, r = 19.6 s)

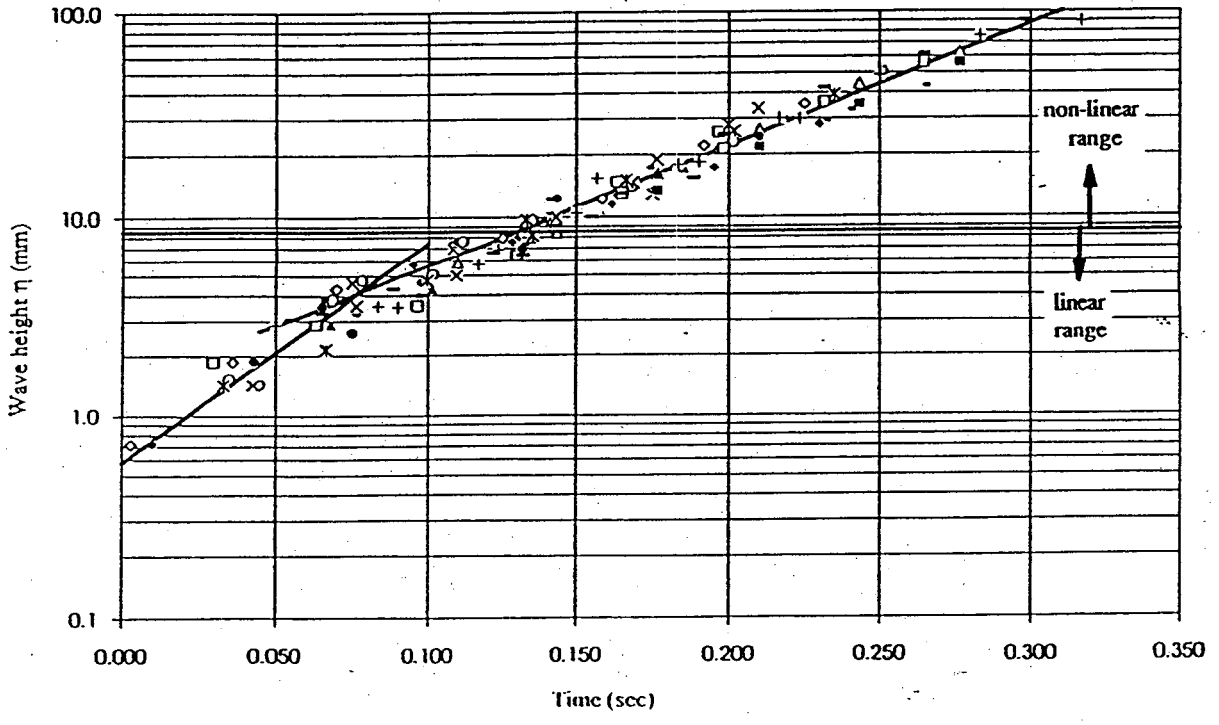

Figure 13 Experimental Curve Fits for Wave Height

4. DESING AND DESCRIPTION OF AIR-WATER TWO-PHASE FLOW LOOP AND INSTRUMENTATION

4.1 Design and Description of Flow Loop

A horizontal flow loop was designed and built for investigating the interfacial structure of horizontal two-phase flow. The overall flow loop schematic is illustrated in Figure 1. The loop basically consists of various flanged lengths of 50.3 mm ID circular Pyrex glass tubings with pressure taps installed between them. However, smaller or larger diameter .I test sections can be easily fitted to the loop. The over-all test section is about 15.4 m in length.

The entire test section is transparent, so that flow visualization, high-speed photography, and high speed cinematography are possible. It is designed such that various local instrumentations for two-phase flow measurements and different mixing chambers can be easily accommodated. In designing the loop, a special emphasis is placed on investigating geometric scaling and phenomenological modeling for a developing horizontal two-phase flow and the effects of entrance mixing geometry.

Because of the large number of flanged joints in the test section, considerable care is taken in the alignment and matching of the joints. This would minimize the flow disturbances caused by a joint. All flanged joints are sealed by the use of O-rings to ensure an even and leak proof joint. In order to support and level the entire test section, an elaborate unistrut support structure is constructed. The support structure consists of one main rail, oriented parallel to and below the test section. This main rail is supported by many support arms, located at 1.2 m intervals. Each of the support arms heights is adjustable for leveling purposes. The glass test section is supported on the unistrut main rail by specially constructed maple wood blocks. The wood blocks have a semicircle machined out of the top side, with a diameter the same as that of the outside diameter of the glass test section. This allows the glass test section to rest on the top of the wood block and be securely clamped in place, and so no movement is possible. The wood blocks are evenly distributed along the glass test section length as required for sufficient support.

Air and water are used as coupling fluids. The air enters the mixing chamber from a 900 vertical leg and is injected into the water flow through a cylindrical porous media to achieve a uniform mixing and a quick development of a bubbly two-phase flow pattern. The porous media is made of pregraded, sintered powder to obtain the desired porosity. Three different sizes of porous media are used. The experimental results presented in this report are based on 100 micron porosity. The cylindrical porous media is centered in the glass test section, and directs the air flow from 90^0 to an axially aligned downstream direction. The water enters the mixing chamber from upstream, with the same central axis as the downstream glass test section. All flow paths for the air and water are designed to be as smooth as possible in order to minimize single-phase flow disturbances in the areas immediately before mixing. A schematic of the mixing chambers are presented in Figure 2 and 3.

After exiting the test section, the two-phase mixture enters an air-water separator. The separator is constructed from $0.4m^3$ circular tank. Aluminum baffles are fastened inside the separator tank to assist the separation process and to prevent the possibility of vortex formation. Once separated, the air is vented to the atmosphere, and the water is returned to the water storage tank. The water storage tank is kept sealed at all times in order to prevent any contamination of the water with foreign debris.

The water flow was supplied by a stainless steel centrifugal pump. The pump has a 20 hp motor and delivers 750 gpm at 1800 rpm. A Toshiba Transistor Inverter model VFP-2220PI motor control is used to control the pump speed. The inverter allows the pump's output capacity to be regulated from 0 to 100 percent of its rated capacity. The pump delivers water from a 500-gallon circular water storage tank to a system of flow regulating valves. All water supply piping is made up of schedule 40 and schedule 80 polyvinyl chloride piping. After the regulating valves, the water passes through a system of three water flow meters. These flow meters are of the paddle wheel type and are assembled in a parallel configuration and have a range of 0 to 750 gpm. They are electrically connected to a digital flow analyzer. The water then passes through a pneumatically controlled butterfly valve and then into the two-phase flow mixing chamber. The butterfly valve is used to shut off the' water flow to the mixing chamber and test section during the period of average void fraction measurements.

The air flow is supplied by a centrally located university air compressor. The central air compressor has a 450 CFM capacity. An additional 100 hp air compressor with 450 CFM capacity is also available if necessary. The central compressor supplies air to the laboratory through a 6 inch diameter steel pipe at 115 psi. Before the air enters the 0.9 m^3 circular air storage tank, it passes through a 0.5 micron Arrow model F4 air filter and then through a Norgren model R18 regulator. The air regulator is used to reduce air flow fluctuations emanating from the air compressor or air supply piping. The air flow regulator is set so that the air pressure in the air storage tank is about 100 psig, or about 10 psig less than the air supply piping. From the air storage tank the air then passes through a second Arrow air filter with a 0.3 micron filter element. The air then goes through a second Norgren air pressure regulator, where the air pressure is reduced to the flow loop operating pressure. This pressure depends on the two-phase flow conditions desired.

The air flow rate is measured by two turbine flow meters. One of the flow meters has a 1/2-inch inside diameter and the other had a 2-inch inside diameter. The larger flow meter has the capacity to measure up to 300 CFM. The two flow meters were connected in a parallel configuration and the appropriate flow meter is used, depending on the desired air flow rate. The output signal of the flow meters is connected to a Masstrol digital flow analyzer. After the flow meters, the air flow passes through a pneumatically controlled ball valve and then enters the two-phase mixing chamber. The pneumatically controlled ball valve is used to shut off the air flow during the period of average void fraction measurements.

The last 1.5 m of the test section incorporates two Quick-closing valves, which are used for average void fraction measurements. These valves, which are pneumatically operated and electrically controlled, have a very high response time in the order of milliseconds and are synchronized through a common electrical switch to ensure simultaneous operation. The distance between the valves is long enough to minimize any experimental error. During experimental runs operation of the Quick-closing valves and measurement of the mass of water entrapped yields the average void fraction.

To protect the system against pressure surges the following features are incorporated:

- Two more Quick-closing valves are added, one in the water line and one in the air line to cut off supply of water and air, respectively. A fifth Quick-closing valve is installed to bypass flow of water from the pump to the tank. All of these valves are also pneumatically operated and electrically controlled. The five valves are connected to a common electrical connection to ensure complete synchronization.
- Two relief valves are installed in the single-phase liquid line after' quick-closing valve to relieve excess pressure.
- Two air pressure relief valves of the pop-up type relieve excess pressure in the air-line after quick-closing valve.

4.2 Pressure Transducers

Pressure transducers of the diaphragm type are utilized for both absolute and differential pressure measurements. The pressure drop in the test section is measured at six intervals with high frequency transducers located at 1.55 m apart from each other. The absolute pressure transducers are located at two locations in the test section, 6.70 m and 8.22 m downstream of the mixing chamber, respectively.

Four pressure measuring parts were located at 0, 90, 180 and 270 degrees around the circumference of each flange. A schematic of the flanges and their orientation is presented in Figures 4 and 5. For each flange, the four pressure measuring ports were connected with an elaborate system of swagelok valves and fittings. This system pressure measuring part connection allowed the used of any combination, of the four pressure parts, an each of the flanges, during a pressure drop measurement period. Depending on the internal flow structure, either all or only the pressure part at the bottom (180 degrees) was used for pressure measurements.

In order to measure the pressure drop along the test section, differential pressure transducers were used. The pressure transducers used were amplified transducers, with a range of 0-5 psid, accuracy of ± 0.15 psid and a frequency response of 300kHz.atotal of six pressure transducers were installed. Each transducers was connected to, two of the pressure measuring flanges, by using ¼ inch plastic tubing. To ensure that no air bubbles developed or accumulated in the connection tubing, an elaborate system of purge valves

were used for each pressure transducer. A schematic of the purge valve system is presented in Figure 6. For purging, pressurized water from the outlet of the pump is passed through all of the transducer connection tubing until it is observed that no bubbles remained in the tubing. This is done before each pressure drop measuring period.

Calibration of the pressure transducers is performed by adjusting two screws on each pressure transducer. One screw adjusted the zero setting of the pressure transducer. When a zero differential pressure is applied to the pressure transducer the zero screw was adjusted until the voltage output signal of the pressure transducer is zero. The second screw adjusted the span of the pressure transducer. When electrical output terminals E and F of the pressure transducer are connected to each other an 80 % full scale output voltage signal was obtained from the pressure transducer. The open screw is adjusted until the output voltage signal match the value given by the manufacturer. Pressure transducer calibration graphs are constructed. The pressure transducers output signal was connected and recorded by the Metrabyte data acquisition system.

4.3. Instrumentation

Summary of instrumentation capabilities developed over the years at the Two-Phase Flow Laboratory is given on Table 1. Details of these instrumentation will be given later.

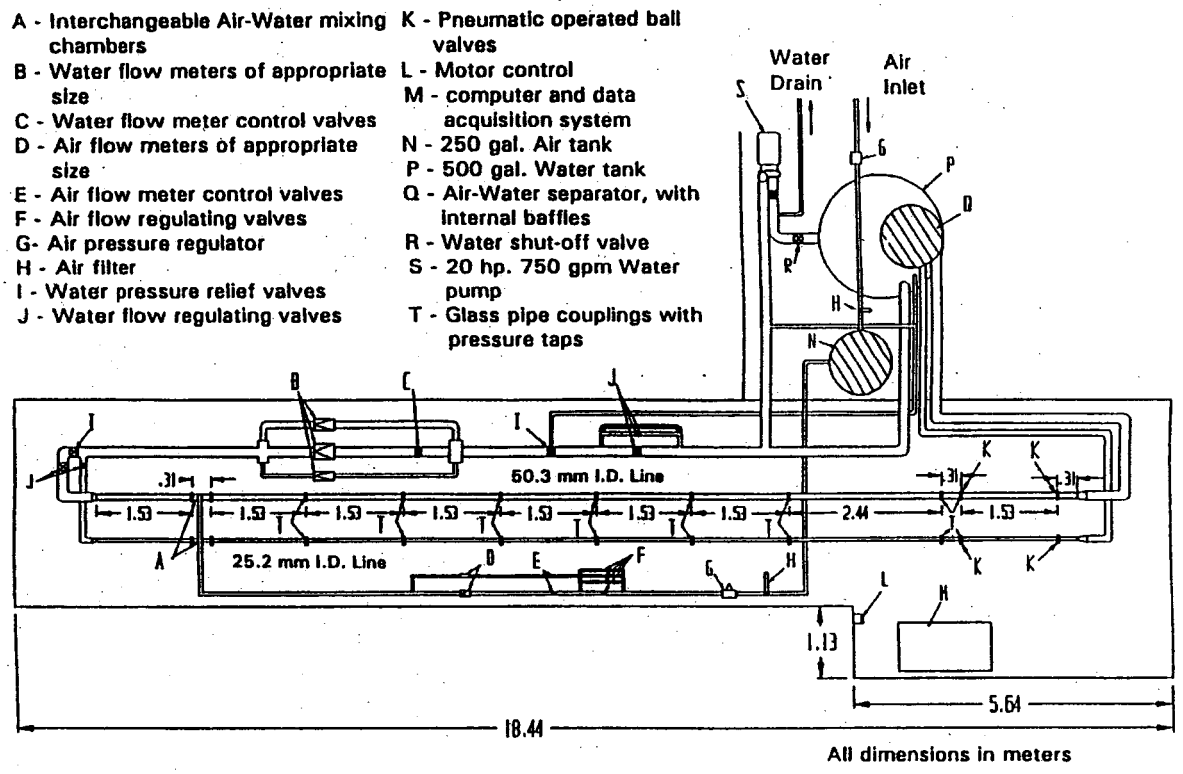

Figure 1. Schematic Diagram of Horizontal Two-Phase flow Experimental Loop

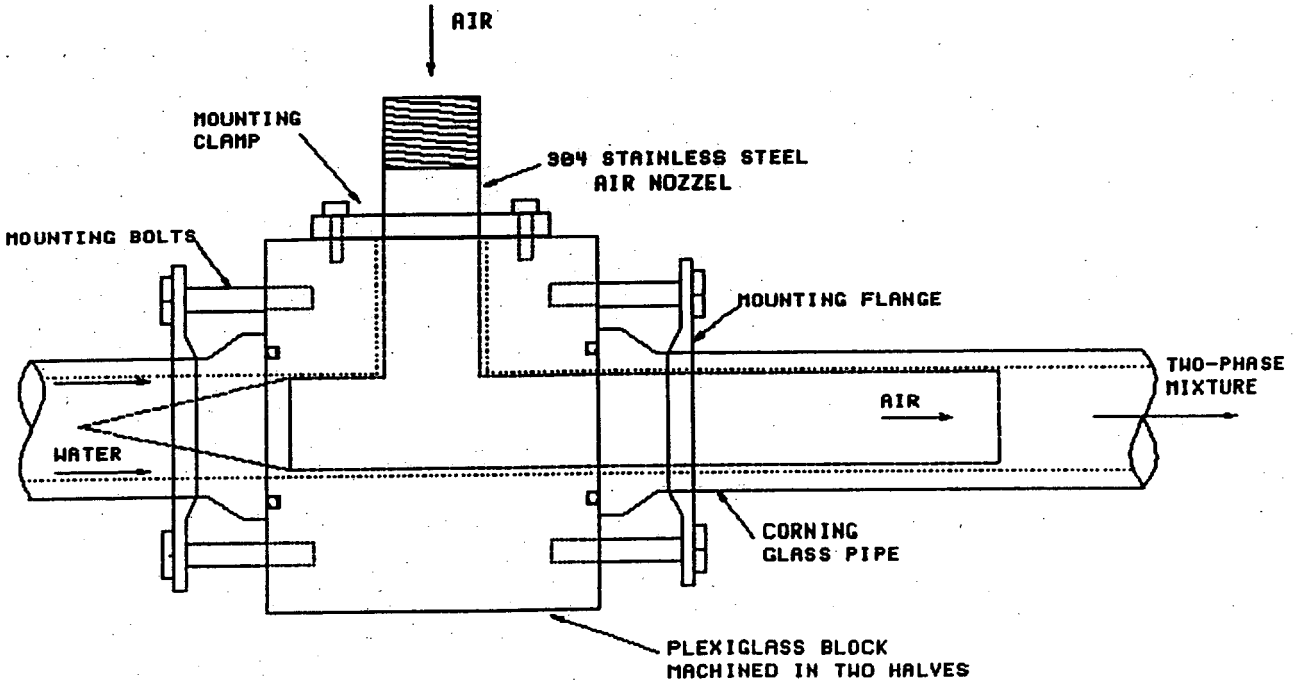

Figure 2. Jet Mixing Chamber for Annular Flow Experiments

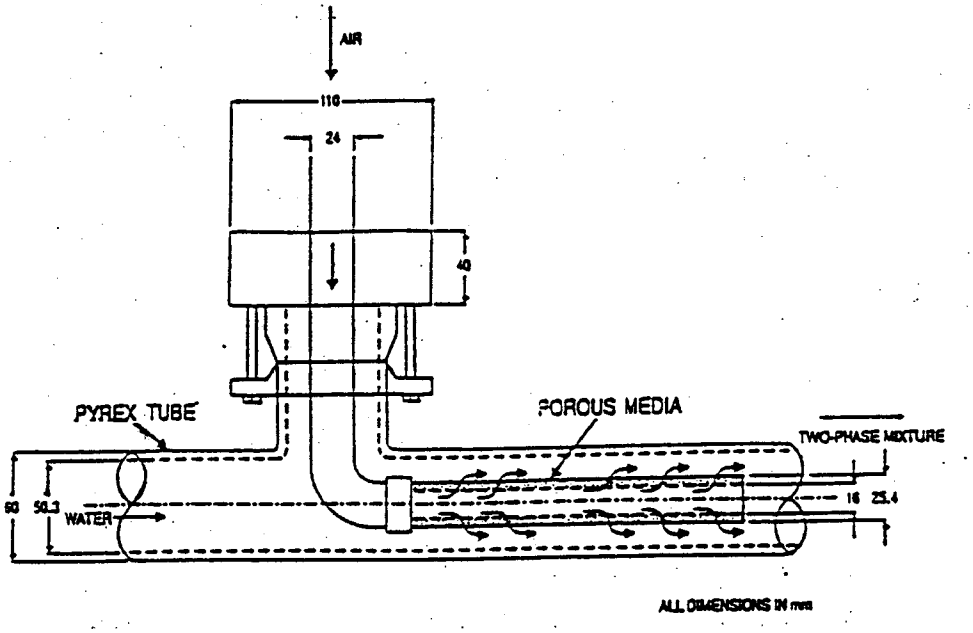

Figure 3. Porous Media Mixing Chamber for Bubbly and Slug Flow Experiments

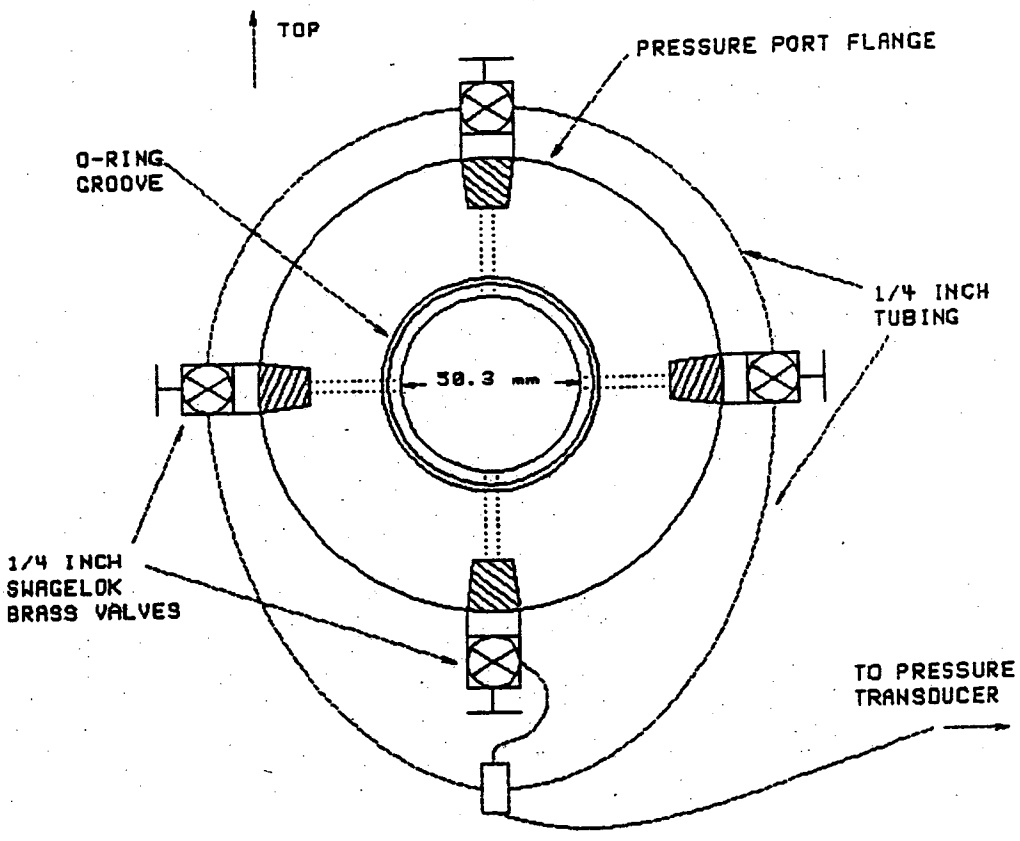

Figure 4. A typical Pressure Port Flange

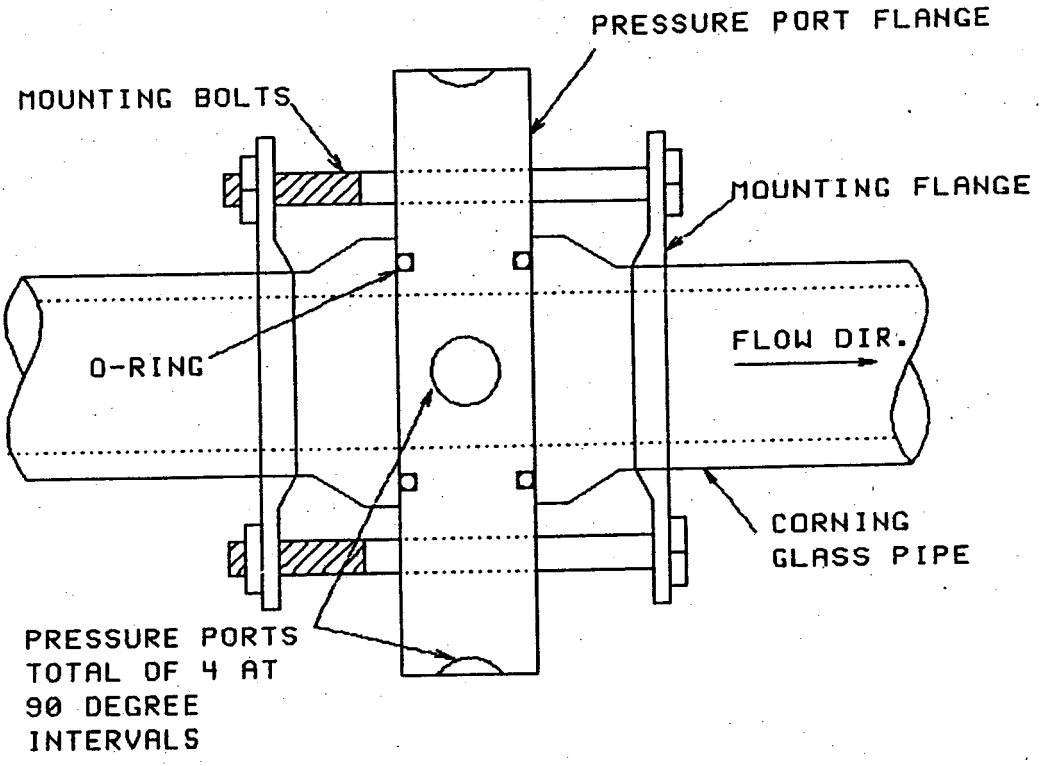

Figure 5. Pressure Port Flange Orientation

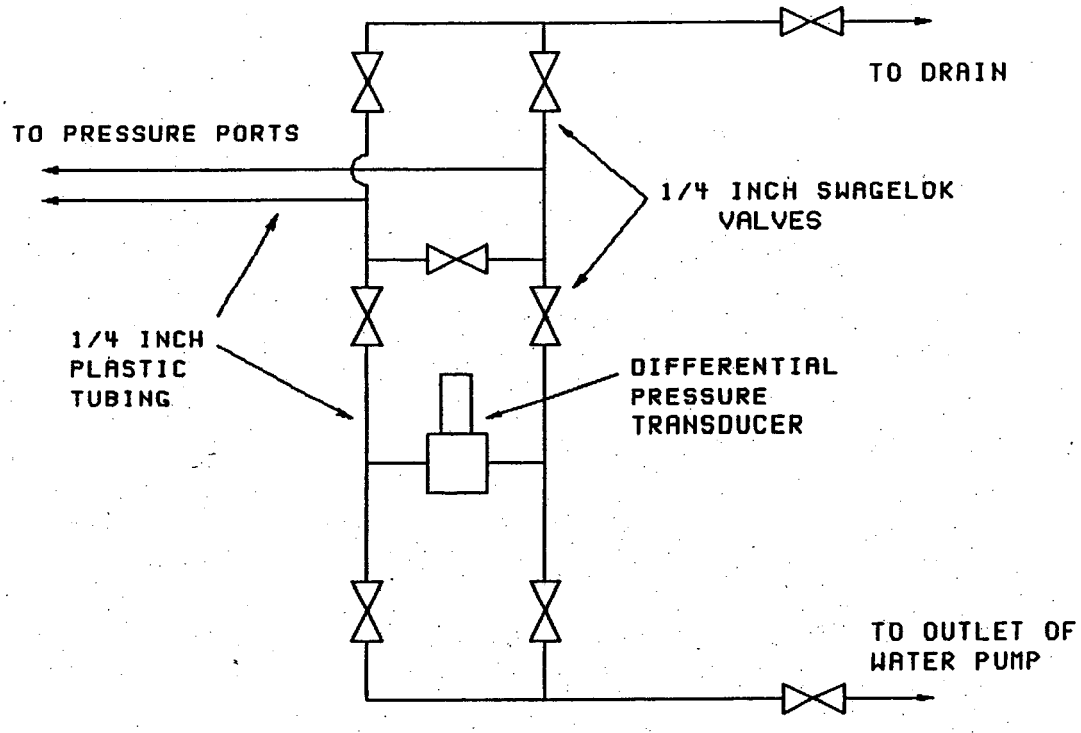

Figure 6. Pressure Transducer Control System

Table 1. Summary of Instrumentation Capabilities in Two-Phase Flow Laboratory at UWM

NAME	MANUFACTURER	APPLICATIONS
Two-Sensor Conductivity Probe for Bubbly Flow	UWM	Interfacial Area Concentration Void Fraction Interfacial Velocity Bubble Frequency Spectrum
Four-Sensor Conductivity Probe for Plug/Slug Flow	UWM	Interfacial Area Concentration Void Fraction Interfacial Velocity Bubble Frequency Spectrum
Double Parallel Wire Resistivity Probe for Stratified Flow	UWM	Mean Liquid Thickness Interfacial Wave Parameters ▪ Amplitude ▪ Propagation velocity ▪ Frequency Spectrum ▪ Wavelength
Single and Double Parallel Wire Resistivity Probe for Annular Flow	UWM	Circumferential Mean Liquid Film Thickness Circumferential Wave Parameters ▪ Amplitude ▪ Frequency Spectrum ▪ Wavelength ▪ Propagation velocity
Hot-Film Anemometer	TSI	Mean Liquid Velocity Turbulence Void Fraction Bubble Frequency Spectrum
High-Speed Film Camera	NAC E-10	Flow Visualization
High-Speed Still Cameral	Nikon-8080	Flow Visualization

5. DEVELOPMENT OF DOUBLE-SENSOR PROBE METHOD FOR BUBBLY FLOW MEASUREMENTS

G. Kojasoy and Z. Wang

Department of Mechanical Engineering

University of Wisconsin-Milwaukee, P.O. Box 784, Milwaukee, WI 53201, U.S.A.

Abstract

The internal phase distribution of cocurrent, air-water bubbly flow in a 50.3 mm diameter transparent pipeline has been experimentally investigated by using a double-sensor resistivity probe. Liquid and gas volumetric superficial velocities ranged from 3.74 to 5.71 and 0.25 to 1.37 m/s. respectively, and average void fractions ranged from 4.30 to 22.5%. The local values of void fractions, interfacial area concentration, mean bubble diameter and bubble interface velocity, chord-length and frequency distributions were measured.

The experimental results indicate that the void fraction, interfacial area concentration and bubble frequency have local maxima near the upper pipe wall, and the profiles tend to flatten with increasing void fraction. The observed peak void fraction can reach 0.65, the peak interfacial area can go to 900-1000 m^2/ m^3, and the bubble frequency can reach a value of 2200/s. These ranges of values have never been reported for vertical bubbly flows. It is found that either decreasing the liquid flow rate or increasing the gas flow would increase the local void fraction, the interfacial area concentration and the bubble frequency.

The axial bubble interface velocity and the Sauter mean diameter profiles show a relatively uniform distribution except near the upper pipe wall, where a sharp reduction in the velocity and mean diameter occurs. The local bubble velocity and the mean diameter generally increase with the gas flow rate.

5.1 Introduction

Advances in the study of the two-phase flow increasingly require detailed internal flow structure information upon which theoretical models can be formulated. The void fraction and interfacial area are two fundamental geometrical parameters characterizing

the internal structure of two-phase flow. The void fraction represents the phase distributions and is a required parameter for hydrodynamic and thermal calculations in various industrial processes. On the other hand, the interfacial area describes the available interfacial area for the interfacial transport of mass, momentum and energy in steady and transient two-phase flows and is a required parameter for two-fluid model formulation. However, little information is currently available on these parameters, and it is limited to vertical two-phase flow configurations. Particularly, there exists very little knowledge on the local interfacial area concentration in spite of its importance in multidimen- sional two-fluid model analysis (Boure 1978; Ishii & Kocamustafaogullari 1982).

Several methods are available at present to measure interfacial area concentration in gas-liquid and liquid-liquid two-phase flows. These are photographic. light attenuation, ultrasonic attenuation, double-sensor probe and chemical absorption methods. Detailed reviews of these methods have been given by Veteau & Morel (1982), Veteau (1981) and Ishii & Mishima (1981). However, these methods for measuring the interfacial area concentration are effective only for certain idealized cases, e.g. only an average interfacial area can be measured by the chemical absorption method (Danckwerts 1970; Sharma & Danckwerts 1970; Schumpe & Deckwer 1980, 1982). The photographic and light attenuation methods cannot be used with opaque walls and are limited to transparent dispersed two-phase flows with volumetric concentrations of less than a few percent (Akita & Yoshida 1974; Yanz et al. 1986; Calderbank 1958; McLaughlin & Rushton 1973; Ohba & Itoh 1978a, b; Ohba et al. 1978). The ultrasonic method is not restricted to such conditions, and thus expands the measurement of the interfacial area concentration beyond the presently available range of fluids and non-opaque systems (Straus et al. 1986; Jones et al. 1986; Bensler et al. 1987). However, the ultrasonic attenuation method is limited to low void fraction bubbly systems and yields a chord-averaged value of the interfacial area concentration.

In view of the intention to measure local interfacial variables in a horizontal bubbly two-phase flow with local void fractions possibly ranging from 0 to 60-65%, it is inevitable that a probe method must be used. An evaluation of potential probe methods resulted in the selection of the electrical resistivity probe because of the relatively simple instrumentation and the positive results for conducting liquids presented in the literature.

In the present work, the local interfacial parameters in a horizontal bubbly two-phase flow have been studied experimentally by using the double-sensor electrical resistivity probe method. Local void fractions, interfacial area concentration, interfacial velocity, local bubble chord-length, size and frequency distributions have been measured, and the results are documented here. Furthermore, the dependence of the local parameters on other flow variables are also presented.

5.2 Double-Sensor Resistivity Probe Method

5.2.1 Measurement principle

The electrical resistivity probe method was first proposed by Neal & Bankoff (1963) for the determination of bubble size and velocity in vertical bubbly flows. Since then the double-sensor resistivity probe has been used by Park et al. (1969) and Rigby et al. (1970) for the determination of bubble parameters in three-phase fluidized beds, by Hoffer & Resnick (1975) for steady- and unsteady-state measurements in liquid-liquid dispersions. by Burgess & Calder bank (1975) for measurements of bubble parameters in single-bubbly flow. by Serizawa et al. (1975), Herringe & Davis (1976) and Liu (1989) for the study of structural parameters as well as of the structural development of gas-liquid bubbly flows, and by Veteau (1981) for the measurement of local interfacial area concentrations.

In principle, the electrical resistivity probe method consists of the instantaneous measurement of local electrical resistivity in the two-phase mixture by means of a sensor electrode. In an air-water flow the air can be considered as electrically insulating, whereas water is electrically conducting. When the sensor is in contact with the liquid, the circuit is closed. On the other hand, when it is in contact with a bubble, the circuit will open. Since.. the circuit is open or closed depending on whether the sensor is in contact with gas or liquid, the voltage drop across a sensor fluctuates between a V_{min} and a V_{max}. In the case of a double-sensor probe method, each sensor and the return electrodes are connected to their own measuring circuits and, therefore, each sensor is used independently as a phase identifying device. Furthermore, from the timing of the shift in the voltage between V_{min} and V_{max}, the time when the gas-liquid interface passes the sensor can be recorded. Therefore, two pieces of parallel and independent information

related to the phase identification and the transit time of the gas-liquid interface are obtained. A schematic diagram indicating a typical time history record of signals from a double-sensor electrical resistivity probe in bubbly flow is illustrated in figure 1(a, b).

As seen from the figure, the signals deviate from the ideal two-state square-wave signals. This deviation is largely due to the finite size of the sensor causing flow disruption and the possible deformation of the interface before the sensor enters from one phase to the other. The trailing edges are generally steeper than the leading edges. This difference is probably due to the wetting of the sensor by the residual liquid when the sensor is in the gas phase. A proper threshold voltage has to be used as a phase identification criterion. The value of the threshold voltage is determined by processing the data for void fraction and comparing it with the average void fraction measured by the quick-closing valve technique.

5.2.2 Double-Sensor Resistivity Probe Design and Signal Processing

A typical double-sensor resistivity probe is shown in figure 2. It consists of two identical stainless-steel wire sensors of 0.25 mm diameter. Their tips are 2.5 mm apart. They are completely insulated from the environment except at their tips. The tips are sharpened to a fine needle point to minimize deformation of bubbles on impact with the sensors. The two sensors are placed next to each other but insulated from each other. The body which holds the sensor acts as the return electrode. These two sensors are welded onto gold-plated wires of 0.8 mm diameter. The complete assembly fits into a probe holder from which coaxial wires run to the electronic circuit. The electronic circuit uses a 4.5 V d.c. power supply. Variable resistors are used to enable adjustment of the maximum and minimum voltage signals.

It was found that the proper distance, L, between two sensors was critical for analyzing the experimental data. Preliminary experiments were conducted to determine a proper distance between two probe tips. The distance was dictated by possible bubble size and bubble velocity. It was decided that 2.5 mm was the appropriate separation distance for the horizontal flow. It is to be noted that a very small distance results in inaccuracies in time duration measurements, since it requires very high sampling frequencies or very small bubble velocities. During the present experiments a sampling

rate of 20 kHz was used. On the other hand, if the distance is too large, then there is a strong possibility of misinterpretation of signals since multi bubble contact may occur between two signals originating from the same bubble. Even though most investigators in the past have used a distance of 5 mm in their vertical bubbly flow experiments, it was found that 5 mm was too large for the horizontal two-phase flow experiments, since maximum packing of bubbles almost always occurs toward the top of the pipe, which requires a smaller separation distance.

As illustrated in figure l(a, b), the experimental data was obtained in the form of a voltage signal I as a function of time from the front and rear sensors of a probe. The correct interpretation of data involves the identification of gas and liquid phases. The first step is to set a threshold voltage at which the signal representing the beginning of the gas phase for an isolated bubble can be identified. However, it was observed that the threshold voltage level may drift during the experiments due to the probe contamination. This difficulty was overcome by dividing the data into several blocks within the total sampling time domain. As an isolated bubble contacts the previously wetted probe, output signals increase from the value of a near V_{min} to near a V_{max}, and decrease abruptly to the value of V_{min} as the bubble moves away. Identification of such a bubble is straightforward. However, for closely compacted bubbles that are observed in a horizontal bubbly flow, the time duration of the liquid phase contacting a probe sensor is very short. Hence, before the sensor tip becomes totally wet, it could be in contact with another bubble. In this case the voltage signal varies between a local minimum above the threshold voltage and the gas level. To identify such a bubble the threshold voltage and the slope of the signal was used in combination for distinguishing phases. A linear programming method was developed to reach a desired convergence.

After distinguishing the phases, the next step is the identification of signals originating from the same bubble. In this case, the right selection of two closely corresponding signals from each sensor is important, since the two signals detected by the front and rear sensors do not always correspond to the same bubble, and the residence time intervals of the gas and or liquid phases at the sensors are not exactly the same. The signal validation was made by judging whether the following series of conditions are satisfied:

1. For a forward motion of the bubbles, the front sensor signal rises or falls before the rear sensor does. Therefore, referring to figure 1, the following condition should be satisfied:

$$t_{f(2j-1)} < t_{f(2j)} \text{ and } t_{r(2j-1)} < t_{r(2j)}; \quad j=1, \ldots, N \tag{1}$$

where f and r, respectively, denote the front and rear sensors; $t_{(2j-1)}$ is the time the front and rear sensor tips enter into the bubble and $t_{(2j)}$ is the time the sensor tips enter into the liquid phase. N is the number of bubbles passing through a given sensor in the total sampling time T.

2. The residence time of a bubble, i.e. the width of the signals, the amplitude and the height above the threshold voltage of the signals for the front and rear sensors should be comparable to ensure that both sensors detect the same bubble. Hence, the following conditions should be also satisfied:

$$t_{f(2j)} - t_{f(2j-1)} \approx t_{r(2j)} - t_{r(2j-1)}; \qquad j=1,\ldots, N$$

$$V_f(t_{f(2j)}) - V_f(t_{f(2j-1)}) \approx V_r(t_{r(2j)}) - V_r(t_{r(2j-1)}); \qquad j=1,\ldots, N$$

and

$$V_f(t_{f(2j-1)}) - V_{fT} \approx V_r(t_{r(2j-1)}) - V_{rT}; \quad j = 1,\ldots, N \tag{2}$$

3. The time difference between the front and rear sensor should be limited by the following condition: The time difference between the front and rear sensor should be limited by the following condition:

$$\Delta t_{min} \leq t_{r(2j)} - t_{f(2j)} \leq \Delta t_{max}$$

$$\Delta t_{min} \leq t_{r(2j-1)} - t_{f(2j-1)} \leq \Delta t_{max} \tag{3}$$

where Δt_{min} and Δt_{max} are the time limits corresponding to the maximum and minimum bubble velocities, respectively. Therefore, Δt_{min} and Δt_{max} should be determined by the combination of the distance between two sensor tips, L, and the flow conditions such as superficial velocities. In our experiments L is fixed to be 2.5 mm, and the flow conditions are limited by $0.25 \leq \langle j_g \rangle \leq 1.59$ m/s. In view of this physical-reasoning, Δt_{min} is equated to the smallest data acquisition time

interval, i.e. 5 x 10^{-5} s, whereas Δt_{max} is taken as 40 time intervals, which becomes 2 x 10^{-3} s for a sampling frequency of 20 kHz. For our experimental conditions and probe distance, these values are believed to be appropriate to cover a relatively wide range of possible bubble velocities.

5.2.3 Local Void Fraction

The local void fraction ε at any location r can be obtained by either front or rear probe sensor tips. It is defined as a time average of the concentration $\delta(r,t)$ by

$$\varepsilon(r) = \lim_{T\to\infty} \frac{1}{T} \int_0^T \delta(r,t)dt \tag{4}$$

where δ as a function of space coordinate r and time t, equals one if the probe tip is in gas and zero if the tip is in liquid phase. As the signal is given in discrete form, Eq. (4) can be written from Figure 1 either for the front or rear probe as follows:

$$\varepsilon(r) = \frac{1}{T} \sum_{j=1}^{N} (t_{2j} - t_{2j-1}) \tag{5}$$

5.2.4 Local Bubble Interface Velocity and Velocity Spectrum

The local bubble interface velocity is determined from the signals of two sensors. A bubble interface which contacts the first sensor will in general subsequently contact with the second sensor. The time delay between the two contact signals is a measure of the bubble interface velocity. The bubble interface velocity component in the axial direction at any location r can be expressed as

$$u_b = \frac{L}{\Delta t} \tag{6}$$

where Δt is the time delay and L is the distance between two sensor tips.

The multichannel method and cross-correlation techniques are used in the determination of the time delay. In the multichannel method, the bubble transport time signals are processed through a computer program to identify signals from the same bubble. This process thus eliminates miscounting of bubbles. The interface velocity for a specified bubble is then given by

$$u_{bj} = \frac{L}{\Delta t_{(2j-1)}}, \qquad j = 1, 2, \cdots, N \tag{7}$$

where the index j refers to a j'th bubble. Then using the multichannel method, the bubble velocity signals are proportionally transferred into equally spaced channels. The local bubble velocity component in the flow direction, $u_b(r)$, and the standard deviation of the bubble velocity spectrum, $s(r)$ are given by

$$u_b(r) = \frac{\sum_{k=1}^{N_k} n_k u_{bk}(r)}{\sum_{k=1}^{N_k} n_k} \tag{8}$$

$$S(r) = \left[\frac{\sum_{k=1}^{N_k} n_k [u_{bk}(r) - u_b(r)]^2}{\sum_{k=1}^{N_k} n_k} \right]^{1/2} \tag{9}$$

where u_{bk} is the instantaneously measured local axial bubble velocity in the k'th channel, n_k is the total count for the k'th channel, and N_k is the number of channels.

The cross-correlation function, which gives the most probable time delay, is also computed. If $u_f(t)$ and $u_r(t)$ are two signals from the front and the rear sensors respectively, then the cross-correlation function $Fu_fu_r(\Delta t_m)$ is given by

$$F_{u_f u_r}(\Delta t_m) = \frac{1}{T} \int_0^T u_f(t - \Delta t_m) u_r(t) dt \tag{10}$$

The maximum value of $Fu_fu_r(\Delta t_m)$ yield the most probable time delay Δt_m, from which the bubble velocity is determined through the use of Eq.(6).

5.2.5 Local Interfacial Area Concentration

The local interfacial area concentration at any spatial location r is given by Ishii[3] as

$$a_i(r) = \frac{1}{T} \sum_{j=1}^{N_i} \frac{1}{\left| \vec{v}_i \cdot \vec{n}_i \right|_j} \tag{11}$$

where T, v_i and n_i are the sampling time, interfacial velocity and unit normal vector of the interface. N_i is the total number of interfaces passing within the sampling time, T.

Physically this local interfacial area concentration represents the probability of the interface occurring at that point.

The form of Eq.(11) indicates a possible measurement technique for determining the local interfacial area concentration. Basically it requires the measurement of the interfacial velocity and the surface direction at the point. A simplified double-sensor resistivity probe suggested by Herringe & Davis (1976), Veteau (1981) and Veteau & Charlot (1981) assumes a unidirectional flow of spherical particles. However, considering the velocity fluctuations due to turbulences or fluid particle motions, Kataoka et al. (1985) suggested an improved statistical model. In this model it was assumed that the direction of the interface velocity fluctuates within a maximum angle of θ_0 from the axial direction with equal probability. Then this angle θ_0 was related to the root-mean-square (r.m.s.) of fluctuating components of the velocity which can be measured by the same double-sensor probe simultaneously with the measurement of the sensor passing velocity u_{bj},. Then the local interfacial area concentrations are given by

$$a_i(r) = \left\{ \frac{2}{T} \sum_{j=1}^{N_i} \frac{1}{|u_{bj}(r)|} \right\} C(\alpha_0) = \frac{2}{LT} \sum_{j=1}^{N_i} \left[\Delta t_{(2j-1)} + \Delta t_{(2j)} \right] \tag{12}$$

where

$$C(\alpha_0) = \left\{ 1 - \cot(\frac{\alpha_0}{2}) \ln[\cos(\frac{\alpha_0}{2})] - \tan(\frac{\alpha_0}{2}) \ln[\sin(\frac{\alpha_0}{2})] \right\}^{-1} \tag{13}$$

The angle α_0 is given approximately by

$$\frac{\sin 2\alpha_0}{2\alpha_0} \approx \frac{1 - S^2/u_b^2}{1 + 3S^2/u_b^2} \tag{14}$$

where S is the root mean square of the fluctuating component of the sensor passing velocity, which is conveniently expressed by Eq. (9).

Knowing the value of α_0, the time-averaged local interfacial area concentration can be calculated from the measured values of $u_b(r)$ at any location r. The measured value of $u_b(r)$ is given by Eq. (8), whereas the value of α_0 can be estimated from measured values of statistical parameters of interfacial velocity as given by Eq. (14). It is to be noted that the root mean square of fluctuations of the axial component of interfacial velocity is assumed to be the root mean square of two other velocity component

fluctuations, i.e., unidirectional assumption. Studies carried out by Hilgert and Hofmann [78] on bubble columns in a vertical pipe using an ultrasonic Doppler technique have shown that the magnitude of axial component root mean square bubble velocity fluctuation is nearly equal to the radial component of root mean square of fluctuation of bubble velocity. In the present study Eq. (12) was used to determine the local interfacial area concentration for the horizontal bubbly flow experiments.

5.3 Experimental Setup and Procedure

5.3.1 Description of the Flow Loop

A horizontal flow loop was designed and built for the purpose of investigating the interfacial structure of horizontal two-phase flow. The overall loop schematic is illustrated in figure 3. The loop basically consists of various flanged lengths of 50.3 mm i.d. circular Pyrex glass tubings with pressure tabs installed between them. However, smaller or larger diameter test sections can be easily fitted to the loop. The entire test section is about 15.4 m in length, and it is all transparent, so that flow visualization, high-speed photography and high-speed cinematography are possible. It is designed such that various local instrumentations for two-phase flow measurements and different mixing chambers can be easily accommodated.

The air and water are used as coupling fluids. The air to the test section is supplied from the University of Wisconsin-Milwaukee central air system. It is, however, regulated through a 0.95 m^3 capacity high-pressure storage tank, and metered by a series of turbine flow meters. The water is recirculated. It is pumped from a 1.9 m^3-capacity storage tank by a stainless-steel centrifugal pump and regulated from 0 to 100% of the pump capacity by a transistor inverter. The water flow rate is measured by a series of paddlewheel flow meters assembled in a parallel configuration. As shown in figure 4 the air enters the mixing chamber from a 90° vertical leg and is injected into the water flow through a cylindrical porous media of 100 μm porosity to achieve a uniform mixing and the quick development of a bubbly two-phase flow pattern. The two-phase mixture from the test section is directed to an air-water separator. The air is vented to the atmosphere, and the water is returned to the water storage tank.

The last 1.5 m of the test section incorporates two quick-closing valves which are used for average void fraction measurements. These valves, which are pneumatically operated and electronically controlled, have a very rapid response time (in the order of milliseconds) and are synchronized through a common electrical switch to ensure simultaneous operation. The distance between the valves is long enough to minimize any experimental error. The system is protected against pressure surges.

Pressure transducers of the diaphragm type are utilized for both absolute pressure and differential pressure measurements. The test-section differential pressure is measured at six intervals with high-frequency transducers located 1.55 m apart. The absolute pressure transducers are located at two locations in the test section, 6.70 and 8.22 m downstream of the mixing chamber, respectively.

5.3.2 Experimental Procedure

The experiments were carried out under fully developed bubbly flow conditions by variations in the liquid flow rate, gas flow rate and the radial position of the probe. The superficial liquid velocities ranged from 3.74 to 5.71 m/s, and the superficial gas velocities covered a range from 0.25 to 1.37 m/s. Details of the experimental conditions are summarized in table 1. At each fixed liquid superficial velocity, the gas superficial velocity was increased as long as the flow pattern was bubbly. Evidence of slug flow was indicated in the output signals and discarded from evaluation. Liquid superficial velocities higher than indicated above could not be reached due to pressure limitations of the Pyrex glass test loop. During the operation of the quick-closing valves, the pressure reached sizable proportions of the loop pressure limitations. The temperature of the water was maintained at room temperature by adding tap water to the storage tank.

The mounting and traversing mechanism for the resistivity probe is shown in figure 5. The probe was inserted through a probe support located at the bottom of a rectangular Plexiglas test section. The test section was 15 cm in length, 15 cm in height and 7.5cm in width. A Vernier, with graduations to an accuracy of 0.0254 mm, was used to traverse the probe in a direction perpendicular to the axis of the tube; 23 locations were selected through the pipe diameter of 50.3 mm. The increments were smaller as the probe traversed toward the wall at the upper half of the tube.

For each preset experimental condition the data, including 23 probe locations, pressure drops at 6 intervals and the absolute system pressure at 2 locations, were recorded. At the end of each experimental run the quick-closing valves were operated to measure average void fraction. Experiments were interfaced with a data acquisition system utilizing a Zenith PC/AT computer with a Metrabyte DASH-16F 16-channel multifunction high-speed analog/digital I/O expansion board, and LabtechNotebo.ok software.

Due to the large volume of data generated, the sampling rate was kept at 20 kHz for each sensor, and the sampling time was 1 s. It was found that this combination provided a sufficiently large volume of data for any statistical analysis. It is to be noted that the total sampling time may seem very short when compared to earlier investigations carried out on vertical bubbly two-phase flows. However, it is also to be noted that in a horizontal bubbly two-phase flow the velocities are very high and thus it becomes essential to have a sampling rate as high as possible to record all the bubbles. This simultaneously leads to a shorter sampling time due to overall limitations on the data acquisition system.

5.4 Experimental Results and Discussion

5.4.1 Local Void Fraction Distribution

The local void fractions were obtained independently with both front and rear sensors of the probe using the average void fraction as a convergence criterion to decide the threshold voltage. Then Eq.(5) was used to calculate the local void fractions. A sample of local void fraction distributions obtained from both sensors is shown in figure 6, and figures 7a, 7b, 8a and 8b illustrate local void fraction profiles for several flow parameter values of $\langle j_g \rangle$ and $\langle j_f \rangle$. In figures 7a, 7b, 8a and 8b only the front sensor measurements are used. The following observations can be made from these figures:

(a) The void fraction distributions obtained by front and rear probes are surprisingly close to each other, indicating the consistency in the signal processing methodology. Although signal validation was made to identify the interfaces by a series of conditions expressed by Eqs.(1)-(3), it might still be possible that some bubbles contact only the front sensor and escape from the rear sensor. As a result,

the front sensor tends to give a slightly higher void fraction than the rear sensor, as barely observed in figure 6.

(b) It is evident from these figures that the bubbles tend to migrate toward the upper wall under the dominating influence of buoyancy force. Thus, the void fraction under all test conditions generally showed a distinct peak near the top wall at about $r / R \approx 0.8$ to 0.9. This range corresponds to that at a 2.5-5 mm distance from the wall. When these values are compared with the observed Sauter mean bubble diameter of 2-5 mm, as documented in section 4.1, the geometry seems to explain the steep decrease in the void fraction. Besides the geometric effects, the possibility of probe interference toward the wall and the increased hydraulic resistance of the liquid path between the bubble and wall may also contribute to the sharp decline in the void fraction. This phenomenon is identical to the one that has been observed in vertical bubbly two-phase flows by Veteau (1981), Serizawa et a/. (1975), Wang (1985) and Wang et al. (1987).

(c) Although the void fraction distributions tend to flatten as the average void fraction increases, the distinct peak always occurs in relatively the same location. The fact that the peak void fraction in all cases never exceeds 0.60-0.65 indicates that the maximum packing exists in the channel. Above the maximum packing limit, coalescence of bubbles occurs resulting in larger slug bubbles.

(d) The effect of increasing the gas flow rate is to increase the average void fraction and to flatten the void fraction distribution toward the bottom channel wall. Again, there was no noticeable change at the peaking positions.

(e) The effect of increasing the liquid flow rate is to decrease the average void fraction. However, there were no noticeable differences in the peaking positions, but there was a significant decrease in the value of the maximum void fraction.

5.4.2 Local Interfacial Area and Bubble Size Distributions

Figures 9a, 9b, 10a and 10b show the local interfacial area concentration profiles based on Eq.(2). It is interesting to note that the interfacial area concentration distributions have similar characteristics to those of the void fraction distributions. The interfacial area reaches a maximum at about the same location as the void fraction peak.

Increasing the gas flow or decreasing the liquid flow would increase the local and overall interfacial area concentration and tend to flatten the interfacial area concentration profile.

It is important to note that the local interfacial area concentration in horizontal bubbly two-phase flow may become as high as 1000 m^2/m^3 toward the top of the channel. This range of the interfacial area concentration has never been reported for vertical bubbly flow. The higher values suggest that in this type of bubbly flow the interfacial transport of mass, momentum and heat transfer is much higher near the top portion of the tube wall.

The interfacial area concentration is strongly affected by bubble sizes, since the surface-to- volume ratio of a small bubble is larger than that of a larger bubble. Furthermore, when the bubbles are not spherical, the volume-to-surface area ratios depend on the shape of the bubble at the same void fraction.

The profiles of the interfacial area concentration and the void fraction can be used to determine the Sauter mean bubble diameter variations along the cross section. The definition of the Sauter mean bubble diameter assumes spherical bubbles and is given by

$$D_{sm} = \frac{\sum_{k=1}^{N_k} n_k D_k^3}{\sum_{k=1}^{N_k} n_k D_k^3} \tag{15}$$

where n_k is the number of bubbles of size D_k and N_k is the total bubble size classes.

On the other hand, the void fraction and the interfacial area concentration can be expressed. respectively, as

$$\varepsilon(r) = \frac{\sum_{k=1}^{N_k} n_k V_k}{V_T} = (\frac{\pi}{6}) \frac{\sum_{k=1}^{N_k} n_k D_k^3}{V_T} \tag{16}$$

and

$$a_i(r) = \frac{\sum_{k=1}^{N_k} n_k A_k}{V_T} = \frac{\pi \sum_{k=1}^{N_k} n_k D_k^2}{V_T} \tag{17}$$

where V_k is the volume of a typical bubble of size D_k in a given class k, A_k is the surface area of a typical bubble in the same class size, and V_T is the total mixture volume.

From Eqs.(15), (16) and (17) it can be shown that

$$D_{sm}(r) = \frac{6\varepsilon(r)}{a_i(r)} \qquad (18)$$

Based on Eq.(8), typical Sauter mean diameter distributions are illustrated in figure 11(a, b) at various gas as well as various liquid fluxes. From this figure it may be observed that the Sauter mean diameters are in the range of 2-5 mm, depending on the location and flow conditions. The profiles show relatively small variations over most of the flow channel cross section except near the wall region. The bubble size tends to reduce close to the wall region. Generally there is no double size peaking found, as reported for vertical bubbly flow by Michiyoshi & Serizawa (1986), Matsui (1984) and Liu (1989). The bubble diameter generally shows an increase with the gas flow rate, although the influence is not significant. By comparing two figures it may be observed that increasing liquid flow rate results in a more homogeneous distribution of the bubbles.

Figure 12 illustrates the variation in the average interfacial area concentration as a function of the averaged void fraction. Figure 12 is not intended to be a correlation between $<a_i>$ and $<\varepsilon>$. It is obvious from Eq.(18) that besides the void fraction, the bubble size also has a very important effect in determining the interfacial area concentration. However, considering small variations in the mean diameter, the behavior observed in figure 12 is not surprising.

5.4.3 Local Bubble Interface Velocity

The local bubble interface velocity in the axial direction was determined from the signal of two resistivity probe tips using Eqs.(6) and (8). Samples of the mean velocity distributions calculated from the bubble velocity spectrum and also from the cross-correlation method are shown in figure 13(a, b). The bubble velocity spectrum at every local position covered a range of bubble velocities approximately following a Poisson distribution. A typical velocity spectrum is also illustrated in figure 14(a, b). The following observations can be made from these figures.

There was no evidence to suggest a proportionate correspondence between local void fraction and bubble velocity distributions, as suggested by Van der Welle (1985) and Beattie (1972) for vertical flow. There were no peaks in bubble velocity profiles corresponding to those observed toward the top wall peaking void and interfacial area

concentration profiles. On the contrary, the velocity profiles show a fairly uniform distribution over a large portion of the flow area, except for the wall region.

It can be observed that an increase in either the liquid flow rate or gas flow rate increases the bubble velocity. The mean bubble velocity near the upper wall decreases, indicating the same tendency as that found in vertical bubbly flows.

Verification of the measured velocities was undertaken by comparing the averaged values u_b and u_G based on the probe measurements and the measured gas volumetric flow rates Q_G, respectively. u_b and u_G are defined as follows:

$$\overline{u}_b \equiv \frac{\int_A \varepsilon \; u_b \, dA}{\int_A \varepsilon \, dA} = \frac{< \varepsilon \, u_b >}{< \varepsilon >} = \frac{< j_b >}{< \varepsilon >} \tag{19}$$

$$\overline{u}_G \equiv \frac{\dot{Q}_G}{< \varepsilon > A} = \frac{< j_G >}{< \varepsilon >} \tag{20}$$

where the brackets, < >, denote area averaged values from integration, and Q_G is the volumetric flow rate of the air.

The corresponding values of the velocity from Eq.(19) were determined by numerical integration, and the values are listed in Table 1. Furthermore, the deviations of $\overline{u}_b$ with respect to $\overline{u}_G$ and of $<j_b>$ with respect to $<j_G>$ which are, respectively, defined as

$$\Delta \overline{u}_b \equiv \frac{\overline{u}_b - \overline{u}_G}{\overline{u}_G} \times 100 \; \% \tag{21}$$

and

$$\Delta < j_b > = (\frac{< j_b > - < j_G >}{< j_G >}) \times 100\% \tag{22}$$

are also listed in Table 1. The mean deviation between the values obtained from integration of the local flow parameters and those obtained from flow rate measurements is ±5.7%. The integrated values are generally lower. This may be explained partially by the fact that we expect the measured values of velocity to be slightly low, both because of the possible deflection of the bubbles when they hit the probe tips and because of missing the smallest size bubbles. In all cases, the difference is < 12% of the value calculated

from the overall gas flow rate. The comparison justifies the reliability of the double-sensor resistivity probe technique for measuring local void fractions and axial velocity components.

Based on the bubble velocity and void fraction measurements, a drift-flux presentation is illustrated in figure 15. As suggested by Ishii (1977) and Wallis (1969), it is given by

$$\bar{u}_G = \bar{u}_{Gj} + C_0 < j > \tag{23}$$

where $\bar{u}_{Gj}$ is the weighted mean drift velocity of the gas phase and Co is the distribution parameter. Figure 15 indicates a linear relationship between $\bar{u}_{Gj}$ and <j>, which is used to determine $\bar{u}_{Gj}$ and Co. Regression analysis on the data yields Co= 1.05 and $\bar{u}_{Gj}$=0.13m/s. It is to be noted that such a representation was obtained from our air-water bubbly flow data which is far from the origin. Therefore, it has the limitations of our data range. It should be checked further for a wider data range.

5.4.4 Bubble Chord-Length and Frequency Distributions

The local bubble chord-length was determined from the bubble residency time measured from the front probe, τ, and from the bubble velocity, u_b, as follows:

$$l_{cl} = u_b \tau \tag{24}$$

A typical bubble chord-length distribution is illustrated in figure 16(a, b). For each experiment, this type of figure has been produced to verify the order of Sauter mean diameter values obtained from Eq.(18).

The local bubble impaction rate or bubble frequency, which is the number of bubbles detected by the front probe in unit time at a specific location, can also be obtained from the experimental data. A typical bubble impaction rate distribution is shown in figure 17(a, b). It is important to note from these figures that the bubble impaction rate distribution has the same behavior as that of the local void fraction distribution. Due to the buoyancy effect, the uniformly generated and distributed bubbles move into the upper sections and crowd together near the top wall of the horizontal flow channel. A distinct peak of bubble impaction rates close to the top wall can be observed in all flow conditions, even though the bubble impaction rate profile tends to flatten as

the average void fraction is increased. A very high bubble frequency on the order of 2200/s may be observed toward the top of the tube. This might explain the high void fractions and interfacial areas observed in the present horizontal bubbly flow experiments.

5.5 Summary and Conclusions

The internal phase distribution of cocurrent, air-water bubbly flow in a 50.3 mm dia transparent pipeline has been experimentally investigated by using a double-sensor resistivity probe technique. Liquid and gas volumetric superficial velocities ranged from 3.74 to 5.71 and 0.25 to 1.37 m/s, respectively, and average void fractions ranged from 4.30 to 22.5%. The local values of void fraction, interfacial area concentration, mean bubble diameter and bubble interfacial velocity, chord-length and frequency distributions were measured.

The experimental results indicated that the void fraction, interfacial area concentration and bubble frequency have local maxima near the upper pipe wall, and that the profiles tended to flatten with increasing void fraction. For the horizontal bubbly flow, the observed peak void fraction can reach 0.65, and the peak interfacial area concentration can go up to 1000 m^2jm^3, whereas the bubble frequency may reach a value of 2200/s. It was found that either decreasing the liquid flow at constant gas flow or increasing the gas flow at a fixed liquid flow would increase the local void fraction, interfacial area concentration 'and the bubble frequency.

The axial bubble interface velocity showed a relatively uniform distribution except near the upper pipe wall, where a sharp reduction in velocity was found. The local bubble interface velocity and the bubble velocity turbulent fluctuations increase with the gas flow.

Using the relation between the local interfacial area concentration, void fraction and the Sauter mean diameter of bubbles, the mean bubble diameter distributions were calculated. It was observed that the mean bubble diameters ranged from 2 to 5 mm, depending on the location and flow conditions. The bubble diameter generally increases with the gas flow rate at a given liquid flow rate, although the effect was not found to be significant.

Finally, it is to be noted that the lateral phase distribution for horizontal flow and bubble size distribution are strongly affected by inlet conditions and boundaries. In the present studies, the mixing chamber that is described in section 3.1 was fixed throughout the experiments, and probe tracing was done along the vertical axis of the pipe. Therefore, it is recommended that future work include a series of experimental studies to understand how inlet conditions and wall affect the lateral phase distribution for horizontal flow.

Acknowledgement

The work reported in this paper was supported by a grant from the U.S. Department of Energy (DF-FGO2-87ER13764).

Nomenclature

- A Area
- a_i Interfacial area concentration
- D Bubble diameter
- D_{sm} Sauter mean bubble diameter
- F Cross correlation function
- j Superficial velocity
- L Distance between two sensor tips
- N Number of bubbles passing through a given sensor in a sampling time T
- n Unit normal vector
- $\dot{Q}_G$ Volumetric flow rate of gas
- r Radial position
- S Standard deviation of bubble velocity spectrum
- T Sampling time
- t Time
- u Axial velocity
- V Voltage
- $\vec{v}_i$ Interfacial velocity vector
- Δt_{min} Time limit corresponding to the minimum bubble velocity

Δt_{max} Time limit corresponding to the maximum bubble velocity

Greek Symbols:

ε Void fraction

Subscripts:

b Bubble

f Front

G Gas

k Identifies the k'th channel

r Rear

References

1. AKITA, K. & YOSHIDA, F., 1974, Bubble size, interfacial area, and liquid-phase mass transfer coefficient in bubble columns. *Ind. Engng Chern. Process Des. Dev.* 13, 84-90.
2. BEATTIE, D. R. H.,,1972, Two-phase flow structure and mixing length theory. *Nuc/. Engng Des.* 2, 46-64.
3. BENSLER. H. P., DELHAYE, J. M. & FAVREAU, C., 1987, Measurement of interfacial area in bubbly flows by means of ultrasonic technique. Presented at the *Natn. Heat Transfer Conf.,* Pittsburgh, Pa.
4. BOURE, J. A., 1978, Mathematical modeling of two-phase flows. In *Proceedings of CSNI Specialist Meeting,* Vol. 1 (Edited by BANERJEE, S. & WEAVER, K. R.), p. 85. AECL, Toronto, Ontario.
5. BURGESS, J. M. & CALDERBANK, P. H., 1975, The measurement of bubble parameters in two-phase dispersions-I. The development of an improved probe technique. *Chern. Engng Sci.* 30, 743-750.
6. CALDERBANK, P. H., 1958, Physical rate processes in industrial fermentation, Parts I and II. *Trans. Inst. chern. Engrs* 36, 443-463.
7. DANCKWERTS, P. V., 1970, *Gas-Liquid Reactions.* McGraw-Hill, New York.

8. HERRINGE, R. A. & DAVIS. M. R., 1976, Structural development of gas-liquid mixture flows. J. *F/uid Mech.* 73, 97-123.
9. HILGERT. W. & HOFMANN, H., 1986, Characterization of gas phase flow in bubble columns of low superficial gas velocities with the aid of ultrasonic Doppler techniques. *Gen. Chem. Engng* 9, 180-190.
10. HOFFER, M. S. & RESNICK, W., 1975, A modified electroresistivity probe technique for steady- and unsteady-state measurements in fine dispersions-I. Hardware and practical operating aspects. *Chem. Engng Sci.* 30, 473-480.
11. ISHII, M. & KOCAMUSTAFAOGULLARI, G., 1982, Two-phase flow models and their limitations. Presented at the *NATO Advanced Research Wkshp on Advances in two-phase Flow and Heat Transfer,* Spitzingsee, Fed. Rep. Germany.
12. ISHII., M. & MISHIMA, K. ,1981, Study of two-fluid model and interfacial area. Argonne National Lab. Report ANL-80-111.
13. JONES, S. W., A. AMBLAND, A. & FAVREAU, C.,1986, Interaction of an ultrasonic wave with a bubbly mixture. *Expts Fluids* 4, 341-349.
14. KATAOKA, I., ISHII, M. & SERIZAWA, A. ,1985, Interfacial area in two-phase flow; formulation and measurement. Presented at the *23rd Natn. Heat Transfer Conf ASME,* Denver, Colo.
15. Liu, T. T.-J., 1989, Experimental investigation of turbulence structure in two-phase bubbly flow. Ph.D. Thesis, Northwestern Univ., Evanston, Ill.
16. MATSUI, G., 1984, Characteristic structure of upward bubble flow under the same flow rate conditions. Presented at the *Japan-U.S. Semin. on Two-phase Flow Dynamics,* Lake Placid, N.Y.
17. McLAUGHLIN. C. M. & RUSHTON, J. H., 1973, Interfacial areas of liquid-liquid dispersions from light transmission measurements. *AIChE Jl, 19,* 813-822.
18. MICHIYOSHI, I. & SERIZAWA, A., 1986, Turbulence in two-phase bubbly flow. *Nuc/. Engng Des.* 95, 253-267.
19. NEAL, L. G. & BANKOFF, S. G., 1963, A high resolution resistivity probe for determination of local void properties in gas-liquid flow. *AIChE* Jl, 9, 490--494.

20. OHBA, K. & ITOH, T., 1978a, Light attenuation technique for void fraction measurement in two-phase bubbly flow-I. Theory. *Techno/. Rep. Osaka Univ.* 28(1448), 487-494.
21. OHBA, K. & ITOH, T., 1978b, Light attenuation technique for void fraction measurement in two-phase bubbly flow-II. Experiment. *Techno/. Rep. Osaka Univ.* 28(1449),495-506.
22. OHBA, K., ITOH. T. & YUHARA, T., 1978, Light attenuation technique for void fraction measurement in two-phase bubbly flow-III. Effect of some parameters on accuracy of measurement. *Techno/. Rep. Osaka Univ.* 28(1450), 507-516.
23. PARK, W. H., KANG, W. K., CAPES, C. E. & OSBERG, G. L., 1969, The properties of bubbles in fluidized beds of conducting particles as measured by an electroresistivity probe. *Chem. Engng Sci.* 24, 851-865.
24. RIGBY, G. R., VAN BLOCKLAND, G. P., PARK, W. H. & CAPES, C. E., 1970, Properties of bubbles in three phase fluidized beds as measured by an electroresistivity probe. *Chem. Engng Sci.* 25,
25. 1729-1741.
26. SCHUMPE, A. & DECKWER, W. D., 1980, Analysis of chemical methods of determination of interfacial area in gas-in-liquid dispersions with non-uniform bubble size. *Chem. Engng Sci.* 35, 2221-2233.
27. SCHUMPE, A. & DECKWER, W. D. 1982 Comparison of the photographic and the sulfite oxidation method for interfacial area determination in bubble columns. *Chem. Engng Commun.* 17, 313-324.
28. SERIZAWA, A., KATAOKA, I. & MICHIYOSHI, I., 1975, Turbulence structure of air-water bubbly flow-I. Measuring techniques. *Int. J. Multiphase Flol1,* 2, 221-233.
29. SHARMA, M. M. & DANCKWERTS, P. V., 1970, Chemical methods for measuring interfacial area and mass transfer coefficients in two-fluid systems. *Br. chem. Engng* 15, 522-528.
30. STRAUS, A. A., VON STOCKER, U. & REILLY, P. J., 1986, Measurement of interfacial areas in aerobic fermentations by ultrasonic pulse transmission. *Biotechnol. Bioengng* 28, 1302-1309.

31. VAN DER WELLE, R., 1985, Void fraction. bubble velocity and bubble size in two-phase flow. *Int.* I *J. Multiphase Flow* 11, 317-345.

32. VETEAU, J. M., 1981, Contribution a l'etude des techniques de measure de l'aire interfacial dans les ecoulements a bulles. Sc.D. Thesis, National Grenoble Polytechnic Inst., France.

33. VETEAU, J. M. & CHARLOT, R., 1981, Techniques de measure des aires interfacials dans les ecoulements a bulles-III. Comparison de la methode d'attenuation d'un faisceau. Lumineux et d'une Methode Locale. CEA Report CEA-R-5122, France.

34. VETEAU, J. M. & MOREL, Y., 1982, Techniques de measures des aires interfacials dans les ecoulements a bulles-II. La methode chimique. CEA Report CEA-R-5092, France.

35. WALLIS, G. B., 1969, *One-dimensional Two-phase Flow,* pp. 261-263. McGraw-Hill, New York.

36. WANG, S. K., 1985, Three-dimensional turbulence structure measurements in air water two-phase flow. Ph.D. Thesis, Rensselaer Polytechnic Inst., Troy, NY.

37. WANG, S. K., LEE, S. J., JONES, O. C. JR and LAHEY, R. T. JR , 1987, Three-dimensional turbulence structure and phase distribution measurements in bubbly two-phase flow. *Int. J. Multiphase Flow, 13,* 327-340.

38. YANZ, N. S., SHEN, Z. Q., CHEN, B. H. & McMILLAN, A. F., 1986, Pressure drop, gas holdup, and interfacial area for gas-liquid contact in karr columns. *Ind. Engng Chem. Process Des. Dev.* 25, 660-664.

Table 1. Experimental conditions and comparisons of velocities

No.	$\langle j_f \rangle$ (m/s)	$\langle \epsilon \rangle$ (%)	$\bar{u}_b$ (m/s)	$\bar{u}_G$ (m/s)	$\Delta\bar{u}_b$ (%)	$\langle j_b \rangle$ (m/s)	$\langle j_G \rangle$ (m/s)	$\Delta\langle j_b \rangle$ (%)
1	3.74	5.70	4.01	4.39	−8.9	0.23	0.25	−8.8
2	3.74	10.50	4.49	4.86	−7.6	0.471	0.51	−7.6
3	3.83	15.18	4.50	4.71	−4.4	0.68	0.72	−5.6
4	3.74	18.30	5.10	5.63	−0.4	0.93	1.03	−9.7
5	4.05	6.48	4.25	4.06	−4.7	0.27	0.26	3.8
6	4.05	10.70	4.69	4.77	−1.7	0.50	0.51	−1.9
7	4.05	15.40	5.02	4.94	−1.6	0.77	0.76	−1.3
8	4.06	18.70	5.53	5.56	−0.5	1.03	1.04	−0.9
9	4.05	21.00	5.89	6.38	−7.7	1.23	1.34	−8.2
10	4.45	4.70	4.64	5.15	−9.9	0.22	0.24	−9.9
11	4.36	10.30	4.89	4.95	−1.2	0.50	0.51	−1.6
12	4.36	14.10	5.41	5.53	−2.1	0.76	0.78	−2.5
13	4.36	21.50	6.32	6.09	3.7	1.36	1.31	3.8
14	4.36	22.50	6.37	7.07	−9.9	1.43	1.59	−10.1
15	4.78	4.30	5.21	5.88	−11.4	0.22	0.25	−10.4
16	4.67	8.70	5.39	6.09	−11.5	0.47	0.53	−11.3
17	4.70	14.30	5.77	5.52	4.5	0.82	0.79	3.8
18	4.77	18.25	6.17	6.52	−5.4	1.12	1.19	−5.6
19	5.10	4.34	5.49	5.61	−2.1	0.24	0.24	0.0
20	5.10	8.02	5.60	6.05	−7.9	0.44	0.48	−6.4
21	4.98	13.90	6.32	5.76	9.7	0.88	0.80	10.0
22	4.98	20.40	6.26	6.57	−4.7	1.27	1.34	−5.2
23	5.29	12.50	6.78	6.40	5.9	0.849	0.80	−6.1
24	5.29	20.80	7.30	6.49	12.4	1.516	1.35	12.3
25	5.71	10.60	7.03	6.75	4.1	0.75	0.71	4.9
26	5.60	21.80	6.04	6.43	−6.0	1.31	1.37	−5.3

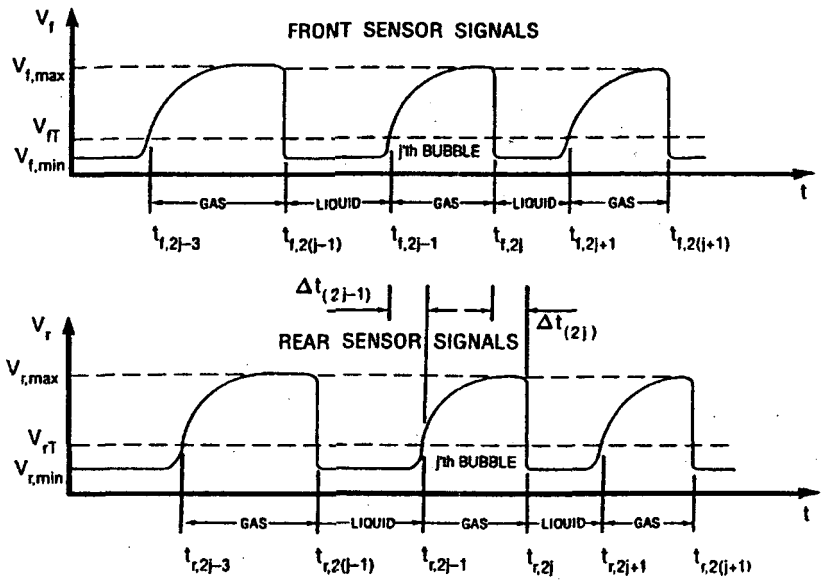

Figure 1. Schematic of the output signals: (a) front sensor; (b) rear sensor.

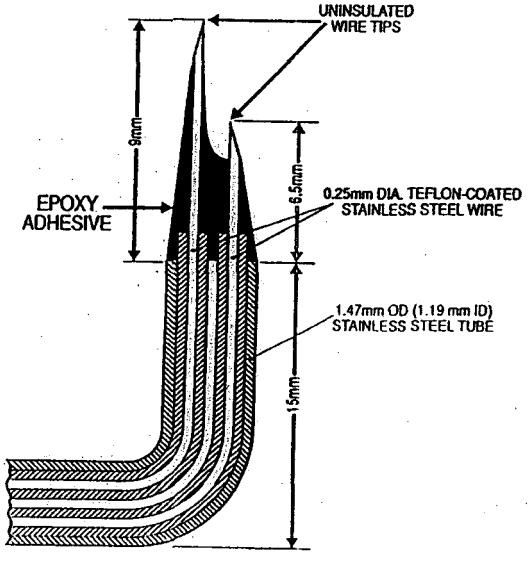

Figure 2. Double-sensor electrical resistivity probe design

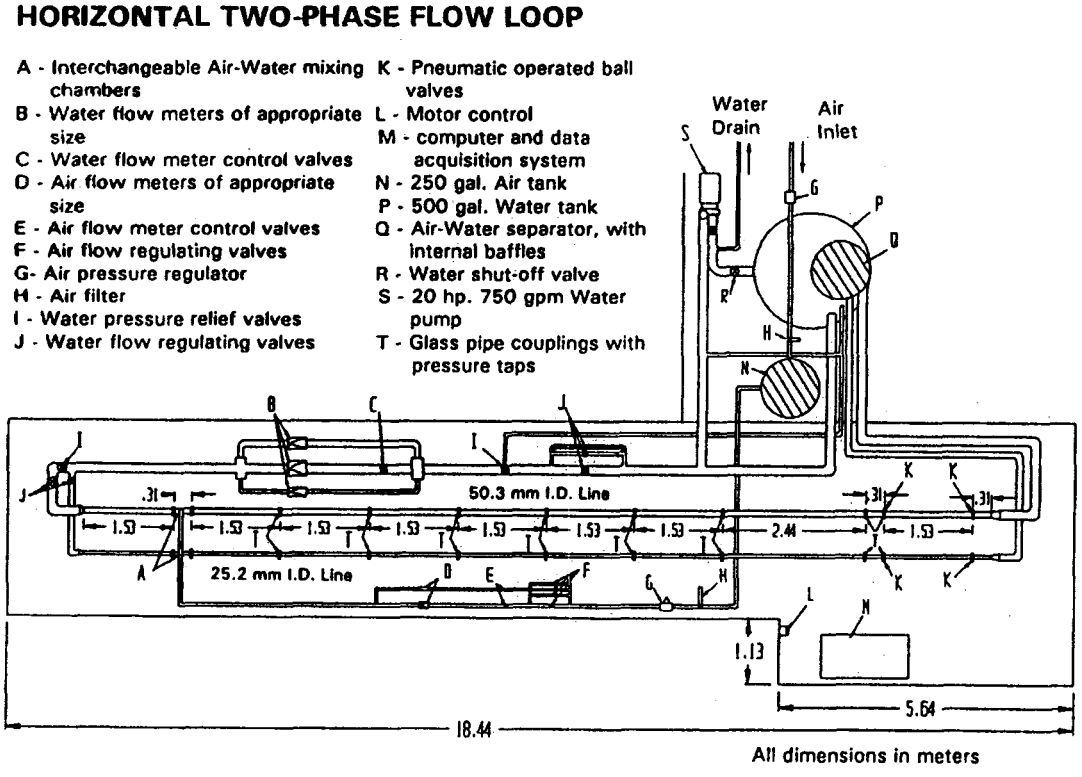

Figure 3. Schematic of the experimental flow loop

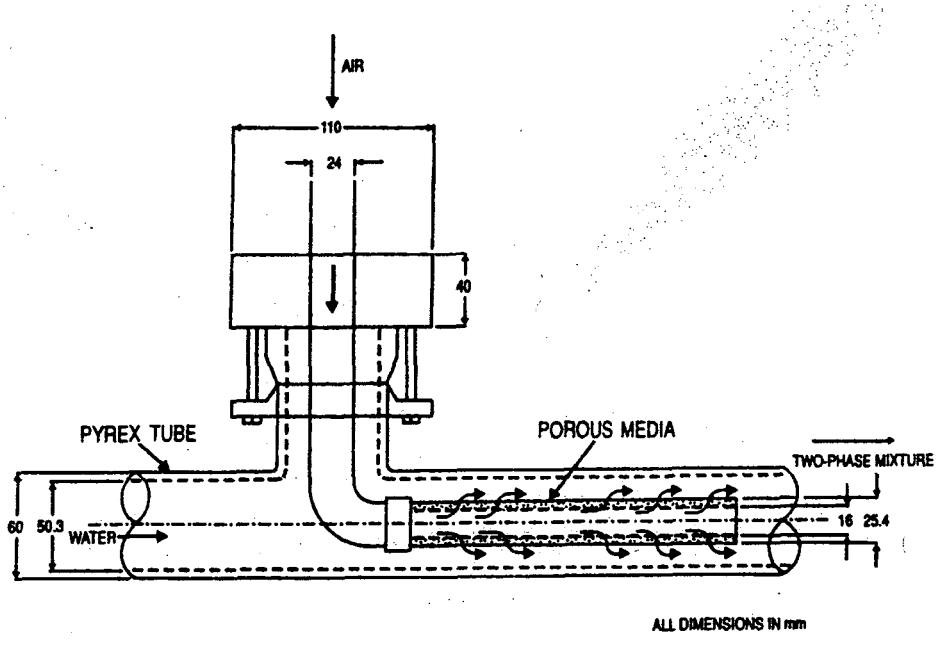

Figure 4. Schematic of air-water mixing chamber

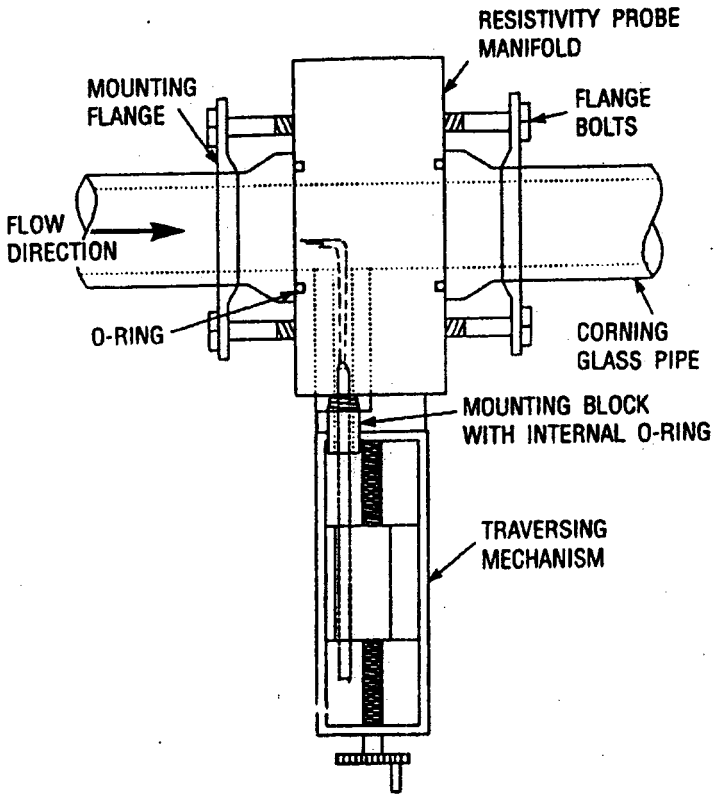

Figure 5. Mounting and traversing mechanism

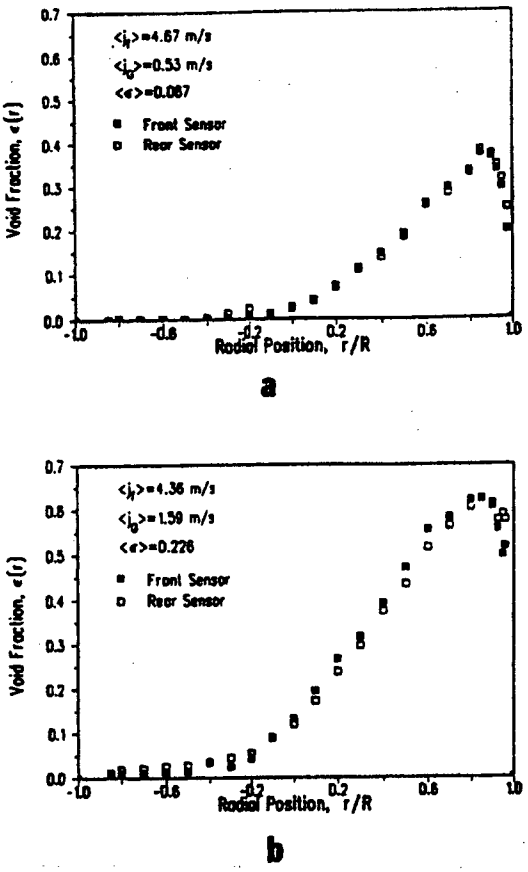

Figure 6. Local void fraction distributions obtained from front sensor and rear sensor

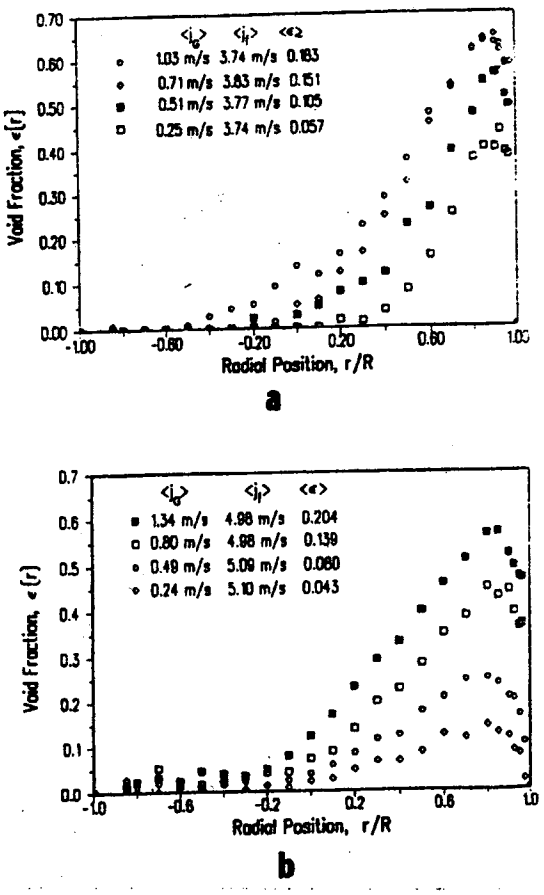

Figure 7(a). Influence of gas flow on the Local void fraction distribution at low liquid flow. (b) Influence of gas flow on the Local void fraction distribution at high liquid flow.

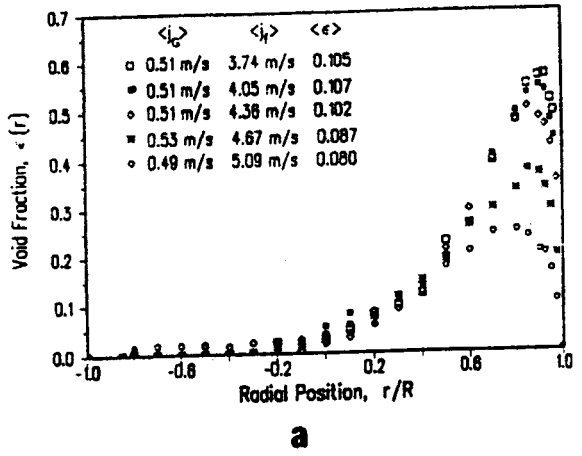

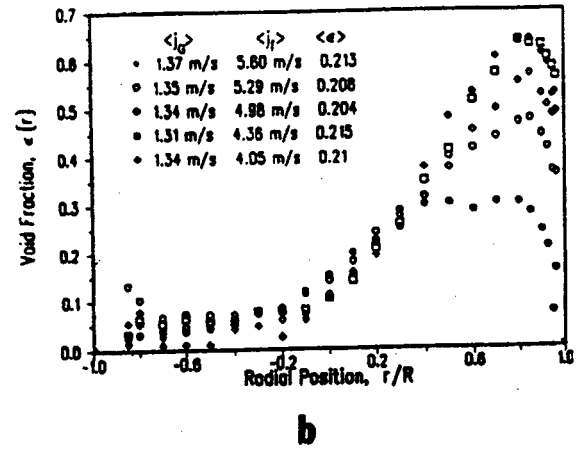

Figure 8(a). Influence of liquid flow on the local void fraction distribution at low gas flow. (b) Influence of liquid flow on the Local void fraction distribution at high gas flow.

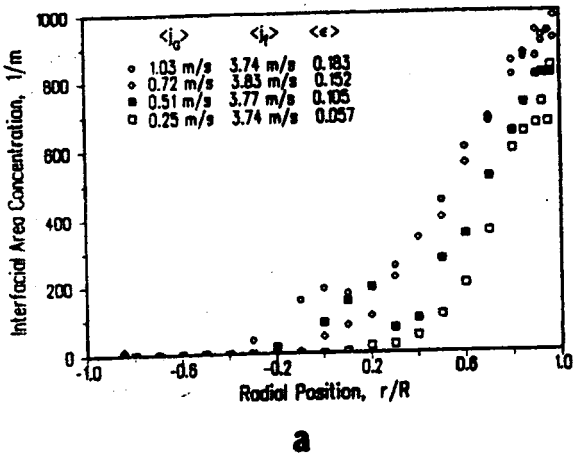

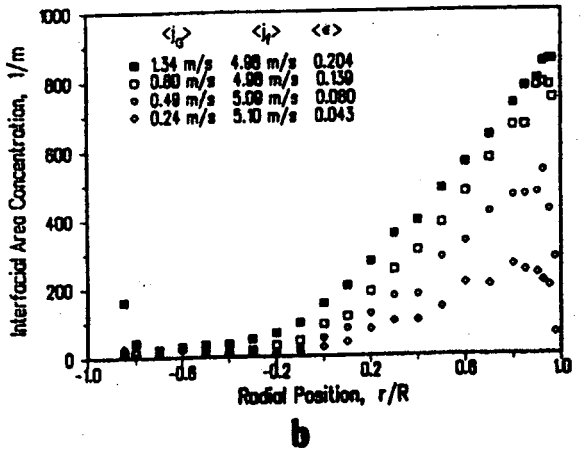

Figure 9(a). Effect of gas flow on the local interfacial area concentration profile at low liquid flow. (b) Effect of gas flow on the local interfacial area concentration profile at high liquid flow.

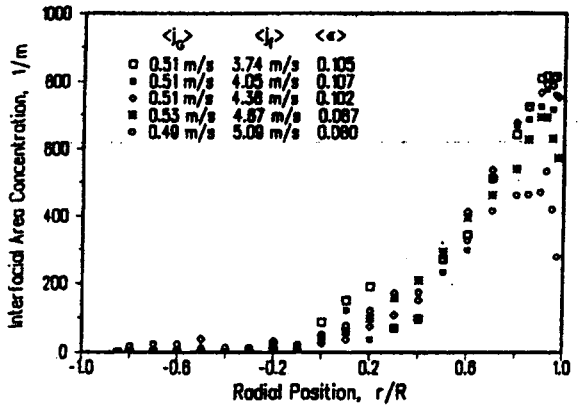

a

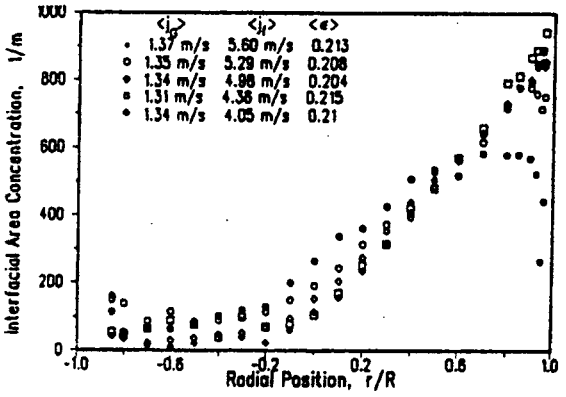

b

Figure 10(a). Effect of liquid flow on the local interfacial area concentration profile at low gas flow. (b) Effect of liquid flow on the local interfacial area concentration profile at high gas flow.

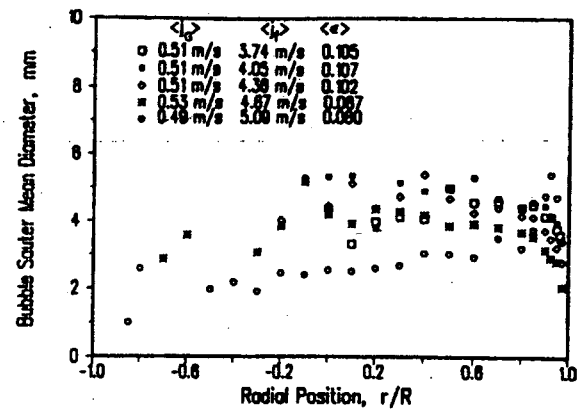

a

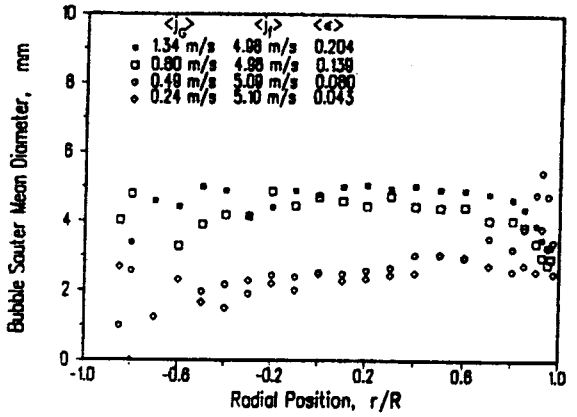

b

Figure 11. Sauter mean diameter profiles:
(a) effect of liquid flow;
(b) effect of gas flow.

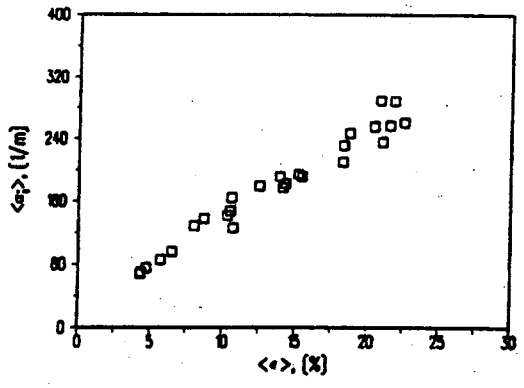

Figure 12. Average interfacial area concentration as a function of void fraction.

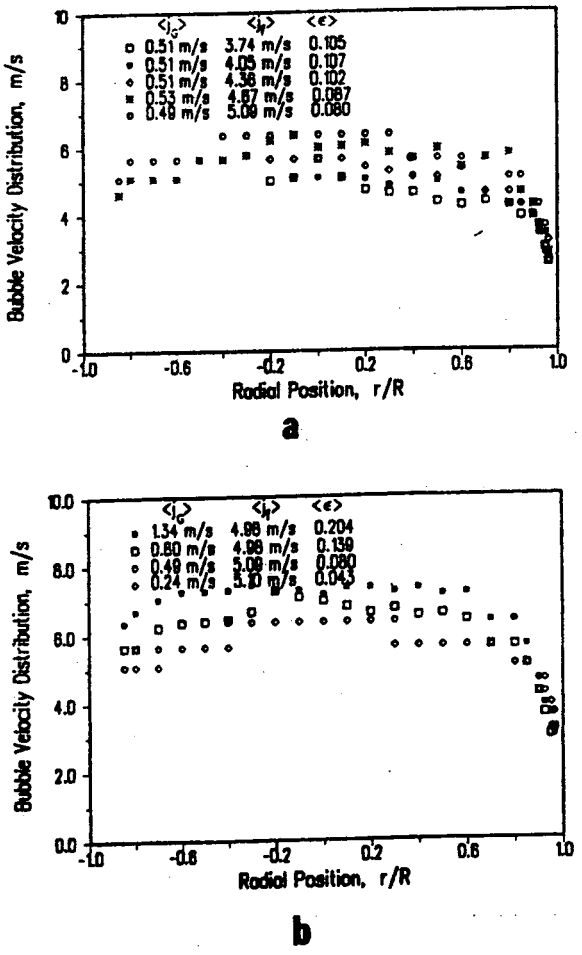

Figure 13. Bubble interfacial velocity distribution: (a) effect of liquid flow; (b) effect of gas flow.

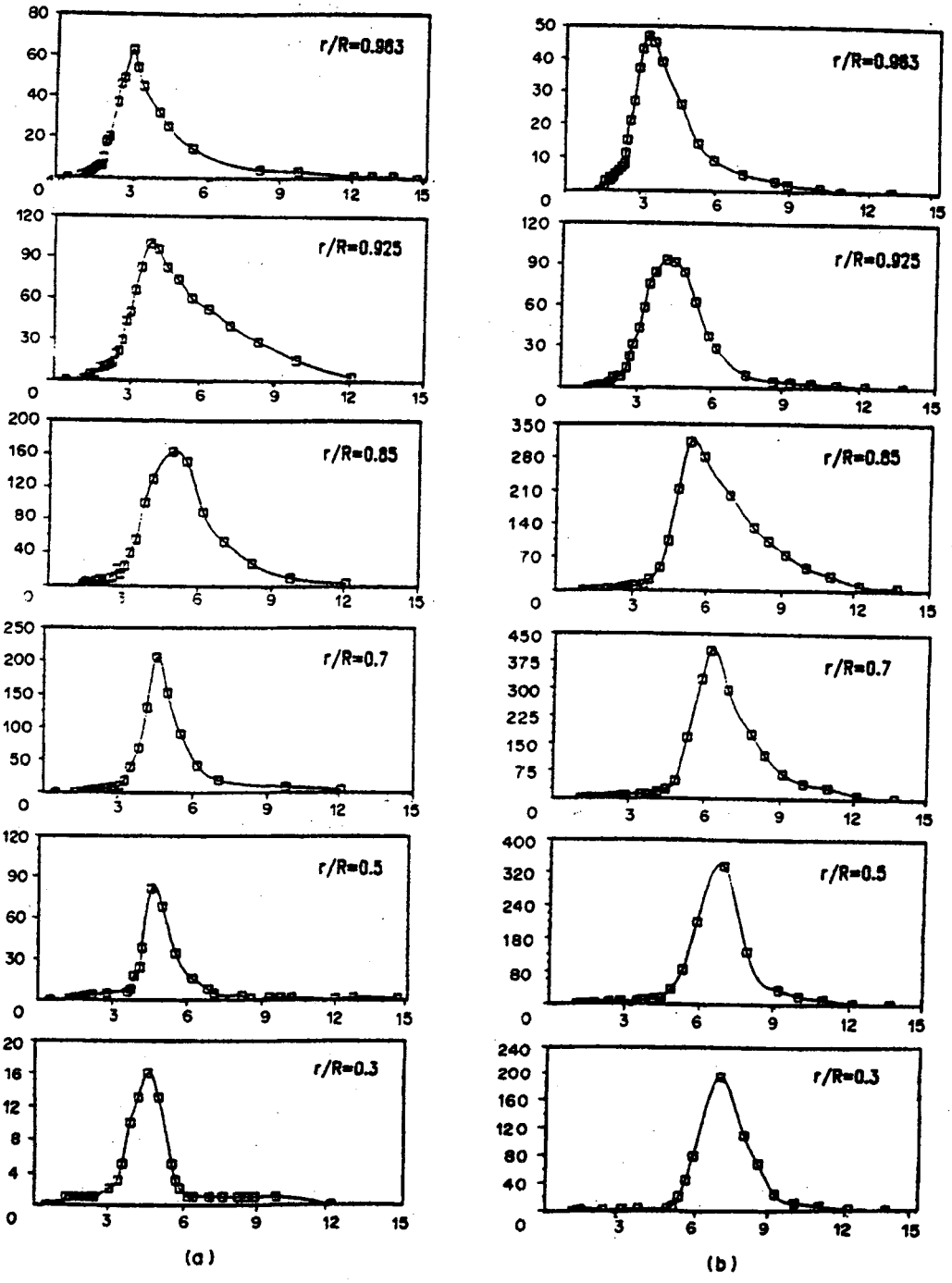

Figure 14. Typical bubble interfacial velocity spectra: (a) $\langle j_f \rangle$=3.83 m/s, $\langle j_G \rangle$=0.72 m/s, $\langle \varepsilon \rangle$=0.152; (b) $\langle j_f \rangle$=4.96 m/s, $\langle j_G \rangle$=1.34 m/s, $\langle \varepsilon \rangle$=0.204.

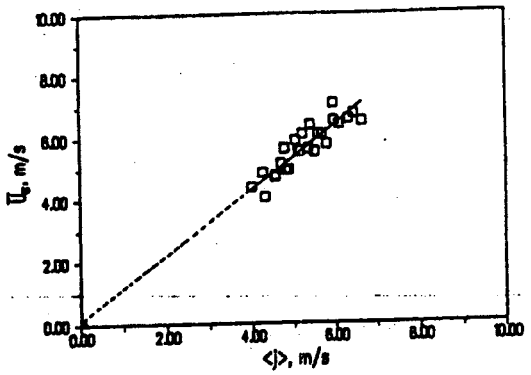

Figure 15. $\overline{u}_G$ ~ <*j* > presentation.

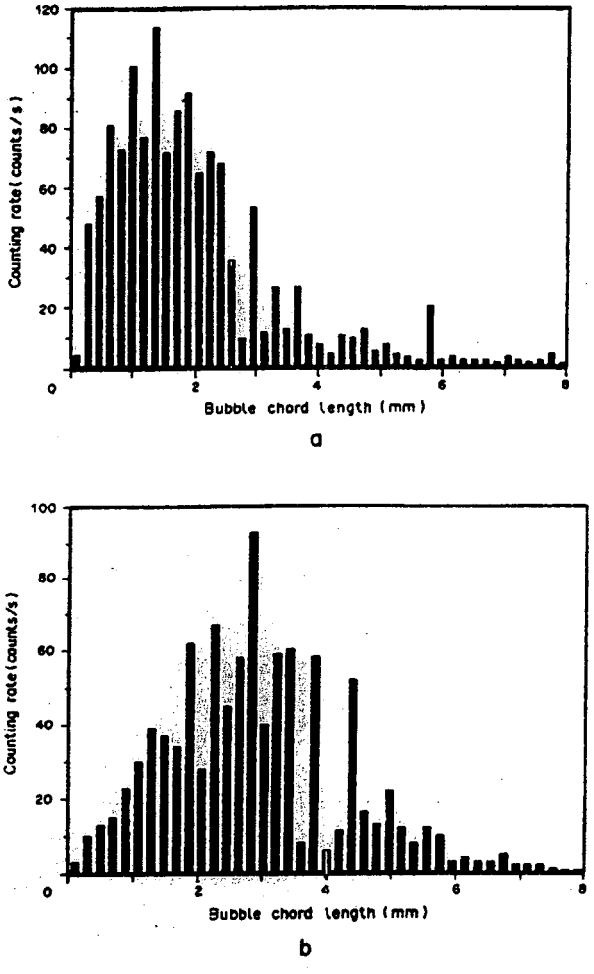

Figure 16. Typical bubble chord-length spectra: <j_f>=4.96 m/s, <j_G>=1.34 m/s, <ε>=0.204 at (a) *r/R*=0.963; (b) *r/R*=0.3.

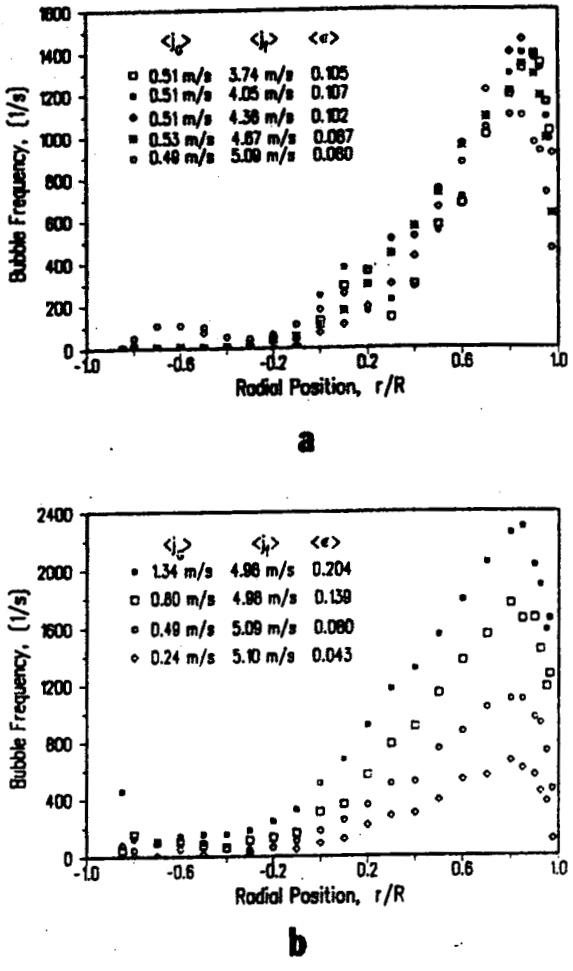

Figure 17. Bubble frequency profiles: (a) effect of liquid flow; (b) effect of gas flow.